Nearshore Oil Spill Modelling Report

Results from Simulations of Fuel Oil Spills in Bull Arm, Trinity Bay, Newfoundland

Prepared in support of the:

Hebron Project
Comprehensive Study Report

For:

Suite 701, Atlantic Place
215 Water Street
St. John's, NL, A1C 6C9

Prepared by:

Applied Science Associates, Inc.
55 Village Square Dr
South Kingstown, RI
02879

July 2011

Prepared for:
Stantec Consulting Ltd.

Nearshore Oil Spill Modelling Report
Results from Simulations of Fuel Oil Spills in Bull Arm, Trinity Bay, Newfoundland

ASA Project 2010–261 **18 July, 2011**

Prepared by:

Chris Galagan
Nicholas Cohn
Rachel Shmookler

Applied Science Associates, Inc.
55 Village Square Dr
South Kingstown, RI 02879

Executive Summary

ASA has used its SIMAP model system to simulate spills of fuel oil in Bull Arm, Trinity Bay, Newfoundland. The model utilizes wind data obtained from model hindcasts and field measurements, and current data from a hydrodynamic model. The SIMAP model was used in stochastic and deterministic modes to determine the range of possible water surface, subsurface and shoreline oiling predicted to occur. Spills simulated at this site are instantaneous surface releases of 100m^3 of marine diesel fuel and 1,000m^3 of intermediate fuel oil (IFO-180). Simulations were performed for both summer and winter environmental conditions. Winter season spills were simulated with and without sea ice present.

Wind data were obtained from the MSC50 Wind Hindcast model that provides winds for the north Atlantic for the period 1954 through 2008. Wind speed and direction data for the most recent 30 years of this period were used in the oil spill modeling. Wind data collected during the construction Hibernia gravity-based structure at the Bull Arm site in 1995 through 1997 were used to supplement the model winds and provide wind forcing specific to the oil release location.

Two separate hydrodynamic simulations were carried out using the HYDROMAP model in order to capture the combined tide and wind-driven currents in Bull Arm and Trinity Bay. Tidal current simulations were conducted using seven astronomical tidal constituents (M2, S2, N2, K2, O1, K1, and P1) to develop tidally driven surface currents over the entire region. Wind driven current simulations were conducted for eight wind directions, each using a constant wind speed of 8 m/s. During simulations, the wind forced currents were scaled depending on the actual wind speed and direction for each simulation time step, these scaled wind forced currents were added to the tidal current simulation to create a combined current. This results in a current field covering Trinity Bay and Bull Arm that accounts for tide and wind driven currents and is used to drive the oil spill simulations.

The stochastic model was used to determine the probability of oil on the water surface, on the shoreline, and in the water column exceeding the following thickness and concentration thresholds:

- Surface oil average thickness > 0.01 mm (10 µm)
- Shoreline oil average thickness > 0.01 mm (10 µm)over the shoreline
- Subsurface oil (entrained in water) average concentration > 10 ppb

Results from the stochastic model simulations are summarized in the table below.

Oil Release	Season	Surface Area Oiled at >0.01 mm (km^2)	Shoreline Oiled at >0.01 mm (km)	Entrained Oil Volume after 30 days (m^3)
100 m^3 Marine Diesel	Summer	581.4	19.8	58.6
	Winter	371.2	10.1	65.3
1,000m^3 IFO 180	Summer	1524.8	144.3	0.017
	Winter	1670.5	137.5	0.024

Individual spill simulations performed as part of the stochastic modeling were ranked to determine the 95th percentile spill for oiled sea surface area, oiled shoreline length and entrained oil volume at the defined thresholds. Maps were prepared showing surface oil, shoreline oil and entrained oil for the 95th percentile cases. Mass balance graphs depicting the volume of oil present on the surface, evaporated to the atmosphere, entrained in the water column, stranded on the shoreline and decayed by natural processes are also generated.

Table of Contents

List of Figures

List of Tables

1. Introduction

ExxonMobil Canada Ltd. has contracted ASA for oil spill modeling services to simulate spills at locations off the coast of Newfoundland and Labrador associated with the Hebron Project. The SIMAP model was used to simulate hypothetical oil spills in Bull Arm, Trinity Bay representative of spill characteristics associated with potential releases from vessels supporting construction of the offshore platform. The SIMAP model was used in both stochastic and deterministic modes to determine the range of possible water surface, subsurface and shoreline oiling predicted to occur. The stochastic modeling provides insight into the spatial extent of probability of oiling in response to the meteorological and oceanographic conditions in the Study Area and the deterministic model results show the predicted oil path and associated weathering for a specific spill event. The dominant environmental factors that influence surface oil transport are winds and currents. For this study, the model scenarios utilized wind data obtained from model hindcasts and field measurements, and current data from multiple hydrodynamic models.

This report presents the model input data and model results for simulations of fuel oil spills performed at the Bull Arm site. A companion report provides the same information for spill simulations performed at the Hebron offshore location. Also included in the report is a description of the model systems used to perform the modeling.

2. Model Inputs and Spill Scenarios

The spill scenarios modeled were defined in consultation with ExxonMobil Canada Properties and ExxonMobil Biomedical Sciences to represent the spills that may occur at the near shore site in Bull Arm. In Bull Arm, the potential spills consist of either marine diesel or intermediate fuel oil releases on the water surface from vessels involved in construction of the platform. These spills may occur at any time of year and under a range of environmental conditions, including partial sea ice coverage.

The SIMAP system was used to simulate all oil spills. The model simulates the transport and weathering of the oil released onto the water surface. This section describes the model inputs characterizing the site and spill scenarios, including wind, current, ice, shore type, and spill characteristics (oil type, volume and duration).

A previous oil spill modeling study was completed for the Hebron project in 2010 (AMEC, 2010). In this study, spill model simulations were run to determine the trajectory of the surface release of fuel oil spills at the Bull Arm site. Simulations were allowed to run until the spill terminated on a coastline or external model boundary (edge of the model grid), or for a maximum of thirty days. A model simulation was commenced on each day of the year for a thirty year period and allowed to run for thirty days or until termination on the shoreline. The results from these simulations for each month of the year were overlain on a grid of the Bull Arm-Trinity Bay region and the number of times surface oil passed through each grid cell was counted to determine the probability that oil released during the month would reach any place within the gridded water surface. This approach is deemed deterministic in that the model is forced using a prescribed set of wind data to generate a set of model trajectories that can be reproduced at any time by

using the same input data set. Results from these model simulations are presented in the AMEC (2010) report as maps of surface oil probability for each of the four seasons.

In contract to the deterministic approach employed in the previous study, this present study utilized a stochastic approach to determine the potential fate of fuel oil spills in Bull Arm. In this approach, a spill trajectory model is run repeatedly but with a randomly selected start date that is determined by a random number generator and a seed value. Using the same MSC50 wind hindcast model data to define the wind field, each oil spill simulation was run using a wind time series that started on the randomly selected date and run for 30 days. In this approach, a sufficient number of model runs will adequately sample all of the variability in the wind speed and direction in the region of interest and result in a prediction of the probability of oil pathways for a spill at the prescribed location. Running multiple spill simulations during a single season will provide a reliable prediction of the oiling probability for a spill occurring during that season.

2.1 Study Area

The Island of Newfoundland is composed of a series of islands off the east coast of Canada, and along with Labrador forms the easternmost Canadian province. The relatively shallow waters of the continental shelf extend eastward up to 500 km from the Newfoundland coast. Known as the Grand Banks, this area contains significant petroleum resources. The Hebron field is located near the edge of the Grand Banks more than 300km east of St John's (map in Figure 2.1-1).

Trinity Bay is an estuary on the northeastern coast of Newfoundland. The long axis of the Bay, approximately 100 km long, is orientated northeast-to-southwest with an opening to the ocean facing the northeast. Bull Arm extends from the southwest corner of the Bay towards the northwest. Trinity Bay and Bull Arm are relatively deep (hundreds of meters), hence tidal currents are small and wind driven circulation is a major component of the currents.

Figure 2.1-1. Map showing location of Bull Arm.

2.2 Model Scenarios

Multiple hypothetical spill scenarios were modeled to assess the fate of oil spilled from the nearshore site in Bull Arm. The hypothetical spills at the Bull Arm site were assumed to be instantaneous releases of either 100 m^3 of marine diesel fuel or 1,000 m^3 of intermediate fuel oil (IFO-180) onto the water surface. Each scenario simulated the transport and weathering of the spilled oil for a period of 30 days following the release. A 30-day period was used as it provides sufficient time for oil weathering and degradation processes to occur and for any remaining surface oil to exit Trinity Bay and enter the open ocean. Six different scenarios were modeled, both stochastic and deterministic, as summarized in Table 2.2-1. The characteristics of the spilled oils are discussed in Section 2.3.

TABLE 2.2-1. OIL SPILL SCENARIOS MODELED AT THE BULL ARM LOCATION.

Scenario	Spill Volume	Spill Duration	Season
Bull Arm (47.818333º N, 53.866667º W)			
Vessel Discharge Marine Diesel	100 m^3	Instantaneous	Summer
		Instantaneous	Winter - No Ice
		Instantaneous	Winter - 65% Ice
Vessel Discharge IFO-180	1,000 m^3	Instantaneous	Summer
		Instantaneous	Winter - No Ice
		Instantaneous	Winter - 65% Ice

2.3 Oil Characterization

The characteristics of the oil types used in the spill simulations are listed in Table 2.3-1. The data used to characterize the fuels come from the Environment Canada Oil Properties database (http://www.etc-cte.ec.gc.ca/databases/oilproperties/). The SIMAP model uses these characteristics to calculate oil weathering simultaneously with oil transport in the environment.

TABLE 2.3-1. CHARACTERISTICS OF OIL USED IN THE SPILL SIMULATIONS.

Oil	Spill	API Gravity	Density (g/cm^3)	Viscosity (cP)
Marine Diesel	Vessel in Bull Arm	37.6	0.82910 @ 25° C	4.0 @ 25° C
IFO-180	Vessel in Bull Arm	14.8	0.9670 @ 25° C	2324.0 @ 25° C

2.4 Wind Data

Wind data for nearshore model simulations were obtained from two sources, an output from a grid point located neat the Study Area from a large-scale model hindcast and observations from a previous GBS construction program near the Study Area. The hindcast wind data was obtained from the MSC50 Wind Hindcast (Swail, et al., 2006), a model reanalysis product that provides hindcast winds for the north Atlantic for the period 1954 through 2008, as provided by Environment Canada, MSC Atlantic Operations. The data are supplied at evenly spaced points 0.1° apart and provide hourly speed and direction. Figure 2.4-1 is a map showing the locations of the MSC50 model data in Trinity Bay. The most recent 30 years (1978 – 2008) of the MSC50 wind data were used in the oil spill model simulations. Wind data were also obtained at the site in Bull Arm during the construction of the Hibernia GBS from January 25, 1995 through May 26, 1997 by Oceans Ltd. These observations included wind speed and direction collected on a 10-minute interval for the 28 month period. The observed data show that wind speed and direction inside Bull Arm differs from wind in Trinity Bay due to the steering effects of the surrounding land.

The requirements of a modeling study utilizing a stochastic approach require multi-year or multi-decade wind time series data covering an area at least as large as the released oil is expected to cover. This is necessary in order to adequately represent the spatially variable range of possible wind conditions over a long time period. Wind data measured at sites within Bull Arm in the past do not meet either of these criteria. The MSC50 wind data are the best available for this modeling study.

The MSC50 Wind and Wave reanalysis project has its roots in three previous oceanographic modeling studies in the North Atlantic, the most recent of which is the AES40 study (Swail, et al., 2006). In AES40, winds for the period 1954 through 2004 were hindcast and supplemented with measured winds from buoys, platforms and C-MAN stations. The wind hindcast was evaluated against satellite altimeter and in-situ wind speed measurements (Swail, et al., 2006). The MSC50 project was intended to improve on the AES40 model by increasing the resolution within the Canadian east coast region and increasing overall model accuracy in order to reduce uncertainties in the hindcast predictions.

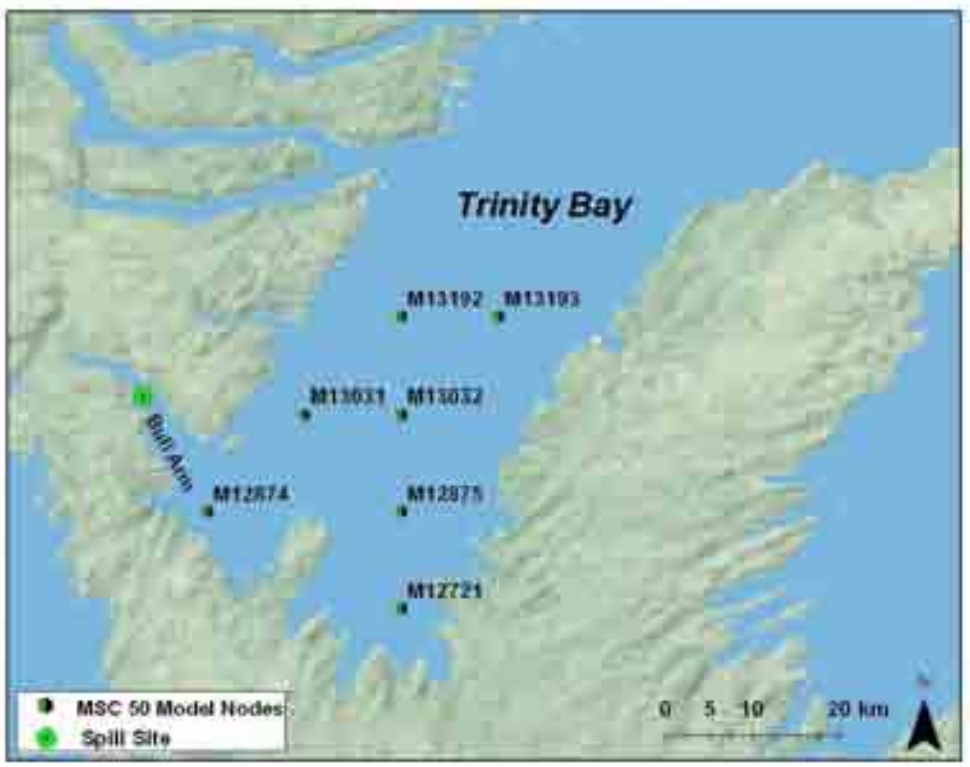

Figure 2.4-1. Map of the Bull Arm, Trinity Bay area showing the location of the potential diesel and fuel oil spills and the MSC50 wind data sites.

The MSC50 wind model hindcast incorporates the passage of storm systems, particularly those that originate along the US New England coast in winter and move into Canadian waters. Sea

ice was also incorporated into the MSC50 model with the ice edge changing on a weekly basis, sufficient to capture changes in sea ice during transition seasons.

Comparison of the in-situ data from the period 1954-2005 with the MSC50 model hindcast show consistent agreement (Swail, et al., 2006). Swail, et al. (2006) state:

> *"The wind and wave data are considered to be of sufficiently high quality to be used in the analysis of long return period statistics, and other engineering applications."*

There were no wind data measurements identified as part of this study within Bull Arm or Trinity Bay that correspond to MSC50 hindcast node locations, so no direct comparisons between the field measurements and model hindcast winds were conducted.

Figure 2.4-2 is a wind rose showing the distribution of wind directions and speeds at the southern end of Trinity Bay according to the MSC50 model hindcast data obtained for location M12874 (see map in Figure 2.4-1). The wind comes from all directions at this site but it comes most frequently from the south through the northwest. Figures 2.4-3 through 2.4-6 are wind roses showing the speed and direction of the wind at MSC50 site 12874 for the four seasons. As can be seen in these plots, summer season winds are predominantly from the southwest with maximum speeds of 10-15 m/s. Winter season winds at this site are predominantly from the west with speeds up to 20-25 m/s. Spring season wind direction is highly variable as is typical for transition seasons at these latitudes. Fall wind direction is somewhat less variable than spring wind with a slightly higher frequency of wind coming from the west.

The wind rose showing the data collected by Oceans Ltd. in Mosquito Cove in 1995-1996 (Figure 2.4-7) shows a predominance of wind coming from the northwest, suggesting that the land bordering Bull Arm is steering the wind along the long axis of the fjord. Comparison of the two wind data sets also shows that winds in Bull Arm are generally of lower speed than the MSC50 wind.

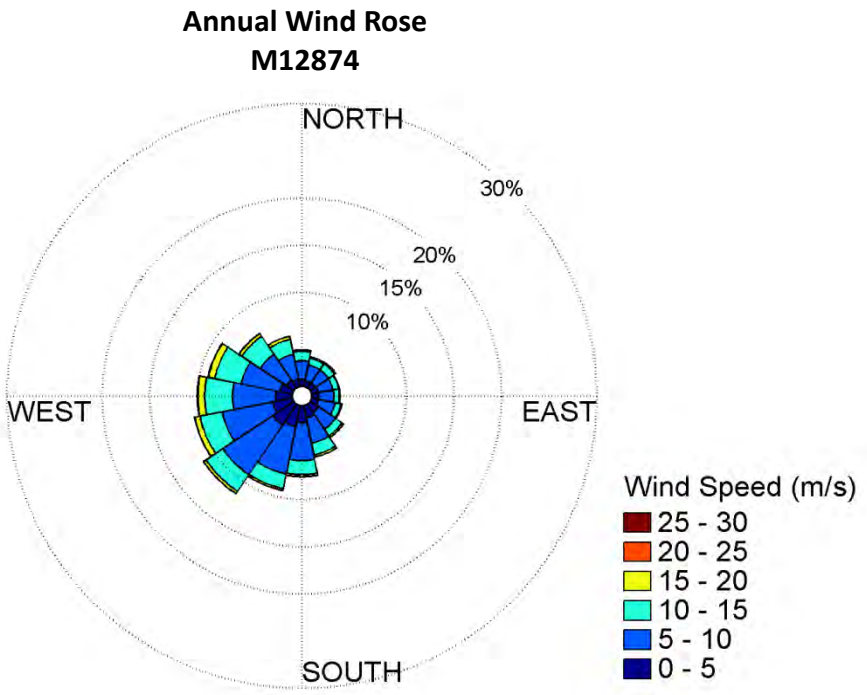

Figure 2.4-2.Wind rose diagram from the MSC50 model hindcast at location M12874.

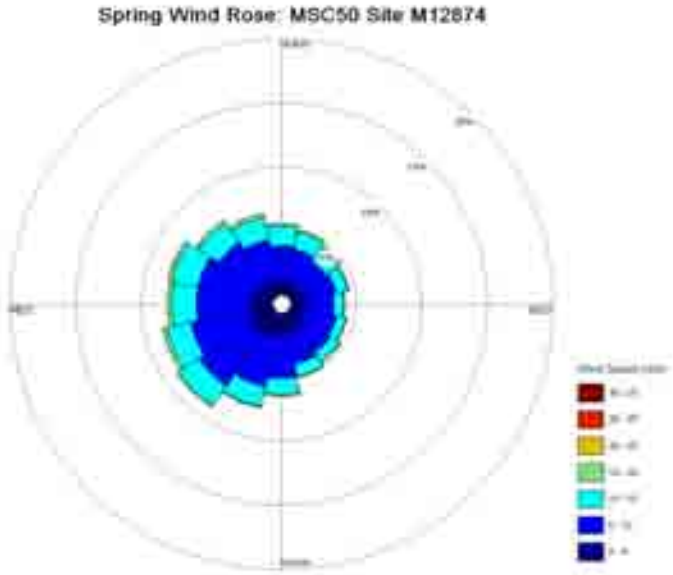

Figure 2.4-3 Wind rose diagram from the MSC50 model hindcast at location M12874 for the Spring season.

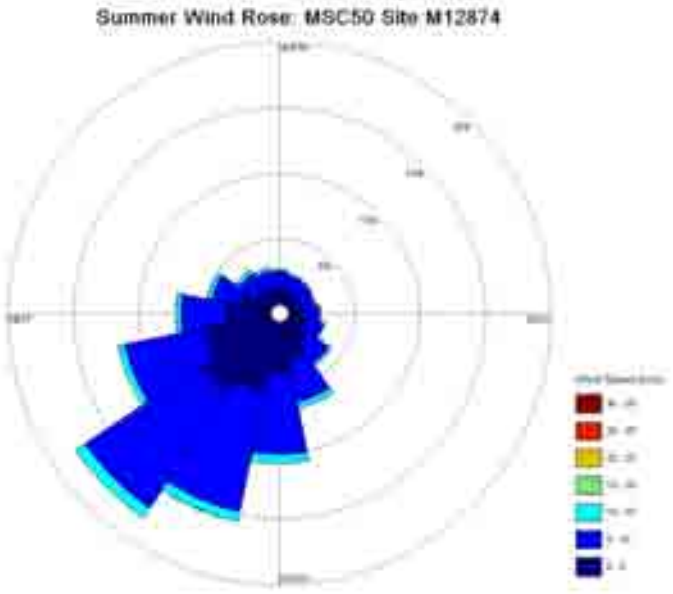

Figure 2.4-4 Wind rose diagram from the MSC50 model hindcast at location M12874 for the Summer season.

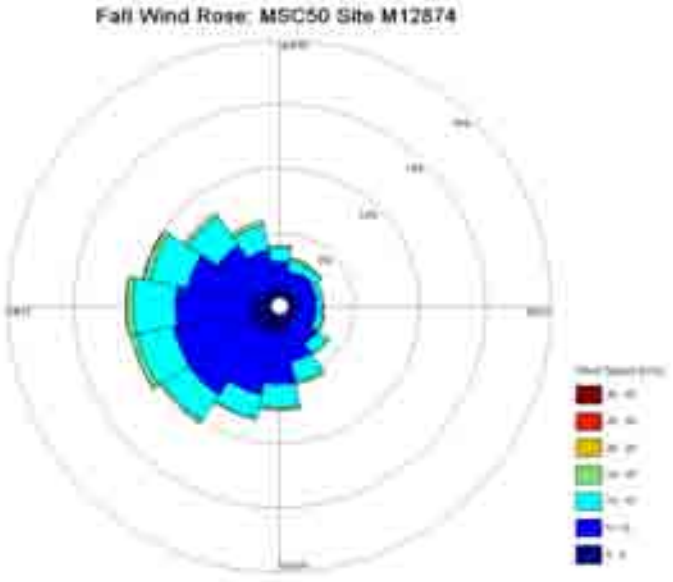

Figure 2.4-5 Wind rose diagram from the MSC50 model hindcast at location M12874 for the Fall season.

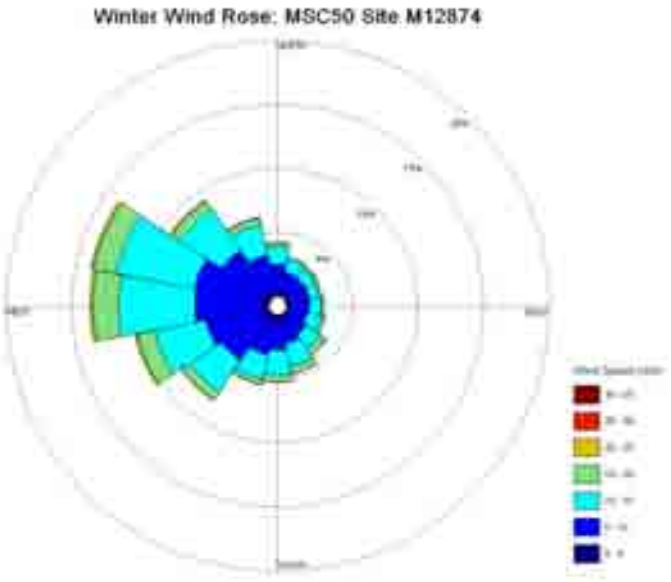

Figure 2.4-6 Wind rose diagram from the MSC50 model hindcast at location M12874 for the Winter season.

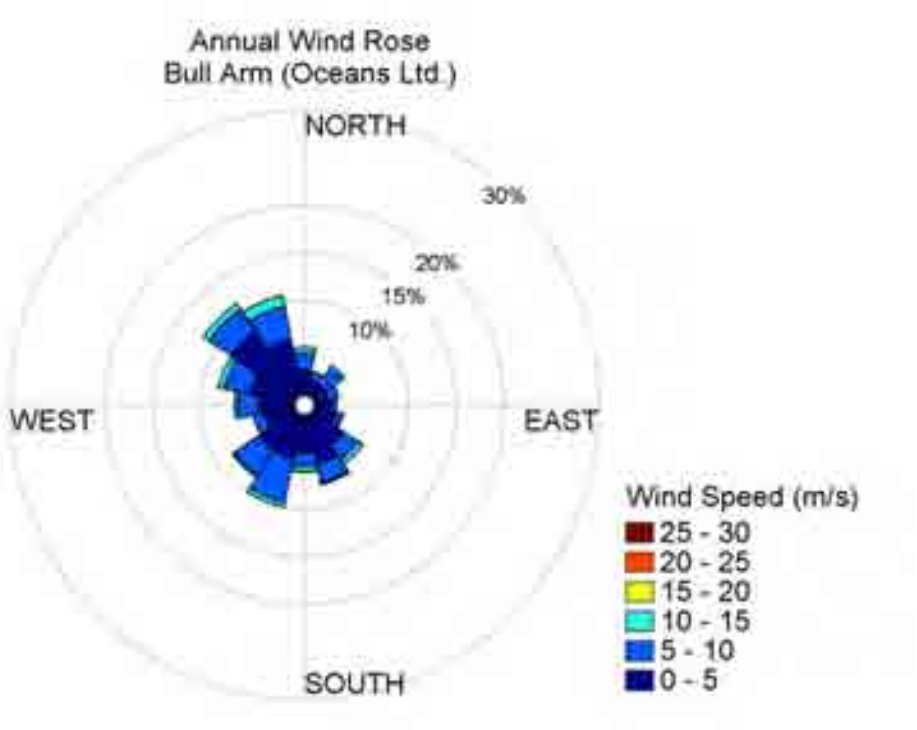

Figure 2.4-7. Wind rose diagram from the Oceans Limited data collected at the Hibernia GBS construction site during 1995 and 1996.

The wind data collected in prior studies are not sufficient to run the simulations defined for this study because the data do not have adequate spatial or temporal coverage. The modeling requires a long-term wind record such as the MSC50 model hindcast provides, but the MSC50 data do not include Bull Arm, so it was necessary to correlate the Oceans Ltd wind data collected in Bull Arm to a nearby MSC50 grid node (M12874) to correct for the difference in wind speed between the two locations and to account for any possible steering affects inside the fjord. Details of the method used to adjust wind data from site M12874 so that it accounts for the change in speed and direction seen in Bull Arm are described in the previous modeling report (AMEC, 2010). The method used the relationship between speed at site M12874 and speed measured at the Bull Arm site to yield a linear regression equation for adjusting the MSC50 wind speeds. The adjustment of wind direction was done using a fixed correction based on the relationship between the directions at site M12874 and the Bull Arm observations (See AMEC, 2010 for details). From this analysis a 30-year wind time series specific to the Bull Arm spill site was produced and used in the oil spill model simulations along with data from the MSC50 sites in Trinity Bay shown in Figure 2.4-1. This provides the SIMAP model with a spatially- and time-varying wind field over Bull Arm and Trinity Bay.

Simulations of the fuel oil spills in Bull Arm use multiple 30-year wind speed and direction time series from the MSC50 model grid nodes in combination with a 30-year modified wind time series in Bull Arm described above. The wind data collected in prior studies is not sufficient to run the simulations defined for this study because the data do not have adequate spatial or temporal coverage. The MSC50 wind data are the best available for the purpose of determining the probabilities of oil trajectories from spills for this kind of risk assessment.

2.5 Current Data

The Labrador Current dominates the large scale ocean circulation in the Newfoundland region. This current originates in the Arctic Ocean and flows south along the coasts of Labrador and Newfoundland, while the North Atlantic current farther offshore flows north and east across the Atlantic Ocean (see the map in Figure 2.5-1). Currents at smaller scales can be highly variable and it was necessary to develop hydrodynamic model datasets to characterize the currents in the Study Area sufficient to simulate the movement of spilled oil.

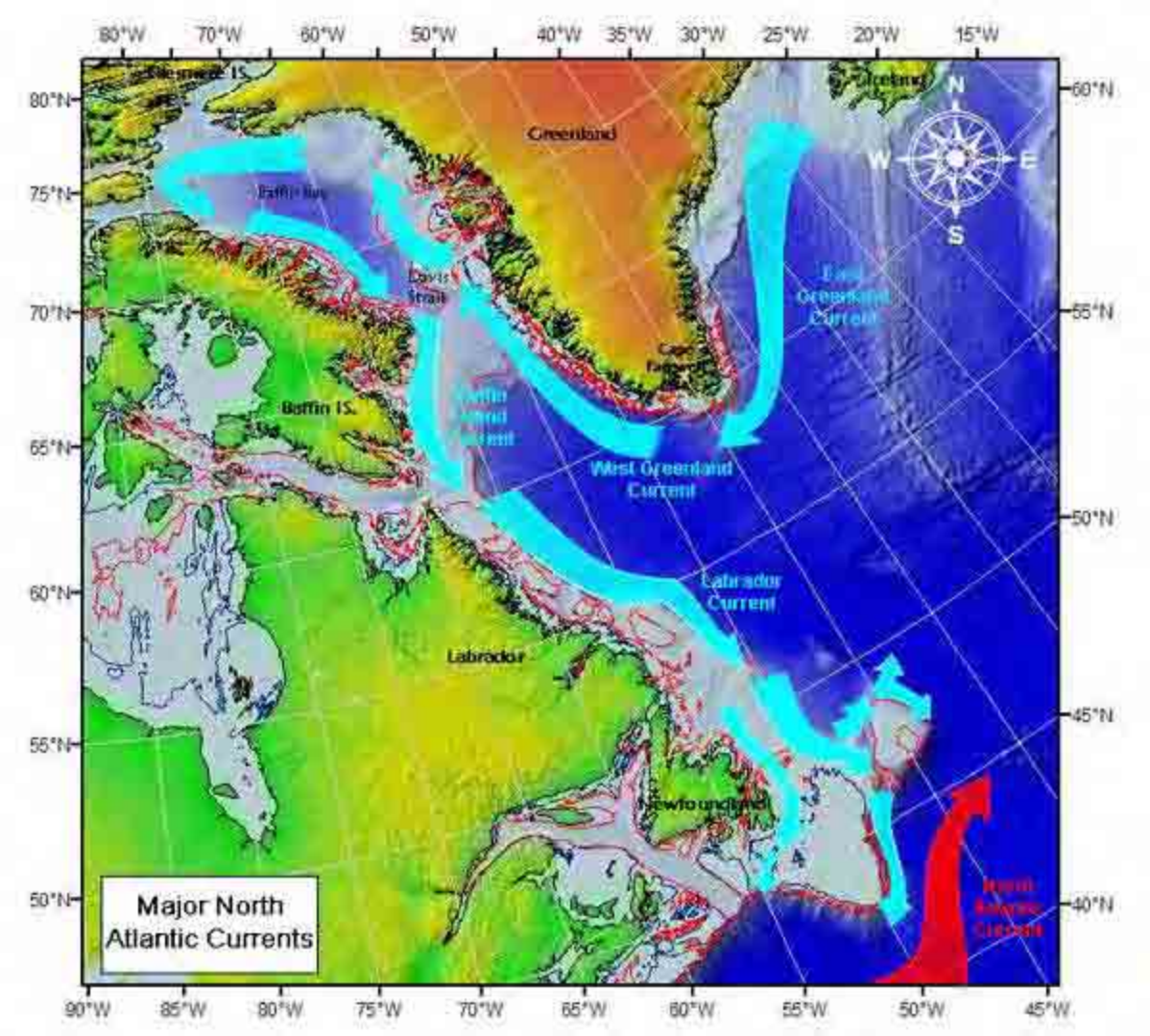

Figure 2.5-1. Map of the large scale ocean currents in the Newfoundland region. (Source: U.S. Coast Guard, International Ice Patrol).

A hydrodynamic model grid covering Trinity Bay and Bull Arm was prepared with a base cell resolution of 2 km (Figure 2.5-2 shows the grid). The grid cell size gets increasingly smaller moving from the mouth of Trinity Bay to Bull Arm (Figure 2.5-3) to provide maximum resolution in the immediate area of the spill site. Depth data used in the model grid were obtained from navigational charts (NOAA/C-MAP) and the RTM30_PLUS (Becker and Sandwell, 2008) database.

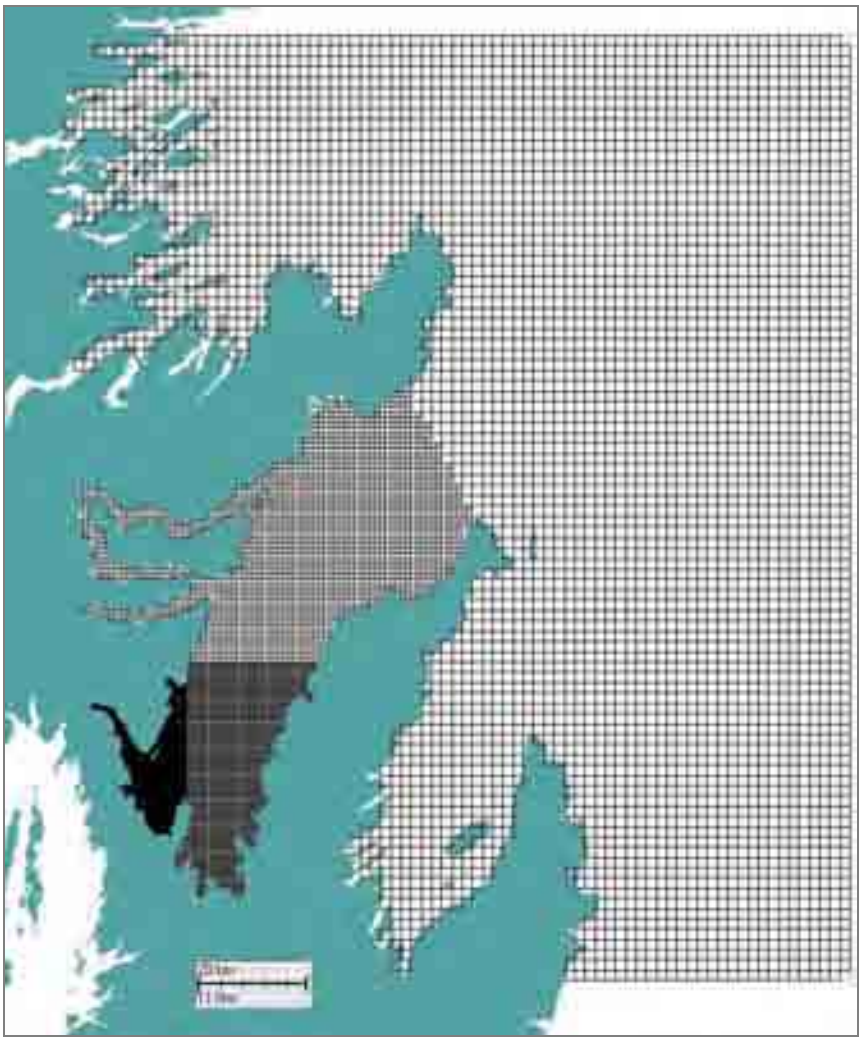

Figure 2.5-2. HYDROMAP model grid of Trinity Bay and Bull Arm.

Figure 2.5-3. Trinity Bay hydrodynamic model grid showing detail in the Bull Arm area.

Two separate hydrodynamic simulations were carried out using the HYDROMAP hydrodynamic model (Isaji, et al., 2001) in order to capture the combined tide and wind-driven currents in the area. Tidal current simulations were conducted for seven astronomical constituents (M2, S2, N2, K2, O1, K1 and P1). The open boundary specification outside Trinity Bay was based on global tide data obtained from the Oregon State University Inverse Tidal Model, TPXO5. TPXO5, which is a data assimilation model constrained by satellite altimetry data, TOPEX/Poseidon, as described by Egbert, Bennett, and Foreman, 1994. Using these tidal constituent characteristics (amplitude and phase) at the open boundaries to force the model, it is possible to predict the associated tidal currents within Trinity Bay and Bull Arm for any given date and time. Figure 2.5-4 shows the observed tidal elevation at Long Cove (top plot) and the model predicted tidal elevation (bottom plot) for the same location. The model prediction compares reasonably well with the observed water elevations except that the model lacks small fluctuations seen in the observed data that are a result of wind forcing. Figures 2.5-5 and 2.5-6 are maps of the model predicted surface currents during mean flood and ebb flow conditions in the vicinity of Bull Arm.

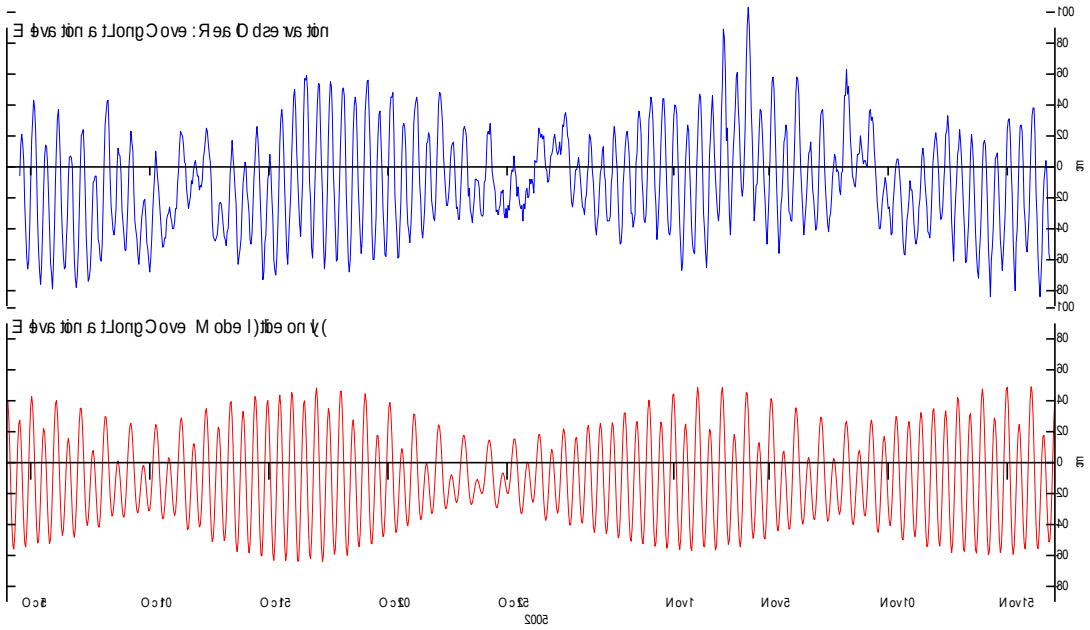

Figure 2.5-4. Comparison of observed water elevation (top plot) versus model predicted water elevation (bottom plot) at Long Cove, Trinity Bay.

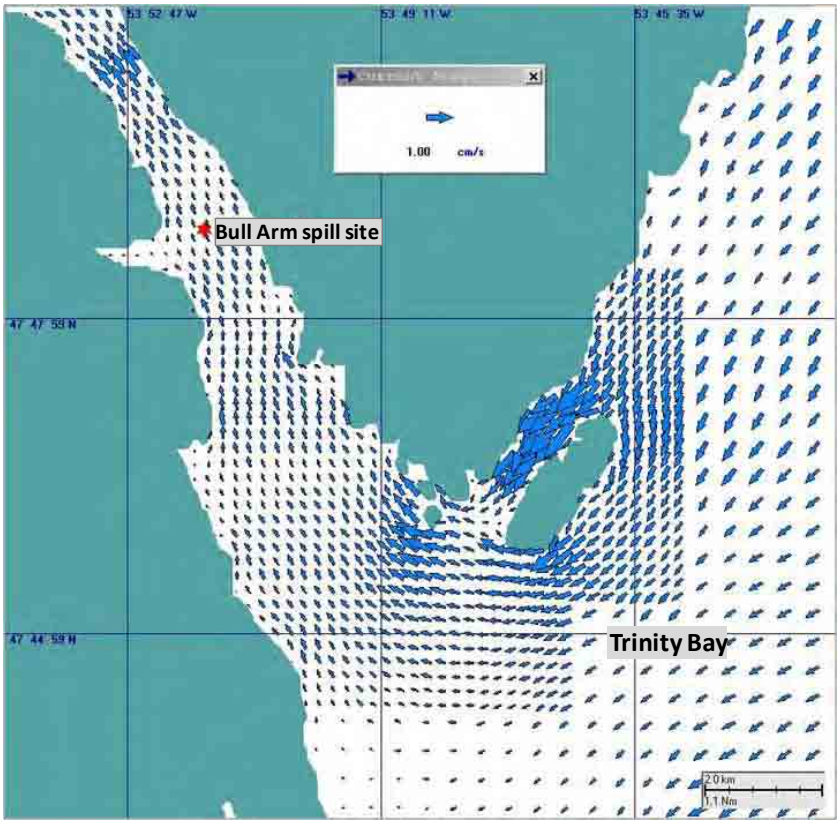

Figure 2.5-5. Model predicted mean surface flood tidal currents in the area of Bull Arm. The current vector in the Current Scale window represents a current speed of 1cm/s (0.02 knots).

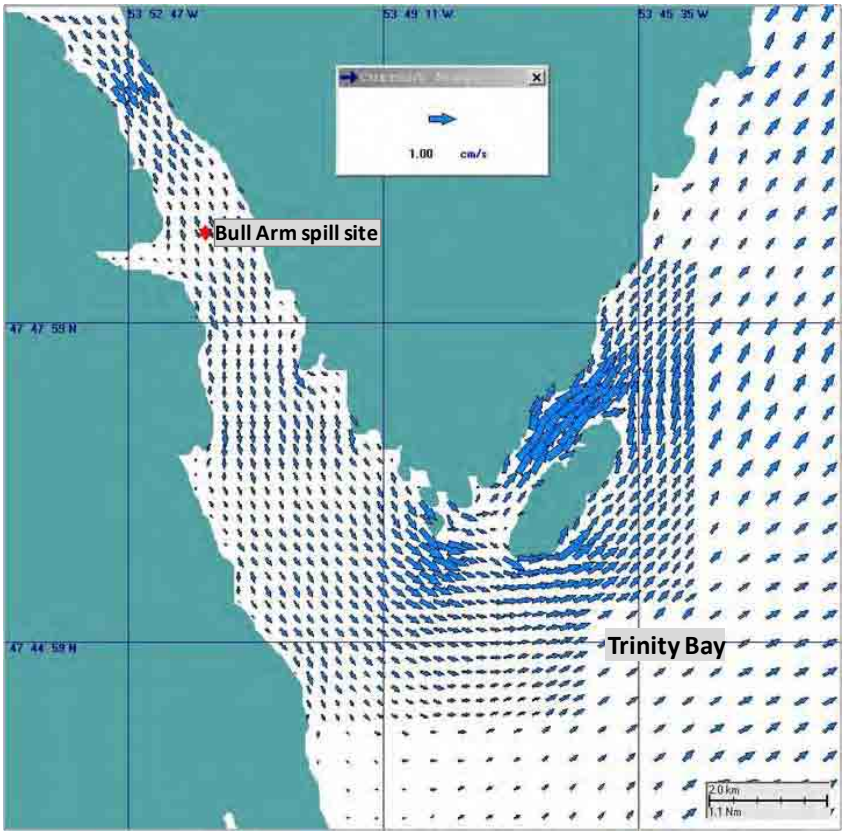

Figure 2.5-6. Model predicted mean surface ebb tidal currents in the area of Bull Arm. The current vector in the Current Scale window represents a current speed of 1cm/s (0.02 knots).

In order to account for the effect of wind on currents in Bull Arm and Trinity bay, wind driven current simulations were generated for eight wind directions each assuming a constant wind speed of 8 m/s. These hydrodynamic simulations provided the wind driven currents for the range of possible wind directions, which can be added to the tidal current simulation to create a combined current. The current generated by each of the eight wind directions represents typical circulation resulting from a day-long wind event with a wind speed of 8 m/s.

In the oil spill model, these tide and wind driven currents are automatically reassembled into a single hydrodynamic field. Astronomic tidal currents are constructed based on the date and time of the spill simulation. Based on the average wind speed and direction occurring at this time, one of the eight wind driven currents is scaled and superimposed on the tidal current. This results in a current field for Trinity Bay and Bull Arm for use in the oil spill model that accounts for tide and wind driven currents.

In hydrodynamic modeling studies of this kind when the effects of wind forcing over the water surface are to be included, it is desirable to model the tide and wind effects simultaneously for the entire period being simulated. The present study utilized a wind dataset spanning 30 years, an extremely long time period over which to simulate a wind forced current. It was deemed not practical to do this because of the extraordinarily large file sizes generated during this process for such an extended time period. It is considered sufficient to utilize the scaling approach described above for the purposes of estimating the statistics of oil spill impacts.

The influence of wind on surface water circulation can be seen in the model predicted surface currents as shown in Figure 2.5-7. In this figure the wind speed and direction time series calculated for the Bull Arm spill site (using the methodology described in the previous section) is compared with the model predicted surface current speed and direction. As can be seen in Figure 2.5-7 the surface current (bottom plot) responds relatively quickly to the changing wind (top plot) inside Bull Arm. An example surface current resulting from an 8 m/s west wind is shown on the map in Figure 5.2-8.

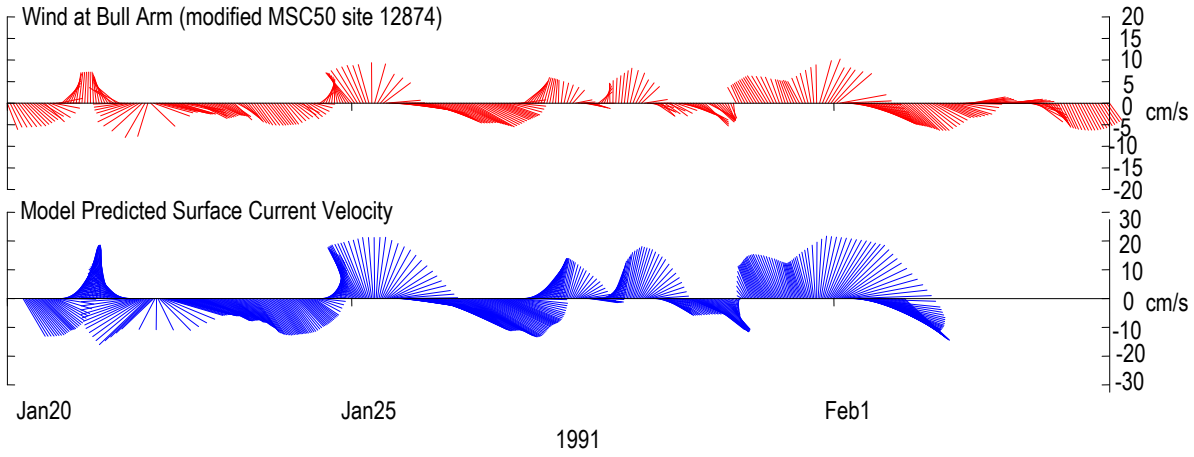

Figure 2.5-7. Wind speed and direction derived from the MSC50 model hindcast data (top plot) and surface current speed and direction (bottom plot) predicted by the hydrodynamic model for the Bull Arm spill site.

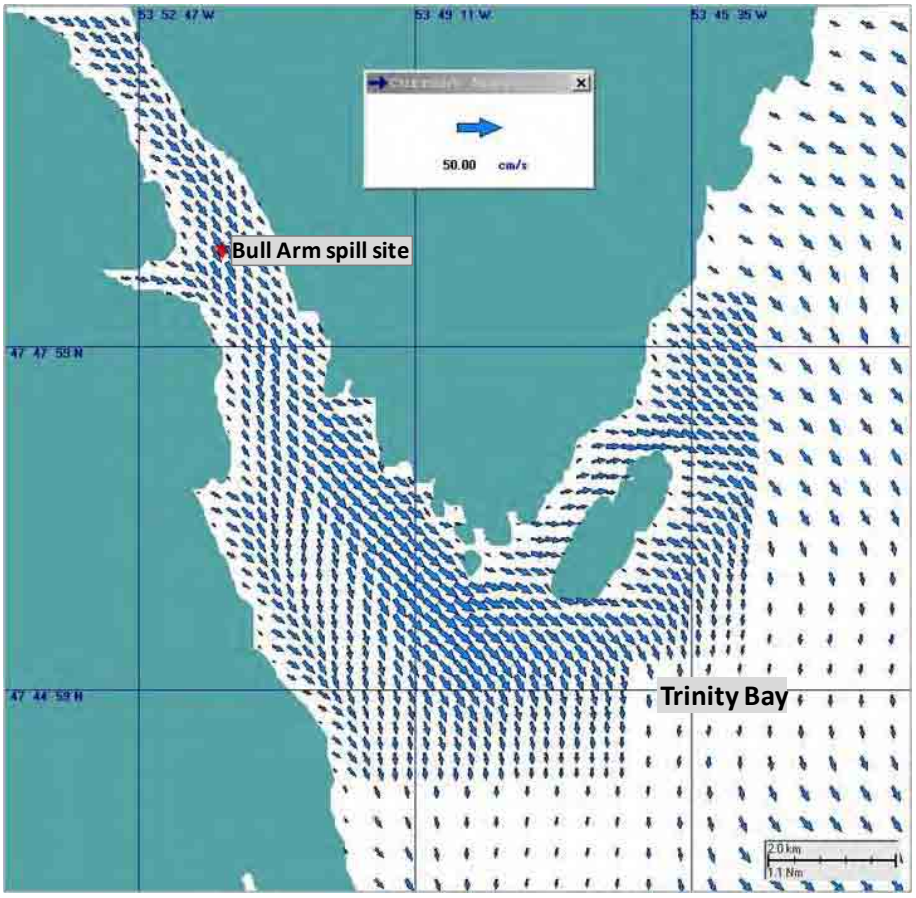

Figure 2.5-8. Model predicted surface currents generated by a west wind in the area of Bull Arm. The current vector in the Current Scale window represents a current speed of 50cm/s (1 knot).

For additional validation of the hydrodynamic model developed for Bull Arm and Trinity Bay, current measurements collected at the Hibernia GBS site from January 20 to February 5, 1991 (Seaconsult, 1991) were compared to the model predicted current direction and velocity. Figure 2.5-9 shows the east-west and north-south components of near-surface currents predicted by the model (top plot) and measured by Seaconsult (Seaconsult, 1991) (bottom plot) at the Bull Arm spill site. The comparison shows that the model is in general agreement with observations in predicting the change in direction of surface currents; however, the model appears to over predict the current magnitude in some instances while under-predicting it in others. This level of agreement is sufficient for a risk assessment study where multiple (hundreds) of individual spill simulations are completed and a range of spill trajectories developed into probability statistics to assess the most likely spill scenarios. The available field measurements of currents in Bull Arm and Trinity Bay do not have sufficient spatial or temporal coverage to drive oil spill model simulations.

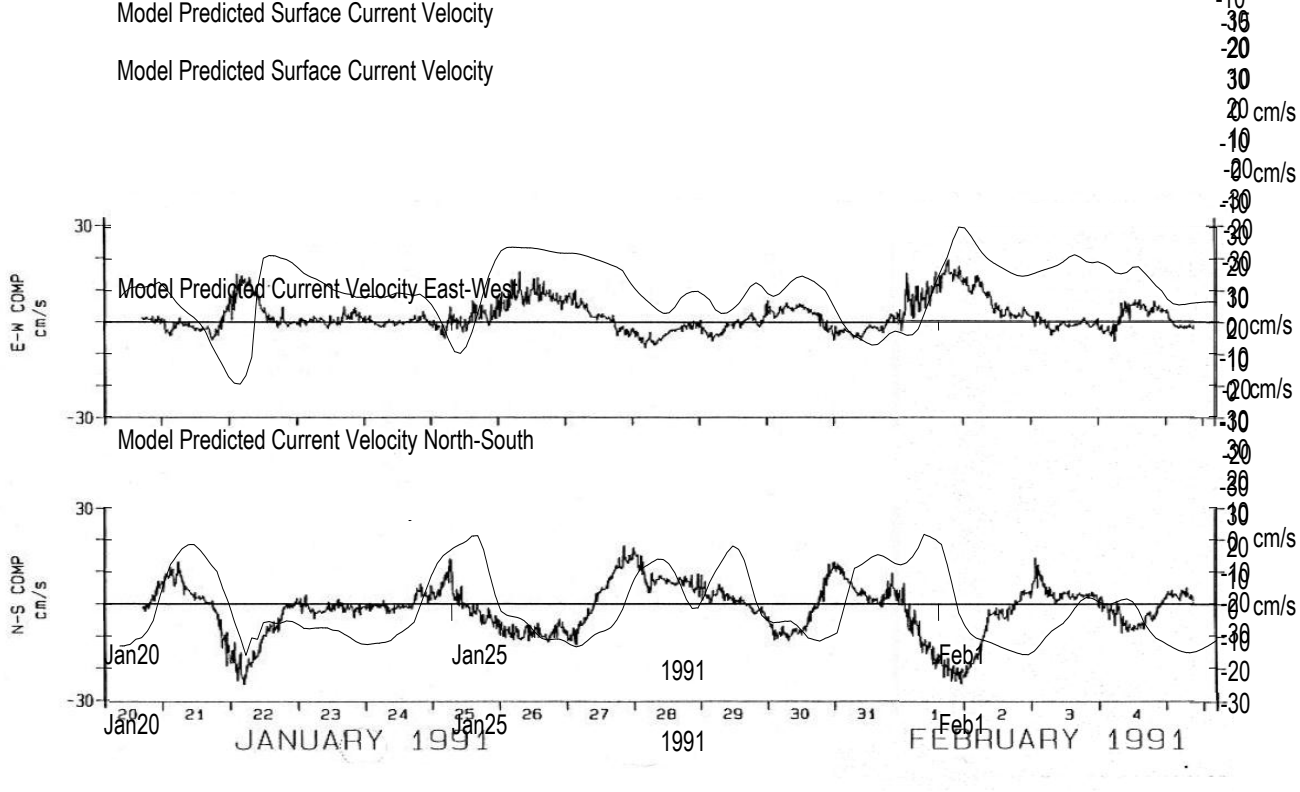

Figure 2.5-9. Overlay of the model-predicted near-surface current (smooth line) on the measured near-surface currents at the Bull Arm spill site for the period January 20 through February 5.

Note: the agreement between the model-predicted currents and the measured currents at the Bull Arm site show that the model both under-predicts and over-predicts currents at times. Considering the data over a 30-day period (the time frame for the oil spill simulations), the model predicted currents are doing a good job of representing flow at the site. The plots show the magnitude of the east-west and north-south components of the near surface currents.

Other effects on the circulation in Bull Arm and Trinity Bay were not considered significant enough to include in the hydrodynamic model application to the region. The lack of major river flow in the region means that stratification is mainly from solar heating. Such stratification may develop in summer, yet the effect is not significant for accurately simulating the trajectory and fate of surface oil spills. Non-linear effects that may, for example, result in advection of momentum of other effects due to bottom stress are only significant in shallow water. Trinity Bay is generally too deep for these terms to become a dominant feature except near shore where spatial scales are too small to consider. Stokes drift is calculated by the SIMAP model using the wind field specified for the spill simulation. In this case the winds come from the MSC50 time series. Spill simulations were not performed using storm event winds, however, the MSC50 wind hindcast includes storm generated winds in its hindcast data. In addition, bay wide oscillations in the circulation would have too high a frequency for the time scales considered in the oil trajectory modeling.

2.6 Ice Data

Sea ice is formed in the autumn in the Arctic and sub-Arctic regions of the world. The growth rate of sea ice depends on surface temperature, the depth of snow cover, and the heat flux in the underlying water. The formation and development of sea ice follows a progression of stages, but the exact timing of these stages at any location is not the same from year to year

because of subtle differences in climatic conditions. In the Northern Hemisphere during September and October, the air temperature lowers sufficiently to form a thin sheet of ice on the sea. Freezing temperature for average northern ocean salt water of approximately 3.5% salt composition by weight (usually designated 35 parts per thousand) is -1.8ºC (28.8ºF).

The presence of sea ice in Newfoundland and Labrador waters was below normal during the winter of 2009-2010 (CIS, 2010), in fact the total accumulated ice coverage in east Newfoundland waters set a new record low during last year's winter season. Figure 2.6-1 shows the total accumulated ice coverage offshore the Canadian east coast measured by the Canadian Ice Service since the winter of 1968-69. With the exception of the 2002-2003 ice season, ice coverage over the past 15 years has been below the 40 year average.

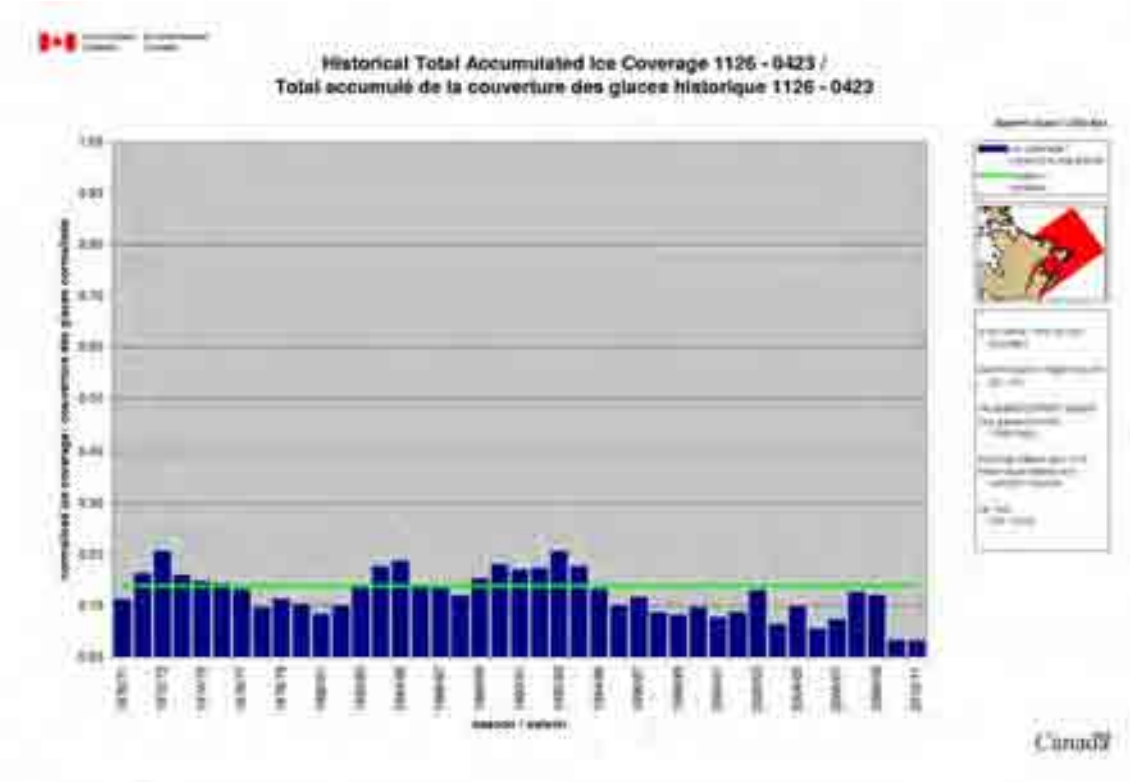

Figure 2.6-1. Total accumulated ice coverage for the period of record from the Canadian Ice Service.

Ice coverage in the winter of 1989-1990 was at a maximum extent according to the data collected by the Canadian Ice Service. Figure 2.6-2 shows a map of ice concentration in the Newfoundland region for the week of March 12, 1990. The red areas on the map in Figure 2.6-2 show that 100% ice concentration covers portions of the offshore area east of Newfoundland as well as the southern half of Trinity Bay.

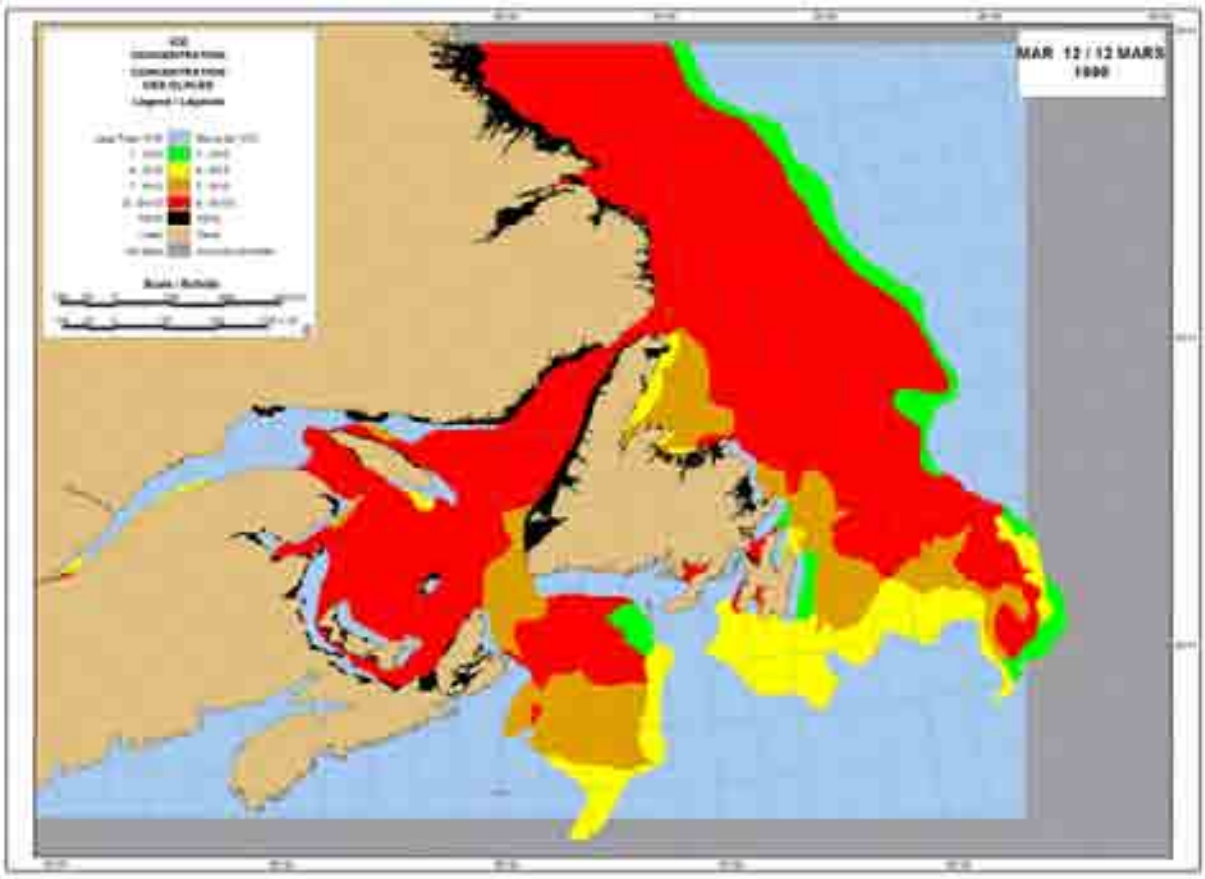

Figure 2.6-2. Ice concentration chart form the Canadian Ice Service for the week of 12 March, 1990.

The fate and behavior of spilled oil is greatly affected by the presence of ice. Oil spilled before, during, or after freeze-up will follow an arrested pattern of weathering compared to oil spilled on open water. Implementation of algorithms for modeling the movement and fate of oil in the presence of sea ice is based on the percent of ice coverage. From 0 to 30% coverage the ice has no effect on the advection or weathering of a surface oil slick. From 30 to 80% ice coverage, oil advection is steered to the right in the northern hemisphere, surface oil thickness generally increases due to ice-restricted spreading, and evaporation and entrainment are both reduced. Above 80% ice coverage, surface oil moves with the ice, evaporation and entrainment cease, and oil thickness, which can vary widely, is calculated as a function of ice thickness. Appendix A contains a brief summary of the algorithms implemented in the SIMAP model for oil spills in sea ice conditions.

The SIMAP model algorithms are based on an early (1980s - 1990s) understanding of oil / ice interactions. Since that time various studies (mostly Norwegian) have improved the understanding of oil / ice interactions, but most of that work was focused on developing oil spill response strategies, not oil spill model algorithms.

The impediment to more robust simulation of the interactions of oil in ice is not a lack of understanding of those processes, as much as it is a lack of data to define the characteristics of the ice over small spatial scales (centimeters to tens of meters) and short time periods (hours to days). A review of oil spill models by Reed, et. al. (1999) identified this as the overriding issue holding back realistic modeling of oil in ice:

> *"… the prognosis for improved representation of oil behavior in ice-infested waters remains bleak until our capability to model ice alone improves. … the processes governing oil behavior occur at scales of a few centimeters to a few tens of meters within an ice field. Ice model resolutions are typically at scales of kilometers, to account for effects at active boundaries, such that very crude, ad hoc parameterizations become necessary."*

Ice coverage in Bull Arm can range from 0 to 100% through the winter season depending on the month and the severity of the winter. Vessel operations during the construction of the Hebron GBS will likely not occur when ice concentration exceeds 65% ice coverage. All winter spill scenarios with sea ice present assume that Bull Arm and Trinity Bay are covered with a 65% ice concentration.

2.7 Shoreline Type Data

The SIMAP model utilizes a specification of the shoreline type in order to simulate oil interactions with the shoreline (see the description of these interactions in Appendix A). The shoreline in Bull Arm was defined as one of two types based on information from the Hebron Project Comprehensive Study Report (EMCP, 2010) as depicted on the map in Figure 2.7-1. The beaches in Bull Arm were classified as Gravel Beach and the remainder of the shoreline was classified as Seaward Rocky Shore. The Eelgrass beds are subtidal habitats and not considered a shoreline type with oil holding capacity. Table 2.7-1 lists the shoreline width, maximum oil thickness and oil removal half-times used in the oil spill modeling.

TABLE 2.7-1 SHORELINE WIDTH, MAXIMUM SHORELINE OIL THICKNESS AND REMOVAL HALF-LIFE TIMES FOR VARIOUS SHORE TYPES (BASED ON GUNDLACH, 1987).

Shore Type	Width (m)	Maximum Oil Thickness (mm)	Oil Removal Half-time (days)
Exposed Rocky Shore	3	0.5	1
Gravel Beach (Capelin Beach)	6	2	10

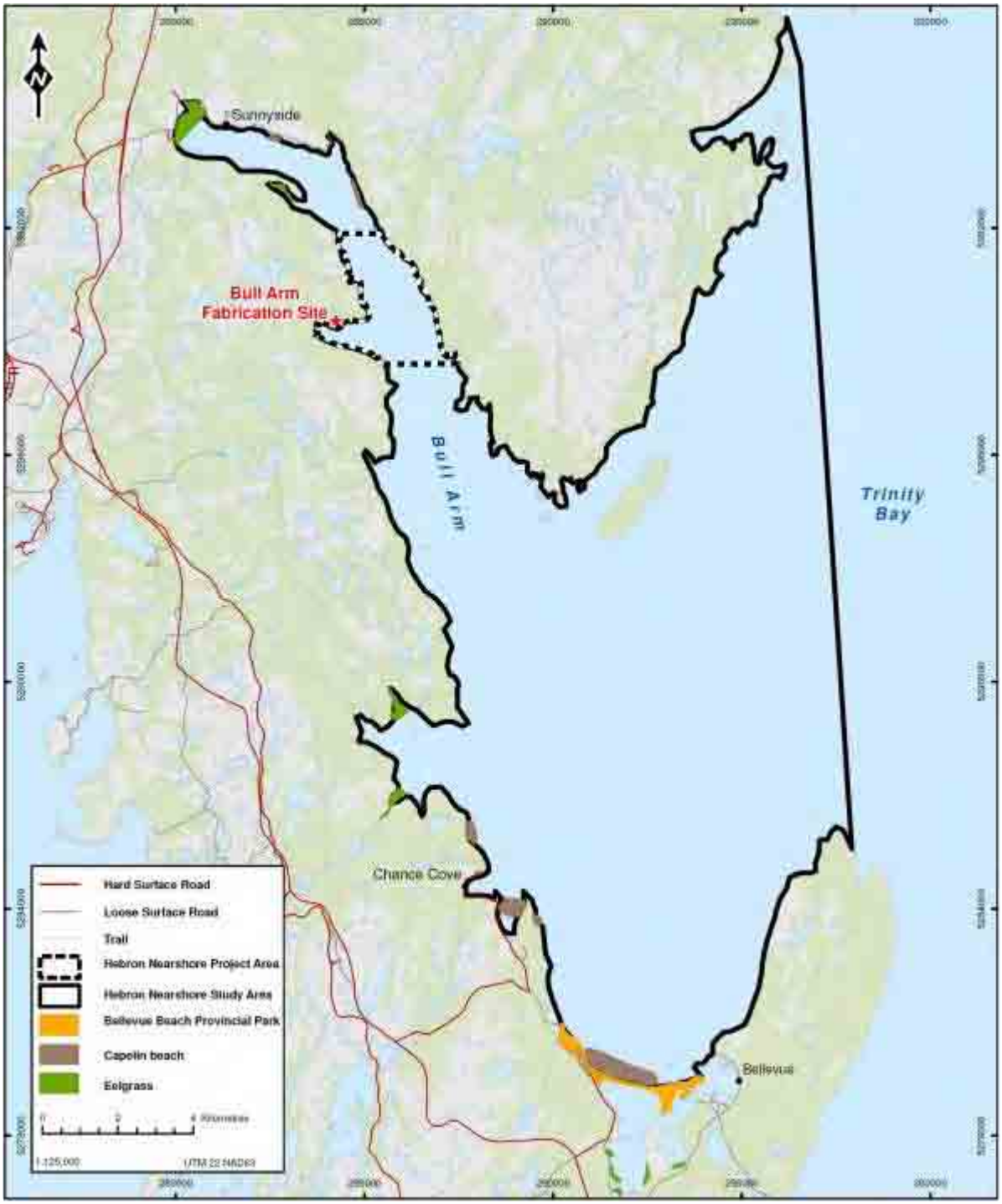

Figure 2.7-1. Bull Arm shoreline type classifications used in the oil spill modeling. (EMCP 2010)

3. Modeling Description

3.1 Surface Releases of Fuel Oils in Bull Arm

Spills of marine diesel and intermediate fuel oil at the near shore site in Bull Arm were modeled using the SIMAP stochastic and deterministic (3D fates) models (Figure 3.1-1 shows the Trinity Bay region with names of local features included). Instantaneous releases of 100 m^3 of marine diesel and 1,000 m^3 of IFO-180 at the Bull Arm site were simulated under summer environmental conditions and winter conditions with and without sea ice present.

Summer and winter seasons were selected because they exhibit winds with different distinct patterns. Summer winds are predominately form the southwest while winter winds are of higher speed and come most frequently from the west. These two wind regimes represent end members of speed and direction, while the spring and fall winds represent transitions between them. It is not necessary to simulate spills occurring spring and fall because those results would be contained within the summer and winter predictions for oil trajectory and fate.

Figure 3.1-1. Map showing Study Area with Bull Arm spill site

To determine risks of various resources being oiled, multiple model runs using a range of environmental conditions were evaluated. The Monte Carlo method implemented in the SIMAP stochastic model was used to characterize the potential consequences, in terms of surface and shoreline oiling, of spills occurring at the near shore site in summer and winter seasons. Each stochastic oil spill scenario included an ensemble of 100 individual simulations, with each run

using a randomly varied spill date and time, so that environmental conditions (currents and winds) were varied within the possible range found in the region.

In order to ensure that the 100 model runs sufficiently sample the range of wind speeds and directions found at the Bull Arm site for a season of interest, a comparison of the wind rose from the long term record for that season was compared to the wind rose of the 100 SIMAP simulations for that season, where similar wind roses indicate that the sample size adequately captured the long term wind speed and direction variability. A demonstration of this evaluation is provided for both summer and winter seasons. Figures 3.1-2 and 3.1-3 are plots of the wind rose comparisons for summer and winter. As can be seen, the comparisons show clearly that the wind data are adequately sampled by the oil spill model and the resulting oil trajectories should be representative of the possible spill pathways.

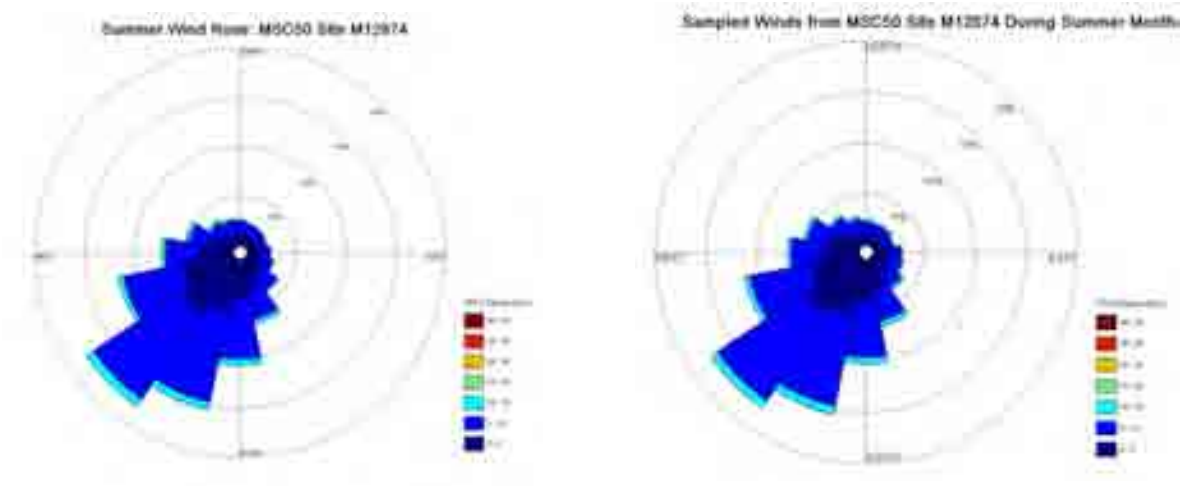

Figure 3.1-2 Rose diagram of all summer winds from MSC50 site 12874 (left plot) compared to wind sampled by the SIMAP model for the summer season spill simulations.

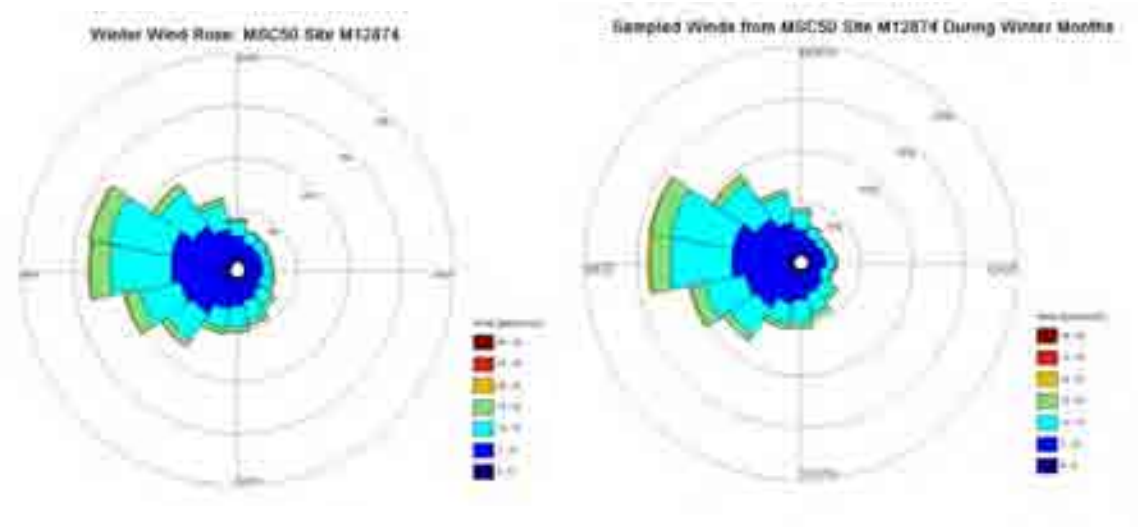

Figure 3.1-3 Rose diagram of all winter winds from MSC50 site 12874 (left plot) compared to wind sampled by the SIMAP model for the winter season spill simulations.

The stochastic analysis provides two types of information to describe the potential spills:

1) areas that might be oiled (as defined by a threshold oil thickness of 0.01mm) and their associated probability of oiling, and
2) the shortest time required for oil to reach any location and/or threshold in the areas predicted to be oiled.

This information is presented for surface oil, shoreline oil, and subsurface oil in maps in Appendix B and in summary tables in subsequent sections of this report. Total hydrocarbons, the group of chemicals that make up crude oil, are divided into two categories, aromatic hydrocarbons, the toxic component of oil, and aliphatic hydrocarbons. For this study only the non-dissolved total hydrocarbons are tracked.

SIMAP's stochastic simulation results provide insight into the probable behavior of potential oil spills under the environmental conditions expected to occur in the Study Area during each season. The 100 individual model simulations from each stochastic model scenario were ranked to determine the individual spill resulting in the 95th percentile for shoreline oiling, water surface oiling and for oil entrained in the water column. For example, the 95th percentile spill for surface oiling is the single spill resulting in a surface area oiled at a thickness exceeding 0.01 mm that is greater than or equal to 95% of all spills simulated. The 95th percentile spills are identified by selecting the individual spill that ranks as the 95th percentile for:

1. Shoreline oiling - shoreline area oiled with an average thickness > 0.01 mm
2. Water surface oiling – surface area oiled by > 0.01 mm thickness
3. Entrained oil - subsurface oil concentration > 10ppb remaining at the end of the simulation

The deterministic trajectory and fate simulations using the 3D fates model were performed for the 95th percentile spills identified in each stochastic analysis as defined above. The spill

scenarios listed in Table 3.1-1 summarize the 95th percentile spills based on the criteria above for surface oiling, shoreline contact and entrained oil amounts.

Results from the 18 simulations (three oil threshold criteria times 6 spill scenarios) listed in Table 3.1-1 provide a time history of oil weathering over the duration of the spill, expressed as the volume of spilled oil on the water surface, on the shore, evaporated, entrained in the water column, and decayed. These results are presented in detail in section 4.

TABLE 3.1-1. SPILLS OF MARINE DIESEL AND INTERMEDIATE FUEL OIL RELEASED AT THE BULL ARM SITE MODELED USING THE 3D FATES MODEL.

Oil Release	95thPercentile for:	Season	Scenario
100 m^3 Marine Diesel	Sea Surface Oiling	Summer	1
		Winter - No Ice	2
		Winter - 65% Ice	3
	Shoreline Oiling	Summer	4
		Winter - No Ice	5
		Winter - 65% Ice	6
	Entrained Oil	Summer	7
		Winter - No Ice	8
		Winter - 65% Ice	9
1,000 m^3 IFO 180	Sea Surface Oiling	Summer	10
		Winter - No Ice	11
		Winter - 65% Ice	12
	Shoreline Oiling	Summer	13
		Winter - No Ice	14
		Winter - 65% Ice	15
	Entrained Oil	Summer	16
		Winter - No Ice	17
		Winter - 65% Ice	18

4. Model Results

Results of the stochastic modeling are presented first, followed by the 3D fates deterministic model results.

4.1 Stochastic Model Results

The stochastic model was used to determine the probability of oiling the water surface, the shoreline and the water column based on specified thickness and concentration thresholds. The thresholds used for the stochastic model simulations in this study are as follows:

- Surface oil average thickness > 0.01 mm (10 µm)
- Shoreline oil average thickness > 0.01 mm (10 µm)
- Subsurface oil (entrained in water) average concentration> 10 ppb

The 0.01 mm (10 micron) surface oil thickness was selected because it is sufficient to provide a lethal dose to seabirds provided they move through the slick a minimum distance (French-McCay, 2009). Smaller surface oil thicknesses that may result in a sub-lethal dose to seabirds were not considered. French-McCay (2009) provides a summary of recent work and discusses the details of wildlife oiling from surface slicks.

Maps of the stochastic model results are contained in Appendix B. The maps show the predicted probability of oiling. The summer maps are shown first followed by the winter season results.

Summary of Stochastic Model Results

Table 4.1-1 summarizes the results from the Bull Arm stochastic modeling. Table 4.1-1 lists the results from the stochastic model simulations for oiled sea surface area, oiled shoreline length and entrained oil volume for the individual spill ranked as the 95th percentile. The 95th percentile results correspond to the maps of the deterministic model results shown in Appendix C.

TABLE 4.1-1. SUMMARY OF SURFACE OILING FROM THE STOCHASTIC SIMULATIONS OF MARINE DIESEL AND INTERMEDIATE FUEL OIL RELEASED AT THE BULL ARM SITE. VALUES IN THE TABLE ARE FROM THE INDIVIDUAL SPILL RANKED AS THE 95TH PERCENTILE IN EACH CATEGORY.

Oil Release	Season	Surface Area Oiled at >0.01 mm (km^2)	Shoreline Oiled at >0.01 mm (km)	Entrained Oil Volume after 30 days (m^3)
100 m^3 Marine Diesel	Summer	581.4	19.8	58.6
	Winter	371.2	10.1	65.3
1,000 m^3 IFO-180	Summer	1524.8	144.3	.017
	Winter	1670.5	137.5	.024

Summer winds are more often from the southwest which drives oil onto the northeast coast of Bull Arm. Any oil exiting Bull Arm in the summer is driven northeastward up Trinity Bay. Winter winds are most often from the northwest which moves surface oil out of Bull Arm and onto the shoreline at the southern end of Trinity Bay and less frequently towards the northeast and the mouth of Trinity Bay.

The smaller volume 100 m^3 marine diesel spills are predicted to have a 10-20% probability of leaving Bull Arm during the summer and a 30-40% probability of leaving Bull Arm under winter conditions. Spills of 1,000 m^3 of IFO-180 have a 60-70% probability of leaving Bull Arm during the summer, and a 70-80% probability of entering Trinity Bay during the winter season.

The model predicts that oil from both the 100 m^3 marine diesel and 1,000 m^3 IFO-180 spills have a small (<5%) probability of leaving Trinity Bay. Some of the surface oil probability maps in Appendix B show oil exiting the northeast corner of the model grid. This oil is >10 days old, the volatile components have evaporated, the oil is at the minimum thickness and moving into open ocean.

Spills of 100 m^3 of marine diesel have a 60% chance of hitting the Bull Arm shoreline in summer, and 30% probability to do so in the winter season. IFO-180 spills of 1,000 m^3 have a 100% chance of impacting the Bull Arm shoreline in the summer and a 90% chance during the winter season.

Entrained marine diesel oil from a 100 m^3 spill is predicted to exceed a concentration of 10 ppb 100% of the time within Bull Arm during the summer and winter seasons. Probabilities drop quickly outside of Bull Arm to 10-30% during summer and winter seasons for a small area of southwest Trinity Bay. IFO 180 is a highly viscous fuel that shows almost no entrainment into the water column for spills of 1000 m^3.

4.2 Deterministic Model Results

Maps of the deterministic model results are contained in Appendix C. Each map in Appendix C depicts the results from one model simulation chosen from the 100 individual simulations completed by the stochastic model. The simulations were selected because they result in the 95^{th} percentile for sea surface oiling area, shoreline oiling length or entrained oil volume. It should be kept in mind that each map in Appendix C displays the results from a different individual simulation and depict one possible outcome for a spill at the Bull Arm site.

The maps appear in Appendix C in the following order: surface oil, shoreline oil and entrained oil. Each map is followed by a mass balance graph depicting the volume of oil present on the surface, evaporated to the atmosphere, entrained in the water column, stranded on the shoreline and decayed by natural processes.

Summary of Deterministic Model Results

Table 4.2-1 lists the mass balance results for all of the deterministic spill scenarios at the end of the 30-day simulation. The table lists oil volumes in cubic meters.

TABLE 4.2-1. SUMMARY OF DETERMINISTIC MODEL MASS BALANCE AT THE END OF THE 30-DAY SIMULATIONS.

Oil Release	95th Percentile for:	Season	Surface Oil (m^3)	Evaporated Oil (m^3)	Entrained Oil (m^3)	Oil Ashore (m^3)	Decayed Oil (m^3)
100 m^3 Marine Diesel	Sea Surface Oiling	Summer	0	52	19	16	13
		Winter - No Ice	0	13	65	0	22
		Winter - Ice	0	49	0	44	7
	Shoreline Oiling	Summer	0	56	18	14	12
		Winter - No Ice	0	25	46	10	19
		Winter - Ice	0	50	1	42	7
	Entrained Oil	Summer	0	18	59	2	21
		Winter - No Ice	0	11	66	1	22
		Winter - Ice	0	51	0	43	6
1,000 m^3 IFO 180	Sea Surface Oiling	Summer*	30	170	0	420	220
		Winter - No Ice*	20	160	0	510	210
		Winter - Ice	0	160	0	680	160
	Shoreline Oiling	Summer	0	170	0	610	220
		Winter - No Ice*	0	160	0	610	220
		Winter - Ice	0	170	0	690	140
	Entrained Oil	Summer*	0	155	0	475	200
		Winter - No Ice	25	155	0	570	210
		Winter - Ice	80	170	0	580	170

Spills of 100 m^3 of marine diesel oil representing the 95th percentile for surface oiling are predicted to remain entirely within Trinity Bay during the winter and to result in small amounts of weathered oil leaving the Bay during summer. In the winter season, roughly 12% of the oil is predicted to evaporate by the end of the 30-day simulation; more than 50% of the diesel fuel is predicted to evaporate in the summer season spill. The difference in evaporation is due to higher winter wind speeds which entrain more oil in the water column making it unavailable for evaporation.

Spills of 100 m^3 of marine diesel oil representing the 95th percentile for shoreline oiling are predicted to impact up to 75% of the Bull Arm shoreline and isolated segments of the Trinity Bay shoreline in both the summer and winter seasons.

Spills of 100 m^3 of marine diesel oil representing the 95th percentile for entrained oil are predicted to exceed the 10 ppb concentration threshold for all of Bull Arm and for an area of southwest Trinity Bay in both the summer and winter seasons.

The presence of 65% ice cover reduces the sea surface area covered by marine diesel oil but results in more widespread shoreline impacts. Ice cover significantly reduces the area predicted to exceed the entrained oil concentration of 10ppb.

Spills of 1,000 m^3 of IFO-180 representing the 95th percentile for surface oiling are predicted to oil Bull Arm and extend the length of Trinity Bay during the summer and winter seasons. Roughly 16% of the IFO-180 is predicted to evaporate by the end of the 30-day simulation during both the summer and winter seasons. The IFO-180 is highly viscous which limits its entrainment and enhances conditions for evaporation.

Spills of 1,000 m^3 of IFO-180 representing the 95th percentile for shoreline oiling are predicted to impact much of the Bull Arm shoreline and segments of the Trinity Bay shoreline in both the summer and winter seasons. The summer shoreline oiling is restricted to the east and west shorelines in the southern half of Trinity Bay. Winter season shoreline oiling is predicted to affect primarily the east coast of Trinity Bay.

Spills of 1,000 m^3 of IFO-180 representing the 95th percentile for entrained oil are predicted to exceed the 10ppb concentration threshold for small areas of Bull Arm close to the release site. The IFO-180 is highly viscous and does not readily entrain.

The presence of 65% ice cover reduces the sea surface area covered by IFO-180 and does not significantly change shoreline impacts compared with the no-ice condition. The presence of 65% ice cover is predicted to eliminate any entrained oil concentrations greater than 10 ppb.

6. References

AMEC, 2010.Spill Trajectory Modeling for the Hebron Project, Prepared by AMEC Earth and Environmental, AMEC Americas Ltd. April 2010, 99 pages.

ASCE Task Committee on Modeling Oil Spills, 1996. State-of-the-art Review of Modeling Transport and Fate of Oil Spills, Water Resources Engineering Division, ASCE, Journal of Hydraulic Engineering 122(11): 594-609.

Becker,J., D. T. Sandwell, 2008, "SRTM30_PLUS: Data fusion of SRTM land topography with measured and estimated seafloor topography",SRTM30_PLUS V4.0 May 20, 2008

Boyer, T., S. Levitus, H. Garcia, R. A. Locarnini, C. Stephens, and J. Antonov, 2004 Objective Analyses of Annual, Seasonal, and Monthly Temperature and Salinity for the World Ocean on a ¼ E Grid, Submitted to International Journal of Climatology April 16, 2004, Ocean Climate Laboratory, National Oceanographic Data Center, Silver Spring, Maryland

Bishnoi, P. R. and Mainik B. B., 1979.Laboratory study of behaviour of oil and gas particles in salt water, relating to deepwater blowouts, Spill Technology Newsletter, Vol. 4 (1), pp. 24-36.

Bishnoi, P. R., Gupta, A. K., Englezos, P., Kalogerakis, N., 1989. Fluid Phase Equilibria, 83, 97.

Bleck, R., 1998: Ocean modeling in isopycnic coordinates. Chapter 18 in Ocean Modeling and Parameterization, E. P. Chassignet and J. Verron, Eds., NATO Science Series C: Mathematical and Physical Sciences, Vol. 516, Kluwer Academic Publishers, 4223-448.

Bleck, R., 2002: An oceanic general circulation model framed in hybrid isopycnic-Cartesian coordinates. *Ocean Modeling*, 4, 55-88.

Boyer, T., S. Levitus, H. Garcia, R. A. Locarnini, C. Stephens, and J. Antonov, 2004 Objective Analyses of Annual, Seasonal, and Monthly Temperature and Salinity for the World Ocean on a ¼ E Grid, Submitted to International Journal of Climatology April 16, 2004, Ocean Climate Laboratory, National Oceanographic Data Center, Silver Spring, Maryland.

Canadian Ice Service, 2010: Seasonal Summary for Eastern Canada, Winter 2009-2010. Produced by the Canadian Ice Service, July, 2010.

Chassignet, E. P., L. T. Smith, R. Bleck, and F. O. Bryan, 1996: A model comparison: numerical simulations of the North and Equatorial Atlantic oceanic circulation in depth and isopycnic coordinates. J. Phys. Oceanogr., 26, 1849-1867.

Egbert, G.D., Bennett, A.F., and M.G.G. Foreman (1994), TOPEX/POSEIDON tides estimated using a global inverse model, J. Geophysical Research, 99, 24821-24852.

Environmental Technology Centre, Environment Canada, 2004. Spills Technology Databases. Oil Properties database. http://www.etc-cte.ec.gc.ca/databases/OilProperties/Default.aspx

French, D., M. Reed, K. Jayko, S. Feng, H. Rines, S. Pavignano, T. Isaji, S. Puckett, A. Keller, F. W. French III, D. Gifford, J. McCue, G. Brown, E. MacDonald, J. Quirk, S. Natzke, R. Bishop, M. Welsh, M. Phillips and B.S. Ingram, 1996a. The CERCLA type A natural

resource damage assessment model for coastal and marine environments (NRDAM/CME), Technical Documentation, Vol. I - Model Description. Final Report, submitted to the Office of Environmental Policy and Compliance, U.S. Dept. of the Interior, Washington, DC, April, 1996, Contract No. 14-0001-91-C-11.

French, D., M. Reed, S. Feng and S. Pavignano, 1996b. The CERCLA type A natural resource damage assessment model for coastal and marine environments (NRDAM/CME), Technical Documentation, Vol. III - Chemical and Environmental Databases. Final Report , Submitted to the Office of Environmental Policy and Compliance, U.S. Dept. of the Interior, Washington, DC, April, 1996, Contract No. 14-01-0001-91-C-11.

Gundlach, E.R., 1987. Oil Holding Capacities and Removal Coefficients for Different Shoreline Types to Computer Simulate Spills in Coastal Waters, in Proceedings of the1987 Oil Spill conference, pp. 451-457.

Halliwell, G. R., Jr., 1997: Simulation of decadal/interdecadal variability the North Atlantic driven by the anomalous wind field. Proceedings, Seventh Conference on Climate Variations, Long Beach, CA, 97-102.

Halliwell, G. R., Jr., 1998: Simulation of North Atlantic decadal/multi-decadal winter SST anomalies driven by basin-scale atmospheric circulation anomalies. Journal of Physical Oceanography, 28, 5-21.

Halliwell, G. R., Jr., R. Bleck, and E. Chassignet, 1998: Atlantic Ocean simulations performed using a new hybrid-coordinate ocean model. EOS, Fall 1998 AGU Meeting.

Halliwell, G .R, R. Bleck, E. P. Chassignet, and L.T. Smith, 2000: mixed layer model validation in Atlantic Ocean simulations using the Hybrid Coordinate Ocean Model (HYCOM). EOS, 80, OS304.

Hu, D., 1996: On the Sensitivity of Thermocline Depth and Meridional Heat Transport to Vertical Diffusivity in OGCMs. J. Physical Oceanography, 26, 1480-1494.

IOC, IHO and BODC (GEBCO) 2003. Centenary Edition of the GEBCO Digital Atlas, published on behalf of the Intergovernmental Oceanographic Commission (IOC) and the International Hydrographic Organization (IHO) as part of the General Bathymetric Chart of the Oceans; British Oceanographic Data Centre (BODC), Liverpool.

Isaji T., E. Howlett, C. Dalton, and E. Anderson, 2001: “Stepwise -Continuous-Variable-Rectangular Grid Hydrodynamics Model”, in Proceedings of the Twenty-fourth Arctic and Marine Oil Spill Program (AMOP) Technical Seminar, Edmonton (Alberta) Canada, pp. 597-610, June 12, 2001

Kullenberg, G. (ed.), 1982. Pollutant transfer and transport in the sea. Volume I. CRC Press, Boca Raton, Florida. 227 p.

Lefebvre, A. H., 1989, Atomization and Sprays, Hemisphere Publishing Corp., New York.

Marsh, R., M. J. Roberts, R. A. Wood, and A. L. New, 1996: An intercomparison of a Bryan-Cox-type ocean model and an isopycnic ocean model, part II: the subtropical gyre and meridional heat transport. J. Phys. Oceanogr., 26, 1528-1551.

McAuliffe, C.D., 1987. Organism exposure to volatile/soluble hydrocarbons from crude oil spills – a field and laboratory comparison. Proceedings of the 1987 Oil Spill Conference, API, p. 275-288.

McDougall, T.J., 1978. Bubble plumes in stratified environments, Journal of Fluid Mechanics, Vol. 85, Part 4, pp. 655-672.

Nafaa, M.G. and O.E. Frihy, 1993. Beach and Nearshore Features Along the Dissipative Coastline of the Nile Delta, Egypt. Journal of Coastal Research, Vol. 9, No. 2 (Spring, 1993), pp. 423-433

National Research Council (NRC), 1985. Oil in the Sea: Inputs, Fates and Effects, National Academy Press, Washington, D.C. 601p.

New, A. and R. Bleck, 1995: An isopycnic model of the North Atlantic, Part II: interdecadal variability of the subtropical gyre. J. Phys. Oceanogr., 25, 2700-2714.

New, A., R. Bleck, Y. Jia, R. Marsh, M. Huddleston, and S. Barnard, 1995: An isopycnic model of the North Atlantic, Part I: model experiments. J. Phys. Oceanogr., 25, 2667-2699.

Okubo, A. 1971. Oceanic diffusion diagrams. Deep-Sea Research 8:789-802.

Okubo, A. and R.V. Ozmidov, 1970. Empirical dependence of the coefficient of horizontal turbulent diffusion in the ocean on the scale of the phenomenon in question atmospheric and ocean physics 6(5):534-536.

Reed, M., et. al., 1999. Oil Spill Modeling Towards the Close of the 20th Century: Overview of the State of the Art. Spill Science and Technology Bulletin, Volume 5, Number 1, pages 3-16.

Roberts, M. J., R. Marsh, A. L. New, and R. A. Wood, 1996: An intercomparison of a Bryan-Cox-type ocean model and an isopycnic ocean model, part I: the subpolar gyre and high latitude processes. J. Phys. Oceanogr., 26, 1495-1527.

Rye, H., Johansen, O., and Kolderup, H. 1998. Drop size formation from deep water blowouts.' *SINTEF Report.*

Seaconsult,1991.*Data Report: Current, Tide and Weather Data Collected in Bull Arm Between January 10 and March 19, 1991*. Prepared for Newfoundland Offshore Development Constructors (NODECO).

Statoil Memo, " ElDabaa Field – Monthly metocean data", Martin Mathiesen, Polytec Foundation, 9 July 2010.

Swail, V.R., Cardone, V.J., Ferguson, M., Gummer, D.J., Harris, E.L., Orelup, E.A. and A.T. Cox.2006: The MSC50 Wind and Wave Hindcast Reanalysis, Ninth International Workshop on Wave Hindcasting and Forecasting, September 25-29, 2006. Victoria, B.C., Canada.

VLIZ (2009). Maritime Boundaries Geodatabase, version 5. Available online at http://www.vliz.be/vmdcdata/marbound. Consulted on 2010-10

Appendix A: SIMAP Model Description

This appendix provides a discussion of the SIMAP model and its important oil fates model algorithms. It is intended to supplement information provided in the spill modeling technical report and help the reader understand the application of the model to the spill simulations performed. It includes an extensive reference list for oil spill modeling in general and a supplementary list of model application and validation study references.

SIMAP includes (1) an oil physical fates model, (2) interfacing to a hydrodynamics model for simulation of currents, (3) a biological effects model, (4) an oil physical, chemical and toxicological database, (5) environmental databases (winds, currents, salinity, temperature), (6) geographical data (in a GIS), (7) a biological database, (8) a response module to analyze effects of response activities, (9) graphical visualization tools for outputs, and (10) exporting tools to produce text format output.

SIMAP originated from the oil fates and biological effects sub-models in the Natural Resource Damage Assessment Model for Coastal and Marine Environments (NRDAM/CME), which ASA developed in the early 1990s for the US Department of the Interior for use in Natural Resource Damage Assessment (NRDA) regulations under the Comprehensive Environmental Response, Compensation and Liability Act of 1980 (CERCLA). The NRDAM/CME (Version 2.4, April 1996) was published as part of the CERCLA type A NRDA Final Rule (Federal Register, May 7, 1996, Vol. 61, No. 89, p. 20559-20614). The technical documentation for the NRDAM/CME is in French et al. (1996a,b,c). This technical development involved several in-depth peer reviews, as described in the Final Rule.

While the NRDAM/CME was developed for simplified natural resource damage assessments of small spills in the United States, SIMAP is designed to evaluate fates and effects of both real and hypothetical spills in marine, estuarine and freshwater environments worldwide. SIMAP may be run in stochastic mode to evaluate a distribution of spill results, rather than just a single result for a specific hind-cast. Additions and modifications to prepare SIMAP were made to increase model resolution, allow modification and site-specificity of input data, allow incorporation of temporally varying current data, evaluate subsurface releases and movements of subsurface oil, track multiple chemical components of the oil, enable stochastic modeling, and facilitate analysis of results. The consideration of the impacts of subsurface oil is important, particularly in the evaluation of impacts on aquatic organisms. Surface floating oil primarily impacts wildlife and intertidal biota, and not aquatic biota in subtidal habitats. At higher wind speeds than about 12 knots (or at lower wind speeds if dispersant is applied), oil will entrain into the water column, unless it has become too viscous to do so after weathering and the formation of mousse. Once oil is entrained in the water in the form of small droplets, monoaromatics (MAHs) and polynuclear aromatic hydrocarbons (PAHs) dissolve into the water column. The dissolved MAHs and PAHs are the most bioavailable and toxic portion of the oil. The dissolution rate is very sensitive to the droplet size (because it involves mass transfer across the surface area of the droplet), and the amount of hydrocarbon mass dissolved is a function of the mass entrained and droplet size distribution. These are in turn a function of soluble hydrocarbon content of the oil, the amount of evaporation of these components before

entrainment, oil viscosity (which increases as the oil weathers and emulsifies), oil surface tension (which may be reduced by surfactant dispersants), and the energy in the system (the higher the energy the smaller the droplets). Large droplets (greater than a few hundred microns in diameter) resurface rapidly, and so dissolution from those is also inconsequential. Dispersant application facilitates the entrainment of oil into the water in a smaller size distribution than would occur naturally, with the median droplet size about 20 m (Lunel, 1993a,b).

Thus, the fate of MAHs and PAHs in surface oil is primarily volatilization to the atmosphere, rather than to the water. If wind speeds exceed 12 knots, entrainment of the surface oil into the water becomes significant. Dispersant application can also facilitate entrainment into the water column. If oil is entrained before it has weathered and lost the lower molecular weight aromatics to the atmosphere, dissolved MAHs and PAHs in the water can reach concentrations where they can affect water column organisms or bottom communities (French McCay and Payne, 2001).

Below is a brief description of the physical fates model implemented in SIMAP. Detailed descriptions of the algorithms and assumptions in the model are in published papers (French McCay 2002, 2003, 2004). The model has been validated with more than 20 case histories, including the Exxon Valdez and other large spills (French and Rines, 1997; French McCay, 2003, 2004; French McCay and Rowe, 2004) as well as test spills designed to verify the model (French et al., 1997).

The three dimensional physical fates model estimates distribution (as mass and concentrations) of whole oil and oil components on the water surface, on shorelines, in the water column, and in sediments. Oil fate processes included are spreading (gravitational and by shearing), evaporation, transport, randomized dispersion, emulsification, entrainment (natural and facilitated by dispersant), dissolution, volatilization of dissolved hydrocarbons from the surface water, adherence of oil droplets to suspended sediments, adsorption of soluble and semi-soluble aromatics to suspended sediments, sedimentation, and degradation.

Oil is a mixture of hydrocarbons of varying physical, chemical, and toxicological characteristics. Thus, oil hydrocarbons have varying fates and impacts on organisms. In the model, oil is represented by component categories, and the fate of each tracked separately. The “pseudo-component” approach (Payne et al., 1984, 1987; French et al., 1996a; Jones 1997; Lehr et al. 2000) is used, where chemicals in the oil mixture are grouped by physical-chemical properties, and the resulting component category behaves as if it were a single chemical with characteristics typical of the chemical group.

SIMAP fates model focuses on tracking the lower molecular weight aromatic components divided into chemical groups based on volatility, solubility, and hydrophobicity. In the model, the oil is treated as eight components (defined in Table A-1). Six of the components (all but the two non-volatile residual components) evaporate at rates specific to the pseudo-component. Solubility is strongly correlated with volatility, and the solubility of aromatics is higher than aliphatics of the same volatility, with the MAHs the most soluble, the 2-ring PAHs semi-soluble, and the 3-ring PAHs slightly soluble Mackay et al. (1992a,b,c,d). Both the solubility and toxicity of the non-aromatic hydrocarbons are much less than for the aromatics and dissolution (and

water concentrations) of non-aromatics is safely ignored. Thus, dissolved concentrations are calculated only for each of the three soluble aromatic pseudo-components.

TABLE A-1. DEFINITION OF FOUR DISTILLATION CUTS AND THE EIGHT PSEUDO-COMPONENTS IN THE MODEL (MONOAROMATIC HYDROCARBONS, MAHS; BENZENE + TOLUENE + ETHYBENZENE + XYLENE, BTEX; POLYNUCLEAR AROMATIC HYDROCARBONS, PAHS).

Characteristic	Volatile and Highly Soluble	Semi-volatile and Soluble	Low Volatility and Slightly Soluble	Residual (non-volatile and insoluble)
Distillation cut	1	2	3	4
Boiling Point (^{o}C)	< 180	180 - 265	265 - 380	>380
Molecular Weight	50 - 125	125 - 168	152 - 215	> 215
Log(K_{ow})	2.1-3.7	3.7-4.4	3.9-5.6	>5.6
Aliphatic pseudo-components: Number of Carbons	volatile aliphatics: C4 – C10	semi-volatile aliphatics: C10 – C15	low-volatility aliphatics: C15 – C20	non-volatile aliphatics: > C20
Aromatic pseudo-component name: included compounds	MAHs: BTEX, MAHs to C3-benzenes	2 ring PAHs: C4-benzenes, naphthalene, C1-, C2-naphthalenes	3 ring PAHs: C3-, C4-naphthalenes, 3-4 ring PAHs with log(K_{ow}) < 5.6	$\geq$4 ring aromatics: PAHs with log(K_{ow}) > 5.6 (insoluble)

This number of components provides sufficient accuracy for the evaporation and dissolution calculations, particularly given the time frame (minutes) over which dissolution occurs from small droplets and the rapid resurfacing of large droplets (see discussion above). The alternative of treating oil as a single compound with empirically-derived rates (e.g., Mackay et al, 1980; Stiver and Mackay, 1984) does not provide sufficient accuracy for impact analyses because the impacts to water column organisms are caused by MAHs and PAHs, which have specific properties that differ from the other volatile and soluble compounds. Use of more pseudo components does not improve accuracy, as the major constituents of concern are well characterized (sufficiently similar in properties within the pseudo-component group of chemicals) by the modeled component properties used in SIMAP. The model has been validated both in predicting dissolved concentrations and resulting toxic effects, supporting the adequacy of the use of this number of pseudo-components (French McCay, 2003).

The lower molecular weight aromatics dissolve from the whole oil and are partitioned in the water column and sediments according to equilibrium partitioning theory (French et al., 1996a; French McCay 2004). The residual fractions in the model are composed on non-volatile and insoluble compounds that remain in the “whole oil” that spreads, is transported on the water surface, strands on shorelines, and disperses into the water column as oil droplets or remains on the surface as tar balls. This is the fraction that composes black oil, mousse, and sheen.

Lagrangian elements (spillets) are used to simulate the movements of oil components in three dimensions over time. Surface floating oil, subsurface droplets, and dissolved components are tracked in separate spillets. Transport is the sum of advective velocities by currents input to the model, surface wind drift, vertical movement according to buoyancy, and randomized turbulent diffusive velocities in three dimensions. The vertical diffusion coefficient is computed as a function of wind speed in the wave-mixed layer. The horizontal and deeper water vertical diffusion coefficients are model inputs.

The oil (whole and as pseudo-components) separates into different phases or parts of the environment, i.e., surface slicks; emulsified oil (mousse) and tar balls; oil droplets suspended in the water column; dissolved lower molecular weight components (MAHs and PAHs) in the water column; oil droplets adhered and hydrocarbons adsorbed to suspended particulate matter in the water; hydrocarbons on and in the sediments; dissolved MAHs and PAHs in the sediment pore water; and hydrocarbons on and in the shoreline sediments and surfaces. The physical fates model creates output files recording the distribution of a spilled substance in three dimensional space and time. The quantities recorded are:

- area covered by oil and thickness on the water surface ("swept area");
- volumes in the water column at various concentrations of dissolved aromatics;
- volumes in the water column at various concentrations of total hydrocarbons in suspended droplets;
- total hydrocarbon concentrations and dissolved aromatic concentrations in surface sediment;
- lengths and locations of shoreline impacted and volume of oil ashore in each segment.

Important Oil Fates Processes

The following section describes the details of the important processes simulated in the SIMAP model.

Wind Drift

If the wind drift of the surface wave-mixed layer is not included in three-dimensional and time varying current data supplied to the fates model, wind drift is added to the advective particle velocity within the oil fates model. Wind drift for surface slicks may be added as a user-specified, constant percentage of wind speed, with the option of including a drift angle clockwise of the down wind direction. Alternatively, wind drift is calculated in the SIMAP fates model.

The wind drift rate is the ratio of oil drift speed relative to the wind speed. Drift velocities due to a wind, u_{wc} and v_{wc} (m/sec), toward the east and north, respectively, are

$$u_{wc} = C_w u_w$$

$$v_{wc} = C_w v_w$$

where

u_w	-	east component of wind speed (m/sec)
v_w	-	north component of wind speed (m/sec)
C_w	-	drift factor (fraction)

The drift factor, C_w, may be set by the user as a constant (Lange and Hufnerfuss, 1978; Wu, 1980; Samuels et al., 1982), where C_w varies between 2.5 and 4.5%. These are values based on observations. The default value in the model is 3.5%, which may be reset by the user.

The wind drift angle is the angle the oil drifts clockwise (to the right in the northern hemisphere, use negative values for southern hemisphere) of the wind direction. The drift angle may be entered by the user as a constant angle in degrees. The default value is zero. For open waters a small positive value may be appropriate. A mean of 20^o has been observed in several spills in mid-latitudes. The angle increases with latitude.

Oil Degradation

Degradation may occur as the result of photolysis, which is a chemical process energized by ultraviolet light from the sun, and by biological breakdown, termed biodegradation.

Most studies of microbe-hydrocarbon interactions have been carried out under controlled laboratory conditions and results are not always applicable to the marine environment. Several parameters can limit biodegradation including the microbial population, temperature, oil composition, toxicity and state of weathering; and availability of nutrients and dissolved oxygen.

In the SIMAP model, degradation occurs on the surface slick, oil on the shore and the entrained oil and aromatics in the water column. A first order decay algorithm is used.

The degradation rate, $\overset{o}{M}_b$ (g/sec), can be defined as:

$$\overset{o}{M}_b = \frac{dM_{b,i}}{dt} = -K_i M_i$$

i	environmental compartment (water or shoreline surface, water column, and sediments)
$M_{b,I}$	mass of oil lost by degradation from i (g)
M_i	mass of oil subjected to degradation from i (g)
K_i	degradation constant for compartment i (1/day)

Many types of marine organisms ingest, metabolize and utilize oil as a carbon source, producing carbon dioxide and water as by-products. The biodegradable fraction of various

crude oils ranges from 11 to 90% (NRC, 1985, 1989). A typical degradation rate results in the loss of 1% of the available oil mass per day.

Shoreline Interactions

The fate of spilled oil that reaches the shoreline depends on characteristics of the oil, the type of shoreline, and the energy environment (Reed et al., 1986, 1988, 1989; Gundlach, 1987; Reed and Gundlach, 1989; Harper and Harvey-Kelly, 1994; Humphrey, 1994). Even when beached, oil will continue to weather. However, several additional processes become important: reflotation, penetration into the substrate, and retention/transport in the beach-groundwater system. Erosion of oiled substrate from the beach to offshore sediments may also occur. Considerable study of shoreline oiling, fates and removal processes was performed as part of the development of the COZOIL model for the U.S. Minerals Management Service (Reed et al., 1986, 1988, 1989; Gundlach, 1987; Reed and Gundlach, 1989). The shoreline interaction algorithms in SIMAP are based on this model.

The maximum oil holding thickness is a function of oil viscosity and shore type (CSE/ASA/BAT, 1986; Gundlach, 1987). Oil removal from the shoreline is by water penetration and flushing, and by wave erosion. Thus, removal is faster on exposed coasts than sheltered shorelines. Each shoreline cell in the SIMAP model grid has an oil holding capacity based on oil type, shore type, beach slope, beach width (Table A2) and shoreline grid length.

Oil deposition occurs when oil intersects the shore surface. Deposition ceases when the holding capacity for the shore surface is reached. Subsequent oil deposited is not allowed to remain on the shore surface, and is refloated as slicks that continue to move along shore. After stranding permanently, the shoreline oil is removed exponentially with time. The removed oil is returned to the water column on a rising tide (sufficiently high to wet the oiled surface) and offshore winds.

TABLE A2: TYPICAL BEACH WIDTHS BY SHORE TYPE (CERC, 1984; FRENCH ET AL, 1996).

Shore Type	Mean Beach Width (m)				
	East Coast[2]	Gulf of Mexico[3]	California[4]	Pacific NW[5]	Gulf of Alaska[6]
1. Exposed rocky	2	1	2	3	3
2. Wave cut platform	2	1	2	3	3
3. Fine sand	10	5-15	10	15	20
4. Coarse sand	10	5	10	15	20
5. Mixed sand/gravel	5	5	5	7	10
6. Gravel	3	2	3	4	6
7. Exposed tidal flats	10	10	10	15	20
8. Sheltered rocky	2	1	2	3	3
9. Sheltered tidal flats	140	20	120	210	300
10. Sheltered marsh	140	50	120	210	300
11. Glacier edge	-	-	-	-	3
12. Artificial[1]	0.1	0.1	0.1	0.1	0.1

[1] Assumed value for vertical bulkhead

[2] These shore widths, as well as the data in Tables 3-4 and 3-5, are included in the default data file "CME-East_Coast.SHR" supplied with the model.

[3] These shore widths, as well as the data in Tables 3-4 and 3-5, are included in the default data file "CME-Gulf_of_Mexico.SHR" supplied with the model.

[4] These shore widths, as well as the data in Tables 3-4 and 3-5, are included in the default data file "CME-California.SHR" supplied with the model.

[5] These shore widths, as well as the data in Tables 3-4 and 3-5, are included in the default data file "CME-Pacific_NW.SHR" supplied with the model.

[6] These shore widths, as well as the data in Tables 3-4 and 3-5, are included in the default data file "CME-Gulf_of_Alaska.SHR" supplied with the model.

Oil Entrainment

As oil on the sea surface is exposed to wind and waves, it is entrained (and dispersed) into the water column. Entrainment is a physical process where globules of oil are transported from the sea surface into the water column by breaking waves. It has been observed that entrained oil is broken into droplets of varying sizes. Smaller droplets spread and diffuse in the water column, while larger ones rise rapidly back to the surface (Delvigne and Sweeney, 1988; Delvigne, 1991). Breaking waves created by the action of wind and waves on the ocean surface are the primary sources of energy for entrainment, although other sources of turbulence can entrain oil (Delvigne et al., 1994). Entrainment is strongly dependent on turbulence and is greater in areas of high wave energy.

It has been observed that entrained oil is subjected to enhanced dissolution and biodegradation processes. The increased surface area represented by these droplets increases the rates of dissolution and photo-oxidation.

Delvigne and Sweeney (1988), using laboratory and flume experimental observations, developed relationships for oil entrainment rate and resulting suspended oil droplet size distribution as functions of turbulent energy level and oil viscosity. Droplet sizes decrease and entrainment rate increases with increasing turbulence. The higher the oil viscosity, the larger is the maximum droplet size and the lower the entrainment rate. Oil viscosity is increased by emulsification, which slows entrainment rate (Spaulding et al., 1992; French et al., 1996; Dahling et al., 1997). The data and relationships in Delvigne and Sweeney (1988) are used to calculate mass and particle size distribution of droplets entrained in SIMAP (as it is in the NRDAM/CME, French et al., 1996). Particle size decreases with higher turbulent energy level and lower oil viscosity, from a low-turbulence and high-viscosity condition where droplet sizes range up to a maximum of 5 mm, to a high-turbulence and low-viscosity condition where droplet sizes range up to a maximum of 0.2 mm (200 m). The natural dispersion particle sizes observed by Delvigne and Sweeney (1988) are confirmed by field observations by Lunel (1993a,b).

Entrained droplets in the water column rise according to Stokes Law, where velocity is related to the difference in density between the particle (droplet) and the water, and to the particle diameter. In addition to rising according to Stoke's Law, entrained droplets are transported by currents and mixed vertically by randomized turbulent diffusion. When droplets intersect the water surface, if their buoyancy can overcome vertical mixing they surface and form sheens and tar balls (modeled as surface spillets of <0.1mm average thickness).

Oil Evaporation

Evaporation can result in the transfer of 20-40% of spilled oil from the sea surface to the atmosphere, depending on the type of oil (Gundlach and Boehm, 1981). The rate of evaporation depends on surface area, thickness, vapor pressure and mass transport coefficient, which in turn are functions of the composition of the oil, wind speed and temperature. As oil evaporates its composition changes, affecting its density and viscosity as well as subsequent evaporation. The most volatile hydrocarbons (low carbon number) evaporate most rapidly, typically in less than a day and sometimes in under an hour (McAuliffe, 1989). As the oil continues to weather, and particularly if it forms a water-in-oil emulsion, evaporation will be significantly decreased.

Evaporation models assume the oil to be well-mixed within the slick. For thick, viscous slicks, the well-mixed assumption is not valid, and virtually fresh oil may remain for several days or even weeks, trapped within viscous oil-water emulsions. A diagram of the evaporative process is in Figure A1.

The Mackay evaporative exposure algorithm (Stiver and Mackay, 1984) is used in many oil spill models such as the Mackay et al. models (Mackay and Leinonen 1977; Mackay et al. 1980a,b, 1982), ADIOS (Lehr et al. 1992), OILMAP (Spaulding et al. 1992), and earlier versions of SIMAP (French et al. 1999). The algorithm is based on accepted evaporation theory, which follows Raoult's Law that each component will evaporate with a rate proportional to the saturation vapor pressure and mole fraction present for that component. For the evaporative exposure model the assumption is that the oil mixture behaves as a single component. It uses an analytical approach to predict the volume fraction evaporated, using distillation data to estimate parameters needed for the analytic equation.

In other models (Payne et al. 1984, 1987; Kirstein et al. 1985; French et al. 1996; Jones 1997; Lehr et al. 2000; Reed et al. 2000) and in SIMAP, so-called pseudo-components (chemical component classes) are evaporated according to an analogous evaporative exposure algorithm, where the flux to the atmosphere is specific to the component's molar volume, vapor pressure, and molecular weight. Jones (1997) simplified this approach into a simplified pseudo-component (SPC) model, relating molar volume, vapor pressure, and molecular weight to the boiling point of the component. Thus, only the boiling points and initial volume fractions of the components need to be specified to implement the model.

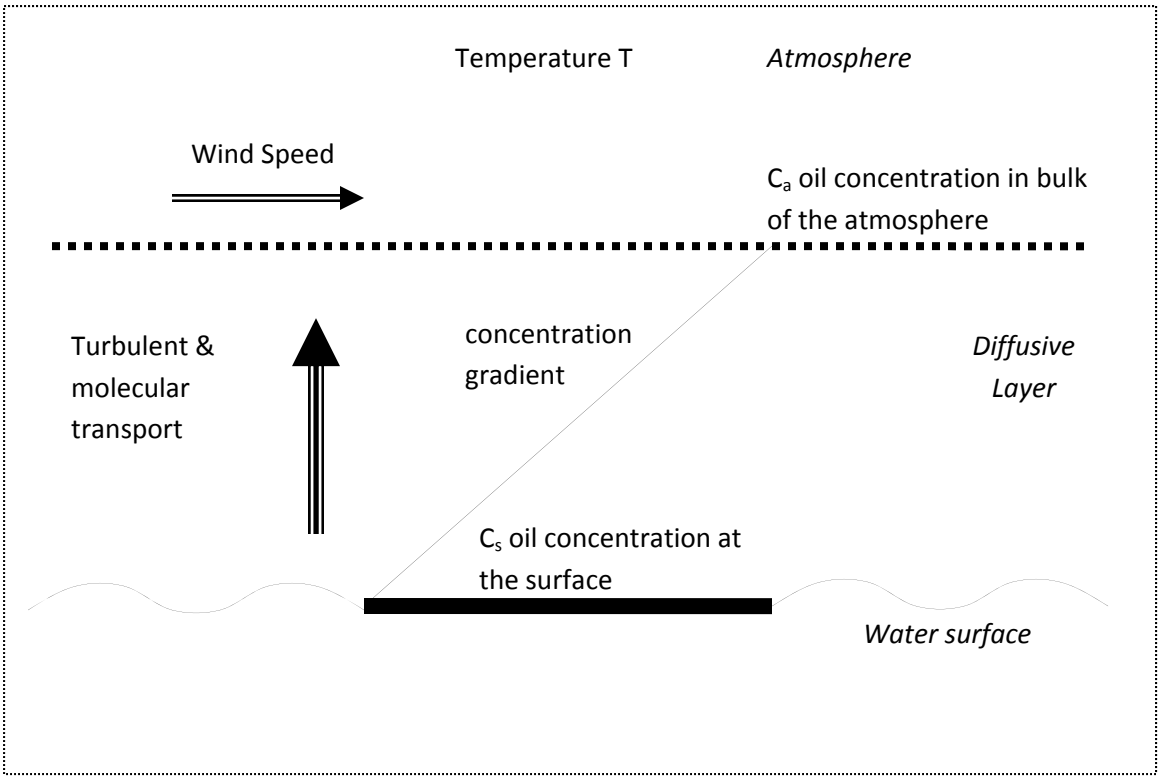

FIGURE A1. SCHEMATIC DIAGRAM OF EVAPORATION PROCESS.

Oil/Ice Interactions

The SIMAP model accounts for the presence of ice when calculating surface oil advection, evaporation, entrainment into the water column and surface oil spreading. Table A3 briefly summarizes how the model deals with oil advection and weathering in the presence of different ice concentrations.

TABLE A3: SUMMARY OF OIL-IN-ICE ADVECTION AND WEATHERING EFFECTS ACCOUNTED FOR IN THE SIMAP MODEL.

Ice Cover (Percent)	Advection	Evaporation	Entrainment	Spreading
0 – 30	No change	No change	No change	No change
30 – 80	15° to right	Linear reduction with ice cover	Linear reduction with ice cover	Terminal thickness increased in proportion to ice coverage
80 - 100	Oil moves with pack ice	No weathering	No weathering	Oil thickness computed as a function of ice thickness

References

CSE/ASA/BAT, 1986. Development of a Coastal Oil Spill Smear Model. Phase 1: Analysis of Available and Proposed Models, Prepared for Minerals Management Service by Coastal Science & Engineering, Inc. (CSE) with Applied Science Associates, Inc. (ASA) and Battelle New England Research Laboratory (BAT), 121p.

French, D., M. Reed, K. Jayko, S. Feng, H. Rines, S. Pavignano, T. Isaji, S. Puckett, A. Keller, F. W. French III, D. Gifford, J. McCue, G. Brown, E. MacDonald, J. Quirk, S. Natzke, R. Bishop, M. Welsh, M. Phillips and B.S. Ingram, 1996a. The CERCLA type A natural resource damage assessment model for coastal and marine environments (NRDAM/CME), Technical Documentation, Vol. I - Model Description. Final Report, submitted to the Office of Environmental Policy and Compliance, U.S. Dept. of the Interior, Washington, DC, April, 1996, Contract No. 14-0001-91-C-11.

French, D., M. Reed, S. Feng and S. Pavignano, 1996b. The CERCLA type A natural resource damage assessment model for coastal and marine environments (NRDAM/CME), Technical Documentation, Vol. III - Chemical and Environmental Databases. Final Report , Submitted to the Office of Environmental Policy and Compliance, U.S. Dept. of the Interior, Washington, DC, April, 1996, Contract No. 14-01-0001-91-C-11.

French, D., S. Pavignano, H. Rines, A. Keller, F.W. French III and D. Gifford, 1996c. The CERCLA type A natural resource damage assessment model for coastal and marine environments (NRDAM/CME), Technical Documentation, Vol.IV - Biological Databases. Final Report , Submitted to the Office of Environmental Policy and Compliance, U.S. Dept. of the Interior, Washington, DC, April, 1996, Contract No. 14-01-0001-91-C-11.

French, D.P., and H. Rines, 1997. Validation and use of spill impact modeling for impact assessment. Proceedings, 1997 International Oil Spill Conference, Fort Lauderdale, Florida, American Petroleum Institute Publication No. 4651, Washington, DC, pp-829-834.

French, D.P., H. Rines and P. Masciangioli, 1997. Validation of an Orimulsion spill fates model using observations from field test spills. In: Proceedings of the Twentieth Arctic and Marine Oilspill Program (AMOP) Technical Seminar, Vancouver, Canada, June 10-13, 1997, Emergencies Science Division, Environment Canada, Ottawa, Ontario, Canada, pp.933-961.

French, D., H. Schuttenberg, and T. Isaji, 1999. Probabilities of oil exceeding thresholds of concern: examples from an evaluation for Florida Power and Light. in Proceedings of the 22nd Arctic and Marine Oil Spill Program (AMOP) Technical Seminar, June 2-4, 1999, Environment Canada, pp.243-270.

French McCay, D.P., 2002. Development and Application of an Oil Toxicity and Exposure Model, OilToxEx. Environmental Toxicology and Chemistry 21(10): 2080-2094.

French McCay, D.P., 2003. Development and Application of Damage Assessment Modeling: Example Assessment for the North Cape Oil Spill. Marine Pollution Bulletin, Volume 47, Issues 9-12, September-December 2003, pp. 341-359.

French McCay, D.P., 2004. Oil spill impact modeling: Development and validation. Environmental Toxicology and Chemistry 23(10): in press.

French McCay, D. and James R. Payne, 2001. Model of oil fate and water concentrations with and without application of dispersants. In: Proceedings of the Twenty-fourth Arctic and Marine Oil spill Program (AMOP) Technical Seminar, Emergencies Science Division, Environment Canada, Ottawa, Ontario, Canada, pp.611-645.

French McCay, D.P., and J.J. Rowe, 2004. Evaluation of Bird Impacts in Historical Oil Spill Cases Using the SIMAP Oil Spill Model. In Proceedings of the 27th Arctic and Marine Oil Spill Program (AMOP) Technical Seminar, Emergencies Science Division, Environment Canada, Ottawa, ON, Canada, pp. 421-452.

Gundlach, E.R., 1987. Oil holding capacities and removal coefficients for different shoreline types to computer simulate spills in coastal waters. In: Proceedings of the 1987 Oil Spill conference, pp. 451-457.

Gundlach, E.R. and P. Boehm, 1981. Fates of several oil spills in coastal and offshore waters. Report to NOAA/Seattle. NOAA Grant No. NA80RAD00060, RPI/R/81/12/31-30.

Gundlach, E.R., P.D. Boehm, M. Marchand, R.M. Atlas, D.M. Ward, and D.A. Wolfe. 1983. The tale of Amoco Cadiz oil. Science. Vol. 332, pp. 122-129, July.

Harper, J. R. and F. Harvey-Kelly, 1994. Subsurface oil retention in coarse sediments beaches. Ottawa, Ontario: Environmental Technology Centre, Environment Canada; Jan 1994; Report Series No. EE-147.

Humphrey, B., 1994. Stranded oil in coarse sediments (SOCS) model. Ottawa, Ontario: Environmental Technology Centre, Environment Canada; Jan 1994; Report Series No. EE-146. 27p.

Jones, R.K., 1997. A Simplified Pseudo-Component of Oil Evaporation Model, in Proceedings of the 20th Arctic and Marine Oil Spill Program (AMOP) Technical Seminar, Environment Canada, pp. 43-61.

Kirstein, B.E., J.R. Clayton, C. Clary, J.R. Payne, D. McNabb, Jr., G. Fauna and R. Redding, 1985 Integration of suspended particulate matter and oil transportation study. Minerals Management Service, Anchorage, Alaska.

Lehr, W.J., R. Overstreet, R. Jones, and G. Watabayashi, 1992. ADIOS-Automatic Data Inquire for Oil Spill, in Proceedings of the 15th Arctic Marine Oilspill Program, Technical Seminar, Environment Canada, Ottawa, Ontario, pp. 31-45.

Lehr, W.J., D. Wesley, D. Simecek-Beatty, R. Jones, G. Kachook and J. Lankford, 2000. Algorithm and interface modifications of the NOAA oil spill behavior model. Proceedings of the 23rd Arctic and Marine Oil Spill Program (AMOP) Technical Seminar, Vancouver, BC, Environmental Protection Service, Environment Canada, pp. 525-539.

Lunel, T. 1993a. Dispersion: Oil droplet size measurements at sea. in Proceedings of the 16th Arctic Marine Oilspill Program (AMOP) Technical Seminar, Environment Canada, Calgary, Alberta, June 7-9, 1993, pp. 1023-1056.

Lunel, T. 1993b. Dispersion: Oil droplet size measurements at sea. in Proceedings of the 1993 Oil Spill Conference, pp. 794-795.

Mackay, D. and P.J. Leinonen, 1977. Mathematical model of the behavior of oil spills on water with natural and chemical dispersion. Prepared for Fisheries and Environment Canada. Economic and Technical Review Report EPS-3-EC-77-19, 39p.

Mackay, D.,S. Paterson and K. Trudel, 1980b. A mathematical model of oil spill behavior, Department of Chemical and Applied Chemistry, University of Toronto, Canada, 39p.

Mackay, D., I. Buist, R. Mascarenhas and S. Peterson, 1980a. Oil spill processes and models. Report EE-8, Environment Protection Service, Canada.

Mackay, D, W.Y. Shiu, K. Hossain, W. Stiver, D. McCurdy and S. Peterson, 1982. Development and calibration of an oil spill behavior model. Report No. CG-D-27-83, U.S. Coast Guard, Research and Development Center, Groton, Connecticut, 83p.

Mackay, D., W.Y. Shiu, and K.C. Ma, 1992a. Illustrated Handbook of Physical-Chemical Properties and Environmental Fate for Organic Chemicals, Vol. I, Monoaromatic Hydrocarbons, Chlorobenzenes, and PCBs. Lewis Publ., Chelsea, Michigan, 668p.

Mackay, D., W.Y. Shiu, and K.C. Ma, 1992b. Illustrated Handbook of Physical-Chemical Properties and Environmental Fate for Organic Chemicals, Vol. II, Polynuclear Aromatic Hydrocarbons, Polychlorinated Dioxins, and Dibenzofurans. Lewis Publ., Chelsea, Michigan, 566p.

Mackay, D., W.Y. Shiu, and K.C. Ma, 1992c. Illustrated Handbook of Physical-Chemical Properties and Environmental Fate for Organic Chemicals, Vol. III, Volatile Organic Chemicals. Lewis Publ., Chelsea, Michigan, 885p.

Mackay, D., W.Y. Shiu and D.C. Ma, 1992d. Illustrated Handbook of Physical-Chemical Properties and Environmental Fate for Organic Chemicals. Volume IV Oxygen, Nitrogen, and Sulfur containing compounds. Lewis Publishers, Inc. Chelsea, Michigan, 930p.

McAuliffe, C.D., 1989. The weathering of volatile hydrocarbons from crude oil slicks on water. In: Proceedings of the 1989 Oil Spill conference. San Antonio, TX. pp. 357-364.

National Research Council (NRC), 1985. Oil in the Sea: Inputs, Fates and Effects, National Academy Press, Washington, D.C., 601 p.

National Research Council (NRC) 1989. Review of the State-of-Knowledge Regarding Dispersant Usage in Open-Ocean Spill Responses. NRC Marine Board, Washington, DC., 306p.

O'Clair, C.E., J.W. Short, and S.D. Rice, 1996. Contamination of intertidal and subtidal sediments by oil from the *Exxon Valdez* oil spill. In Rice SD, Spies RB, Wolfe DA,

Wright BA, eds. *Proceedings* of the *Exxon Valdez* oil spill symposium. American Fisheries Society Symposium 18:17-28.

Payne, J.R., B.E. Kirstein, G.D. McNabb, Jr., J.L. Lambach, R. Redding R.E. Jordan, W. Hom, C. deOliveria, G.S. Smith, D.M. Baxter, and R. Gaegel, 1984. Multivariate analysis of petroleum weathering in the marine environment – sub Arctic , Environmental Assessment of the Alaskan Continental Shelf, OCEAP, Final Report of Principal Investigators, Vol. 21 and 22, Feb. 1984, 690p.

Payne, J.R., B.E. Kirstein, J.R. Clayton, Jr., C. Clary, R. Redding, G.D. McNabb, Jr., and G. Farmer, 1987. Integration of suspended particulate matter and oil transportation study. Final Report. Minerals Management Service, Environmental Studies Branch, Anchorage, AK. Contract No. 14-12-0001-30146, 216 p.

Reed, M. and E. Gundlach. 1989. Hindcast of the Amoco Cadiz event with a coastal zone oil spill model. Oil and Chemical Pollution, Vol. 5, pp. 451-476.

Reed, M., E. Gundlach and T. Kana, 1989. A coastal zone oil spill model: development and sensitivity studies. Oil & Chemical Pollution 5:411-449.

Reed, M., T. Kana, and E. Gundlach, 1988. Development, testing and verification of an oil spill surf-zone mass-transport model. Final Report to: Mineral Management Service, Alaska OCS Region, Contract No. 14-12-0001-30130; by Applied Science Associates, Inc. (ASA), Coastal Science & Engineering, Inc. (CSE), and E-Tech, Inc., June 1988, 343p.

Reed, M., M.L. Spaulding, E.R. Gundlach, T.W. Kana and S.J. Siah, 1986. Formulation of a shoreline/oil spill interaction model. In: Proceedings 1986 Arctic Marine Oil Program (AMOP), Edmonton, Canada, Ottowa, Ontario, pp. 77-101.

Spaulding, M.L., E. Howlett, E. Anderson and K. Jayko, 1992. OILMAP: A global approach to spill modeling. 15th Arctic and Marine oil Spill Program, Technical Seminar, Edmonton, Alberta, Canada, June 9-11, 1992, pp. 15-21.

Stiver, W. and D. Mackay, 1984. Evaporation rate of oil spills of hydrocarbons and petroleum mixtures. Environmental Science and Technology 18: 834-840.

References - SIMAP Example Applications and Validations

French, D.P., and H. Rines, 1997. Validation and use of spill impact modeling for impact assessment. In *Proceedings, 1997 International Oil Spill Conference*, Fort Lauderdale, Florida, American Petroleum Institute Publication No. 4651, Washington, DC, pp-829-834.

French, D. P., 1998a. Estimate of Injuries to Marine Communities Resulting from the North Cape Oil Spill Based on Modeling of Fates and Effects. Report to US Department of Commerce, National Oceanic and Atmospheric Administration (NOAA), Damage Assessment Center, Silver Spring, MD, January 1998.

French, D. P., 1998b. Updated Estimate of Injuries to Marine Communities Resulting from the North Cape Oil Spill Based on Modeling of Fates and Effects. Report to US Department of Commerce, National Oceanic and Atmospheric Administration (NOAA), Damage Assessment Center, Silver Spring, MD, December 1998.

French, D.P., 1998c. Modeling the Impacts of the *North Cape,* p. 387-430. In *Proceedings, 21st Arctic and Marine Oilspill Program (AMOP) Technical Seminar*, June 10-12, 1998, West Edmonton Mall Hotel Edmonton, Alberta, Canada, Emergencies Science Division, Environment Canada, Ottawa, ON, Canada.

French McCay, D. and James R. Payne, 2001. Model of Oil Fate and Water concentrations with and with out application of dispersants. In *Proceedings of the 2001 24th Arctic and Marine Oil spill Program (AMOP) Technical Seminar*, June 12-14, 2001, Environment Canada, pp.611-645.

French, D. P., Jones, M. A., and Coakley, L., 2001. Use of Oil Spill Modeling for Contingency Planning and Impact Assessment: Application for Florida Power and Light. In *Proceedings of the 20 01 International Oil Spill Conference & Exposition*, American Petroleum Institute, March 26-29, 2001, Tampa, Florida.

French, D.P. and H. Schuttenberg, 1999. Evaluation of net environmental benefit using fates and effects modeling. Paper ID #321. In *Proceedings, 1 999 International Oil Spill Conference*, American Petroleum Institute.

French McCay, D. 2002. Modeling Evaluation of Water Concentrations and Impacts Resulting from Oil Spills With and Without the Application of Dispersants. International Marine Environmental Seminar 2001, Journal of Marine Systems, Special Issue 2002.

French McCay, D., N. Whittier, S. Sankaranarayanan, J. Jennings, and D. S. Etkin, 2002. Modeling Fates and Impacts for Bio-Economic Analysis of Hypothetical Oil Spill Scenarios in San Francisco Bay. In *Proceedings of the T wenty Fifth Arctic and Marine Oil Spill Program (AMOP) Technical Seminar*, Environment Canada, Calgary, AB, Canada, 2002, p. 1051-1074.

French McCay, D., N. Whittier, T. Isaji, and W.Saunders, 2003. Assessment of the Potential Impacts of Oil Spills in the James River, Virginia. In Proceedings of the 26th Arctic and Marine Oil Spill Program (AMOP) Technical Seminar, Emergencies Science Division, Environment Canada, Ottawa, ON, Canada, p. 857-878.

French McCay, D., N. Whittier, S. Sankaranarayanan, J. Jennings, and D. S. Etkin, 2003. Estimation of Potential Impacts and Natural Resource Damages of Oil. J. Hazardous Materials (in press).

French McCay, D. and N. Whittier, 2003. Modeling Assessment of Potential Fates and Exposure for Orimulsion and Heavy Fuel Oil Spills. In: Proceedings, International Oil Spill Conference, April 2003, Paper 157, American Petroleum Institute, Washington, DC.

French McCay, D.P., 2003. Development and Application of Damage Assessment Modeling: Example Assessment for the North Cape Oil Spill. Marine Pollution Bulletin, Volume 47, Issues 9-12, September-December 2003, pp. 341-359.

French McCay, D.P., and J.J. Rowe, 2004. Evaluation of Bird Impacts in Historical Oil Spill Cases Using the SIMAP Oil Spill Model. In Proceedings of the 27th Arctic and Marine Oil Spill Program (AMOP) Technical Seminar, Emergencies Science Division, Environment Canada, Ottawa, ON, Canada, pp. 421-452.

French-McCay, D.P., J.J. Rowe, N. Whittier, S. Sankaranarayanan, D. S. Etkin, and L. Pilkey-Jarvis, 2005. Evaluation of the Consequences of Various Response Options Using Modeling of Fate, Effects and NRDA Costs of Oil Spills into Washington Waters. In: Proceedings, International Oil Spill Conference, May 2005, Paper 395, American Petroleum Institute, Washington, DC.

French-McCay, D.P., N. Whittier, C. Dalton, J.J. Rowe, and S. Sankaranarayanan, 2005. Modeling fates and impacts of hypothetical oil spills in Delaware, Florida, Texas, California, and Alaska waters, varying response options including use of dispersants. In: Proceedings, International Oil Spill Conference, May 2005, Paper 399, American Petroleum Institute, Washington, DC.

French McCay, D., N. Whittier, J.J. Rowe, S. Sankaranarayanan and H.-S. Kim, 2005. Use of Probabilistic Trajectory and Impact Modeling to Assess Consequences of Oil Spills with Various Response Strategies. In Proceedings of the 28th Arctic and Marine Oil Spill Program (AMOP) Technical Seminar, Emergencies Science Division, Environment Canada, Ottawa, ON, Canada, pp. 253-271, 2005.

Appendix B: Stochastic Model Results

This Appendix contains maps of the stochastic model results from spill simulations at the Bull Arm site. The summer maps are shown first, followed by the winter season results.

- For water surface oiling, the map shows the predicted probability that surface oil will exceed the 0.01 mm thickness threshold.
- For shoreline contact, the map shows the predicted probability that shoreline oil will exceed the 0.01 mm thickness threshold.
- For entrained oil, the map shows the predicted probability that entrained oil will exceed the 10 ppb concentration threshold.

Figure B1. Probability of surface contact from a release of 100 m^3 of marine diesel at the Bull Arm site in summer.

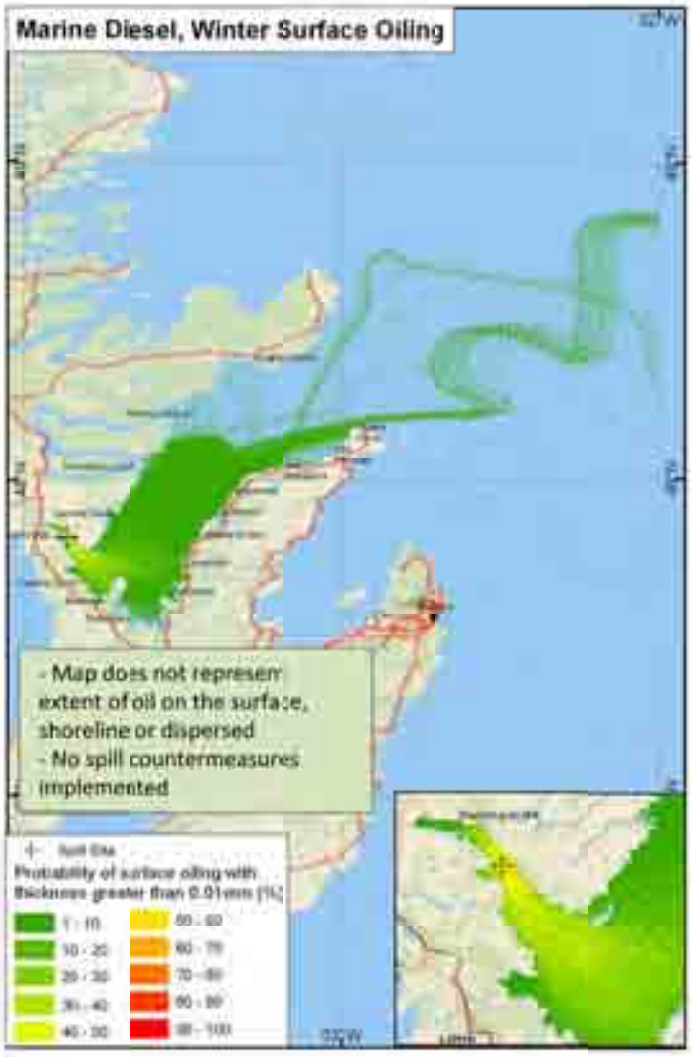

Figure B2. Probability of surface contact from a release of 100 m^3 of marine diesel at the Bull Arm site in winter.

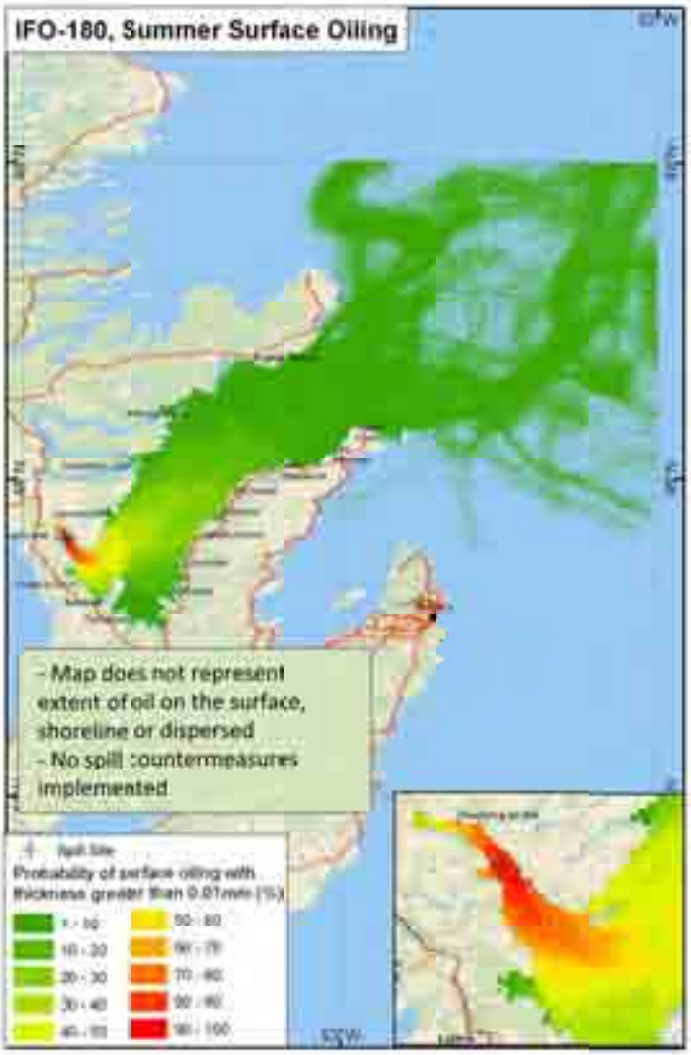

Figure B3. Probability of surface contact from a release of 1,000 m^3 of Intermediate Fuel Oil (IFO-180) at the Bull Arm site in summer.

Figure B4. Probability of surface contact from a release of 1,000 m^3 of Intermediate Fuel Oil (IFO-180) at the Bull Arm site in winter.

Figure B5. Probability of shoreline contact from a release of 100 m^3 of Marine Diesel at the Bull Arm site in summer.

Figure B6. Probability of shoreline contact from a release of 100 m^3 of marine diesel at the Bull Arm site in winter.

Figure B7. Probability of shoreline contact from a release of 1,000 m^3 of Intermediate Fuel Oil (IFO-180) at the Bull Arm site in summer.

Figure B8. Probability of shoreline contact from a release of 1,000 m^3 of Intermediate Fuel Oil (IFO-180) at the Bull Arm site in winter.

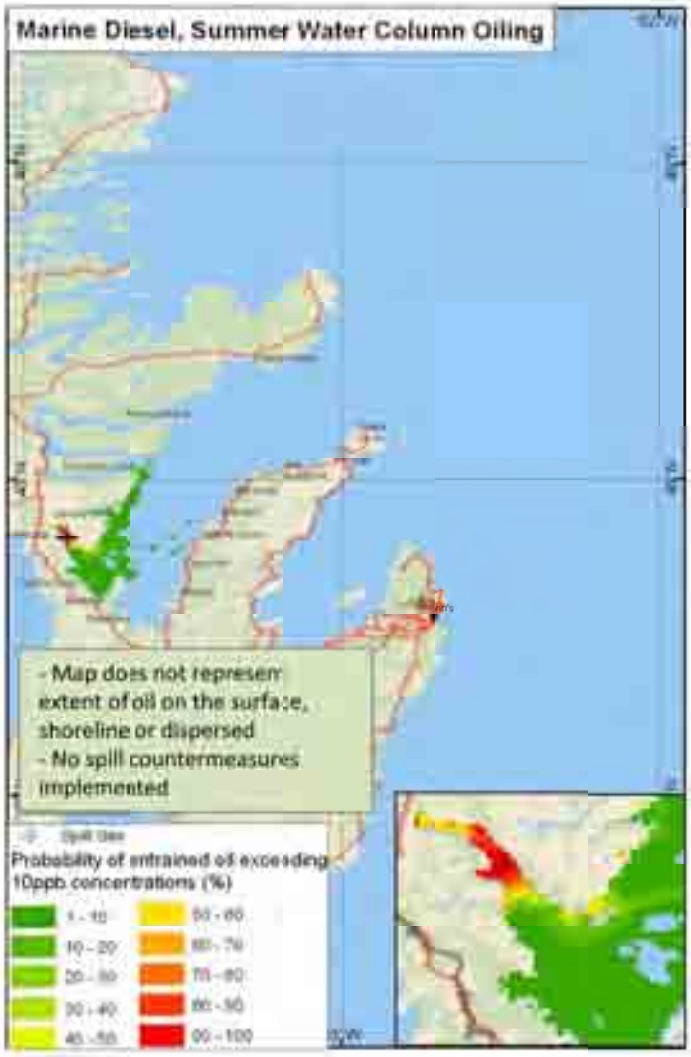

Figure B9. Probability entrained oil from a release of 100 m^3 of marine diesel at the Bull Arm site in summer.

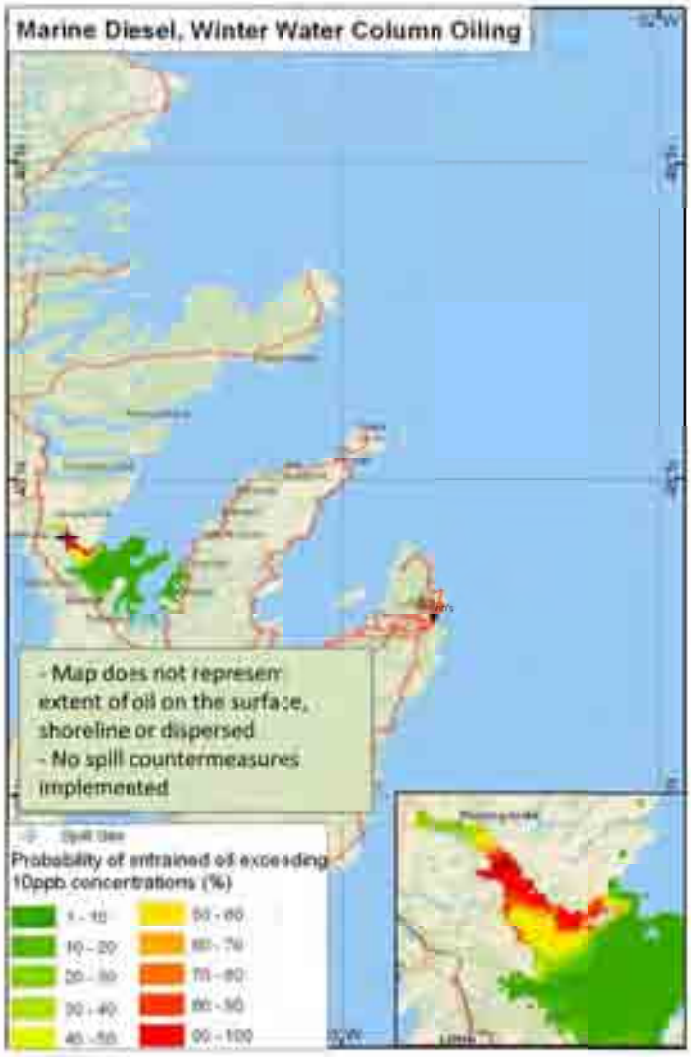

Figure B10. Probability of entrained oil from a release of 100 m^3 of marine diesel at the Bull Arm site in winter.

Figure B11. Probability of entrained oil from a release of 1,000 m^3 of Intermediate Fuel Oil (IFO-180) at the Bull Arm site in summer.

Figure B12. Probability of entrained oil from a release of 1,000 m^3 of Intermediate Fuel Oil (IFO-180) at the Bull Arm site in winter.

Appendix C: Deterministic Model Results

This Appendix contains maps and graphs of the deterministic model results from spill simulations at the Bull Arm site. Maps of the surface, shoreline or entrained oil are shown first, followed by a graph of the oil mass balance for the spill. On the maps, gray depicts the water surface area swept by surface oil at any time during the 30-day simulation. Black on the map depicts the location of surface oil at the end of the 30-day simulation. Areas of the shoreline highlighted in red indicate where oil is predicted to come in contact with the shoreline. The mass balance graphs depict the change in oil volume over the duration of the spill simulation for surface, shoreline, evaporated, decayed and water column oil.

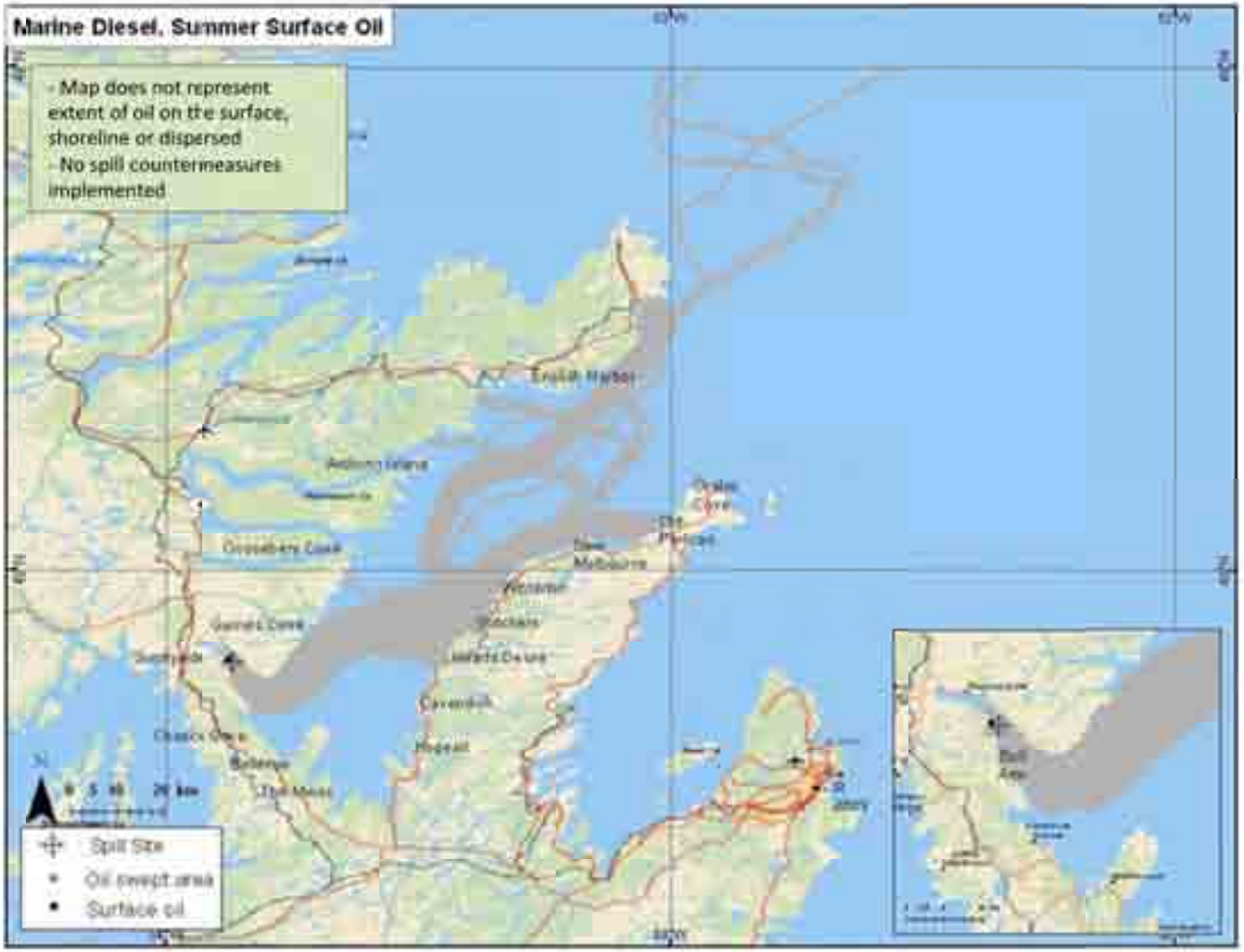

Figure C1. Water surface exposure to surface oil for 95th percentile run based on water surface area exposed to oil with average thickness greater than 0.01mm (dark brown sheen) for a 100 m^3 release of marine diesel in the summer. Gray depicts the area of the sea surface swept by surface oil over the 30-day period, not a continuous surface slick. Black areas depict oil on the water surface at the end of the 30 day simulation.

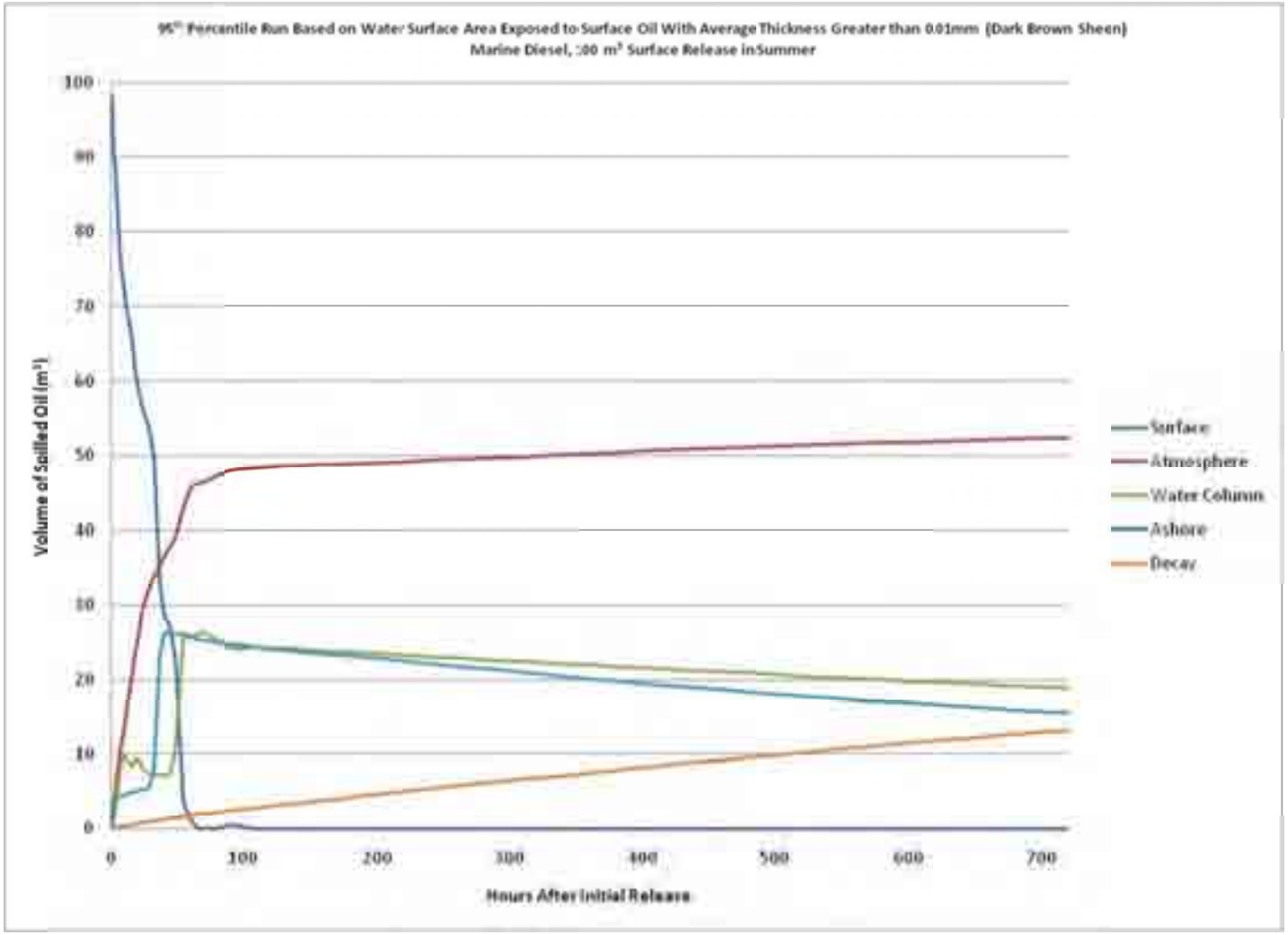

Figure C2. Mass balance graph for 95th percentile run based on water surface area exposed to surface oil with average thickness greater than 0.01mm (dark brown sheen) for a 100 m^3 release of marine diesel in the summer.

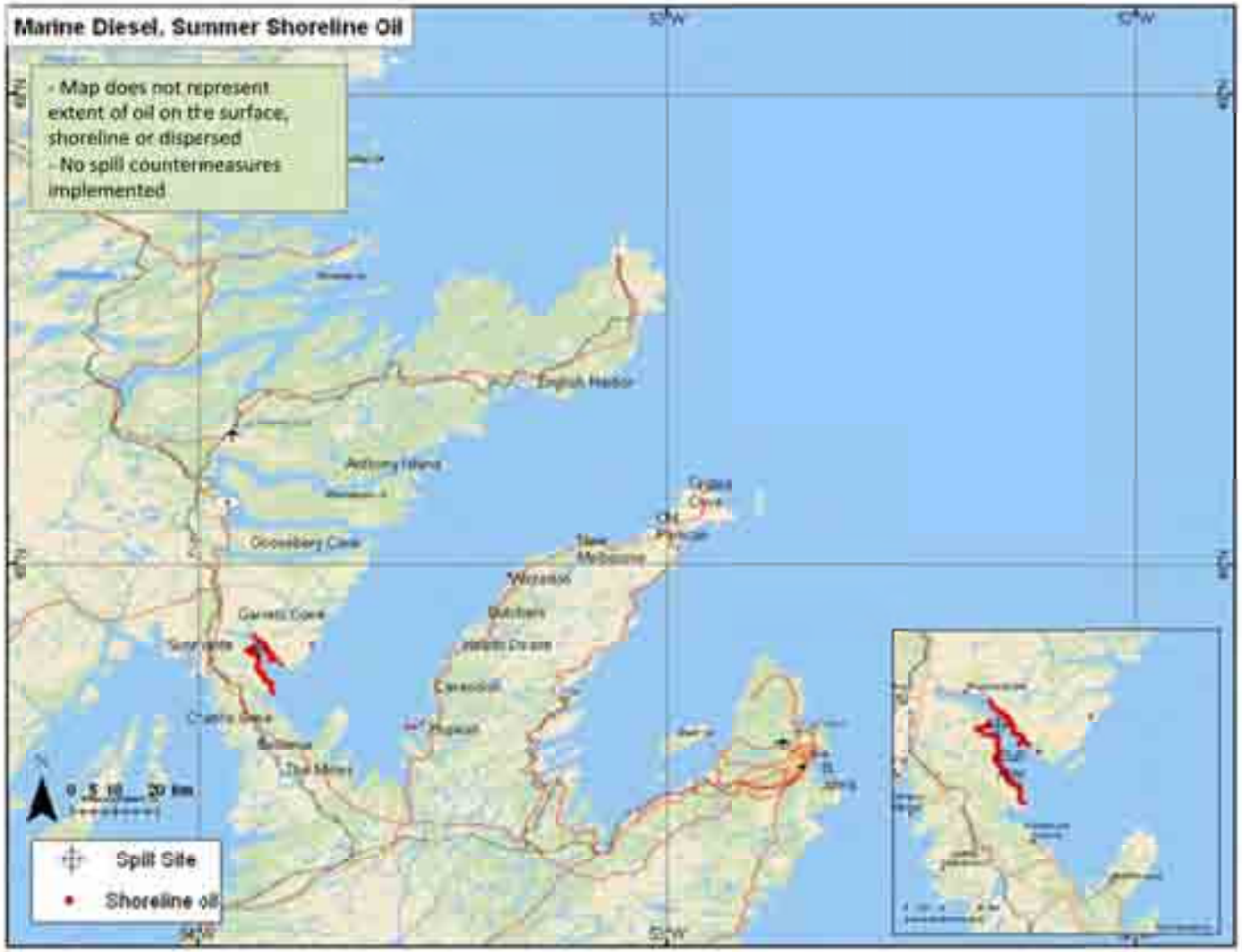

Figure C3. Shoreline exposure to hydrocarbons (mm) for 95th percentile run based on area of shoreline oiled with average thickness greater than 0.01mm (dark brown sheen) for a 100 m^3 release of marine diesel in the summer. Red color highlights the areas of predicted shoreline oiling.

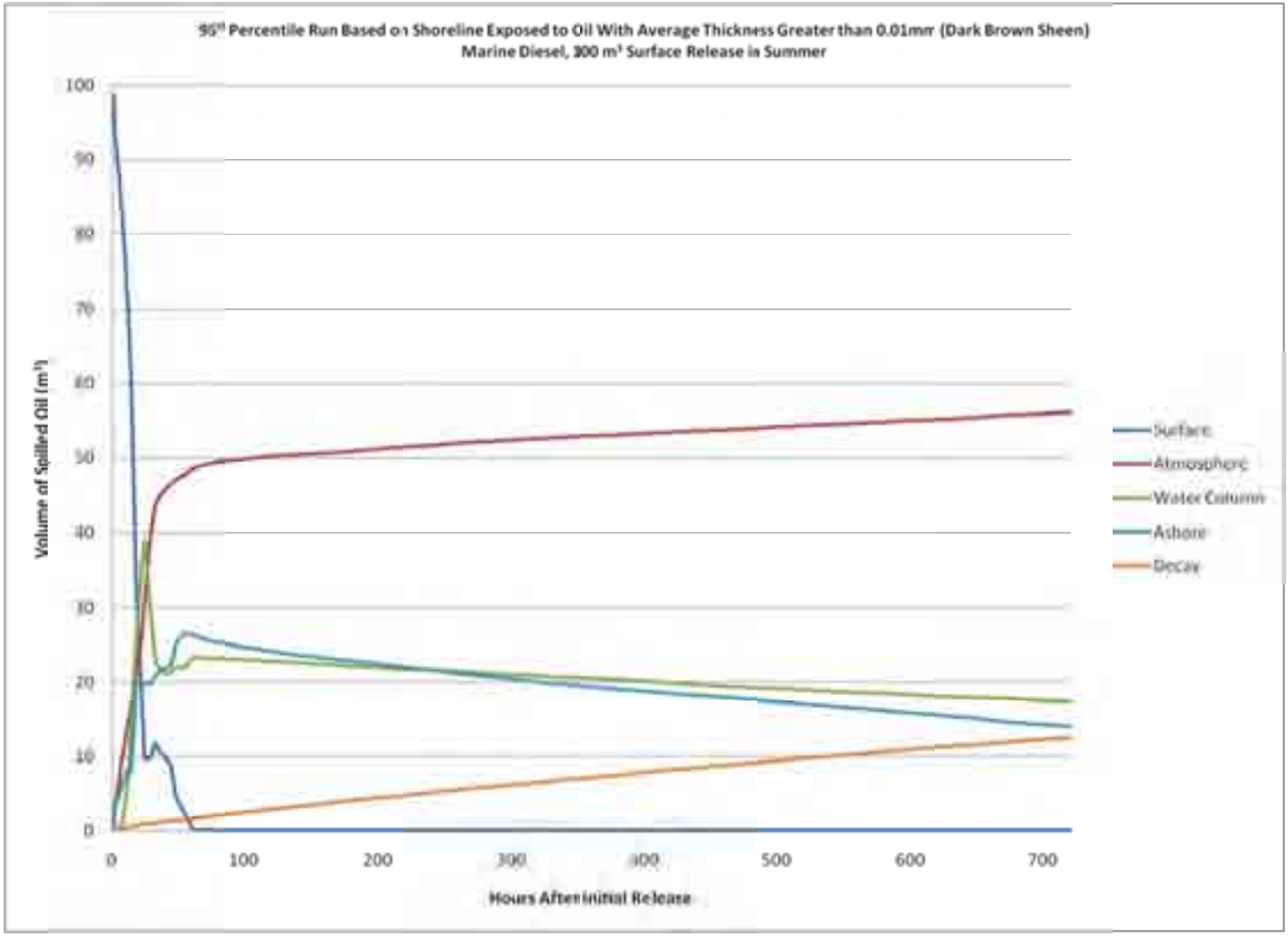

Figure C4. Mass balance graph for 95th percentile run based on area of shoreline oiled with average thickness greater than 0.01mm (dark brown sheen) for a 100 m^3 release of marine diesel in the summer.

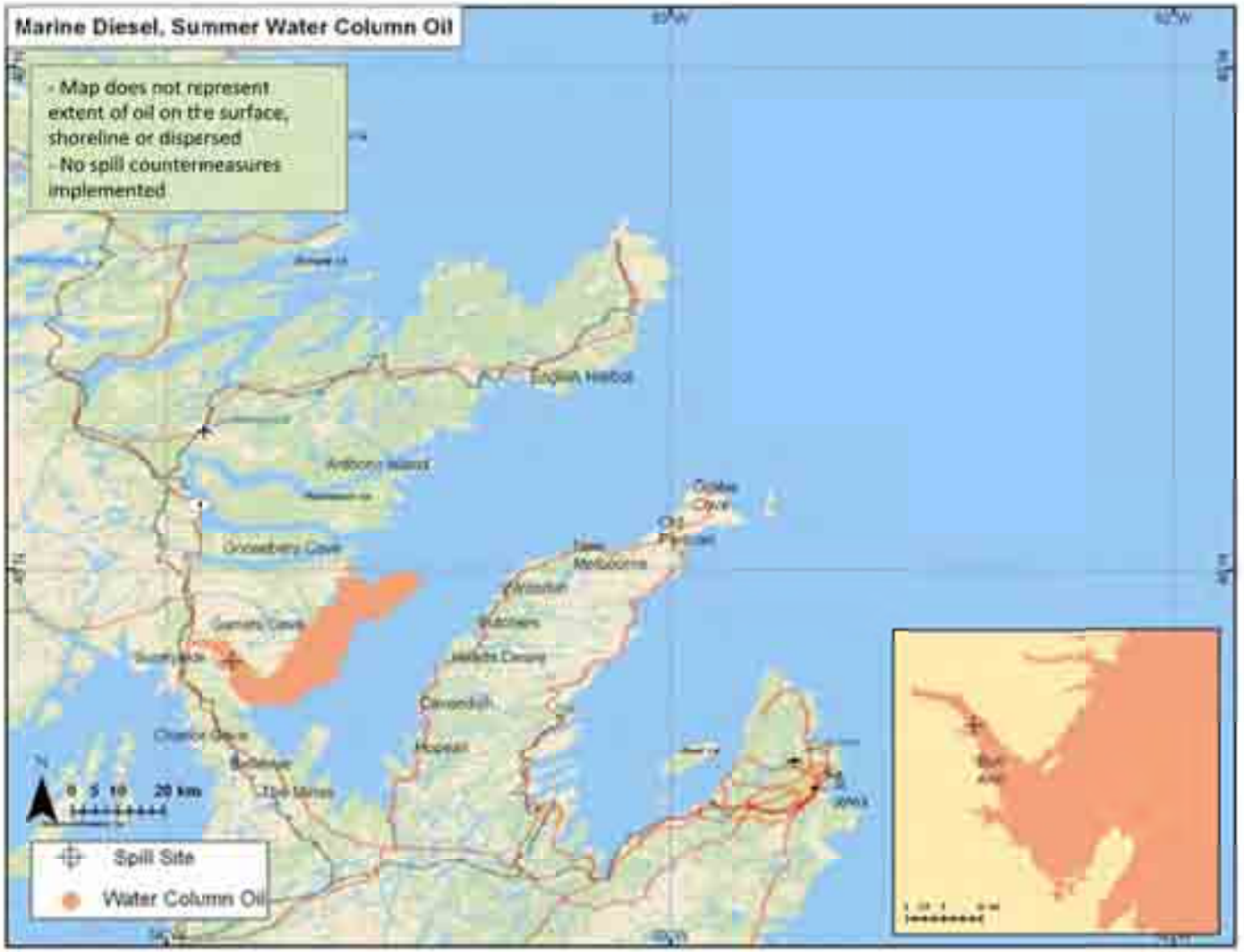

Figure C5. Area where the water column is exposed to a total hydrocarbon concentration exceeding 10ppb based on the 95th percentile run for a 100 m^3 release of marine diesel in the summer.

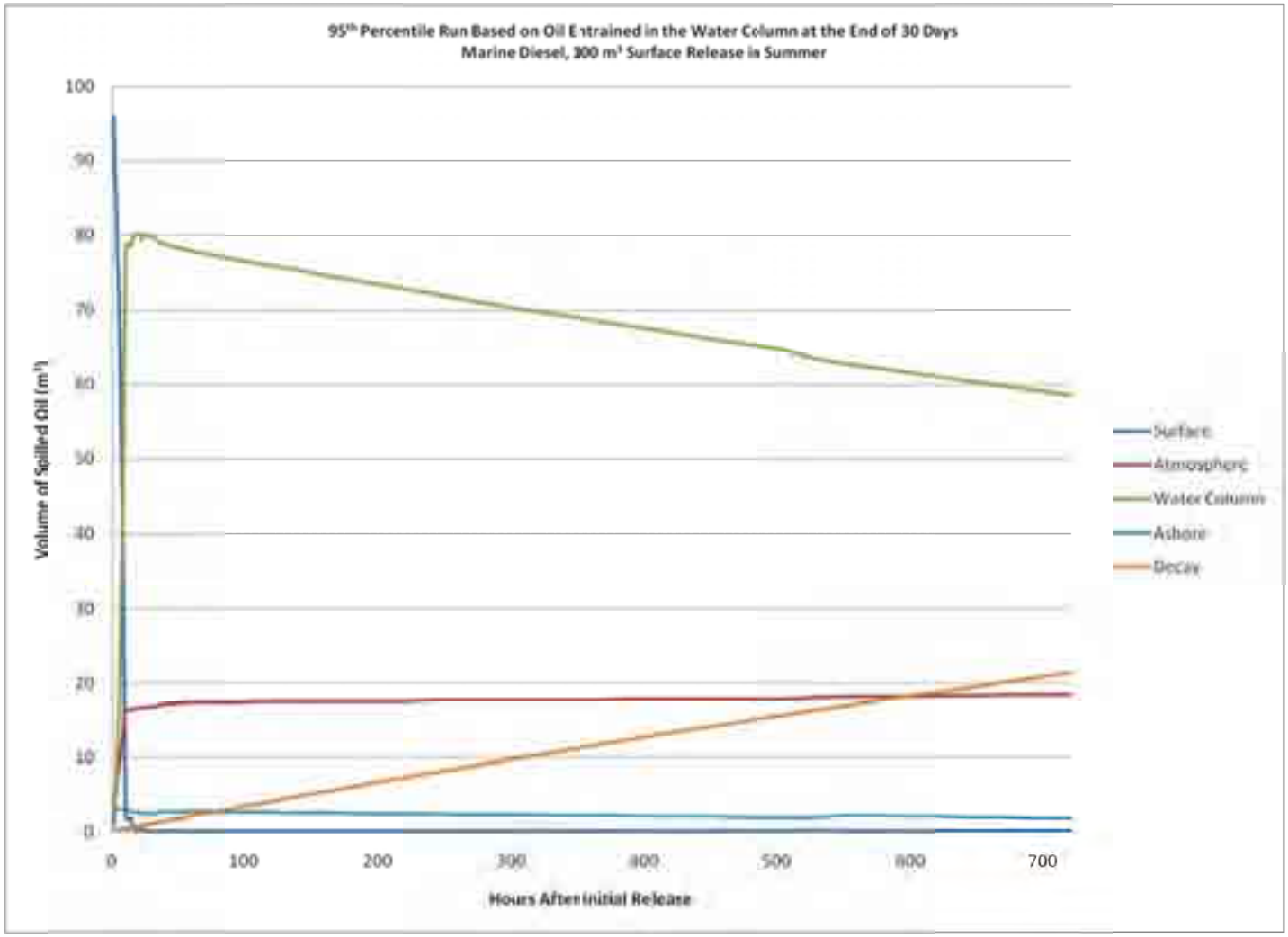

Figure C6. Mass balance graph for 95th percentile run based on subsurface oil entrained in the water column after 30 days for a 100 m^3 release of marine diesel in the summer.

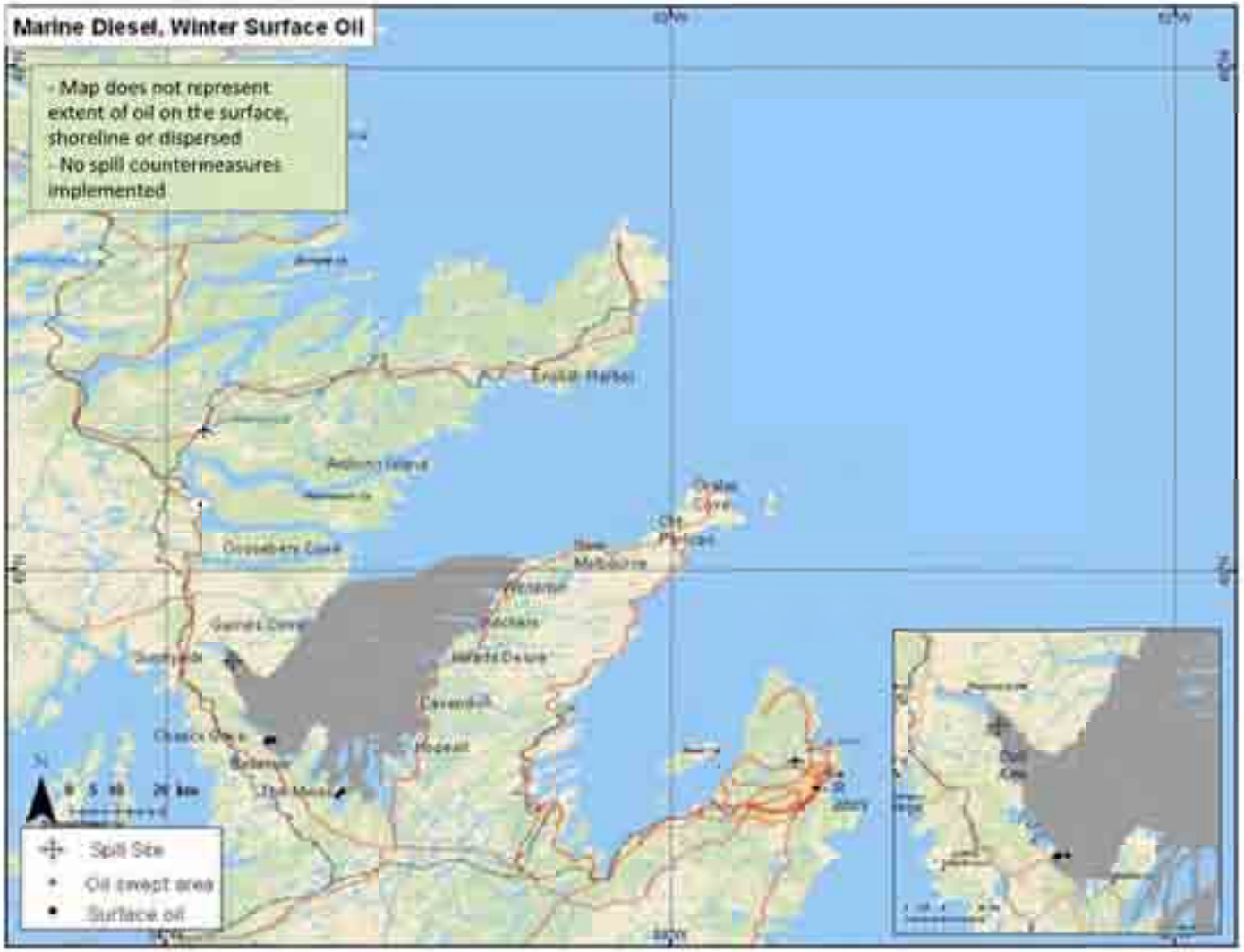

Figure C7. Water surface exposure to surface oil for 95th percentile run based on water surface area exposed to surface oil with average thickness greater than 0.01mm (dark brown sheen) for a 100 m^3 release of marine diesel in the winter. Gray depicts the area of the sea surface swept by surface oil over the 30-day period, not a continuous surface slick. Black areas depict oil on the water surface at the end of the 30 day simulation.

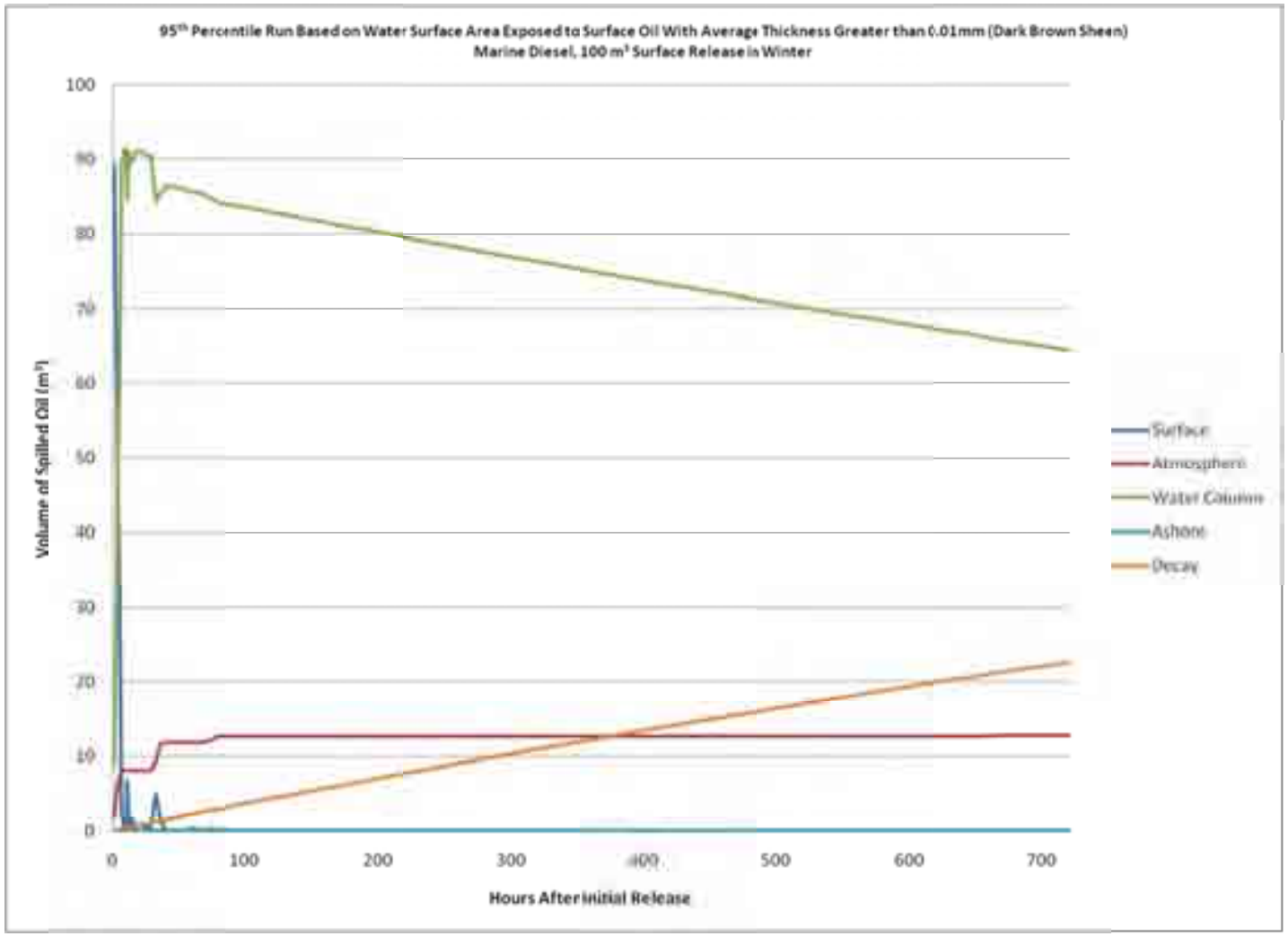

Figure C8. Mass balance graph for 95th percentile run based on water surface area exposed to surface oil with average thickness greater than 0.01mm (dark brown sheen) for a 100 m^3 release of marine diesel in the winter.

Figure C9. Shoreline exposure to hydrocarbons (mm) for 95th percentile run based on area of shoreline oiled with average thickness greater than 0.01mm (dark brown sheen) for a 100 m^3 release of marine diesel in the winter. Red color highlights the areas of predicted shoreline oiling.

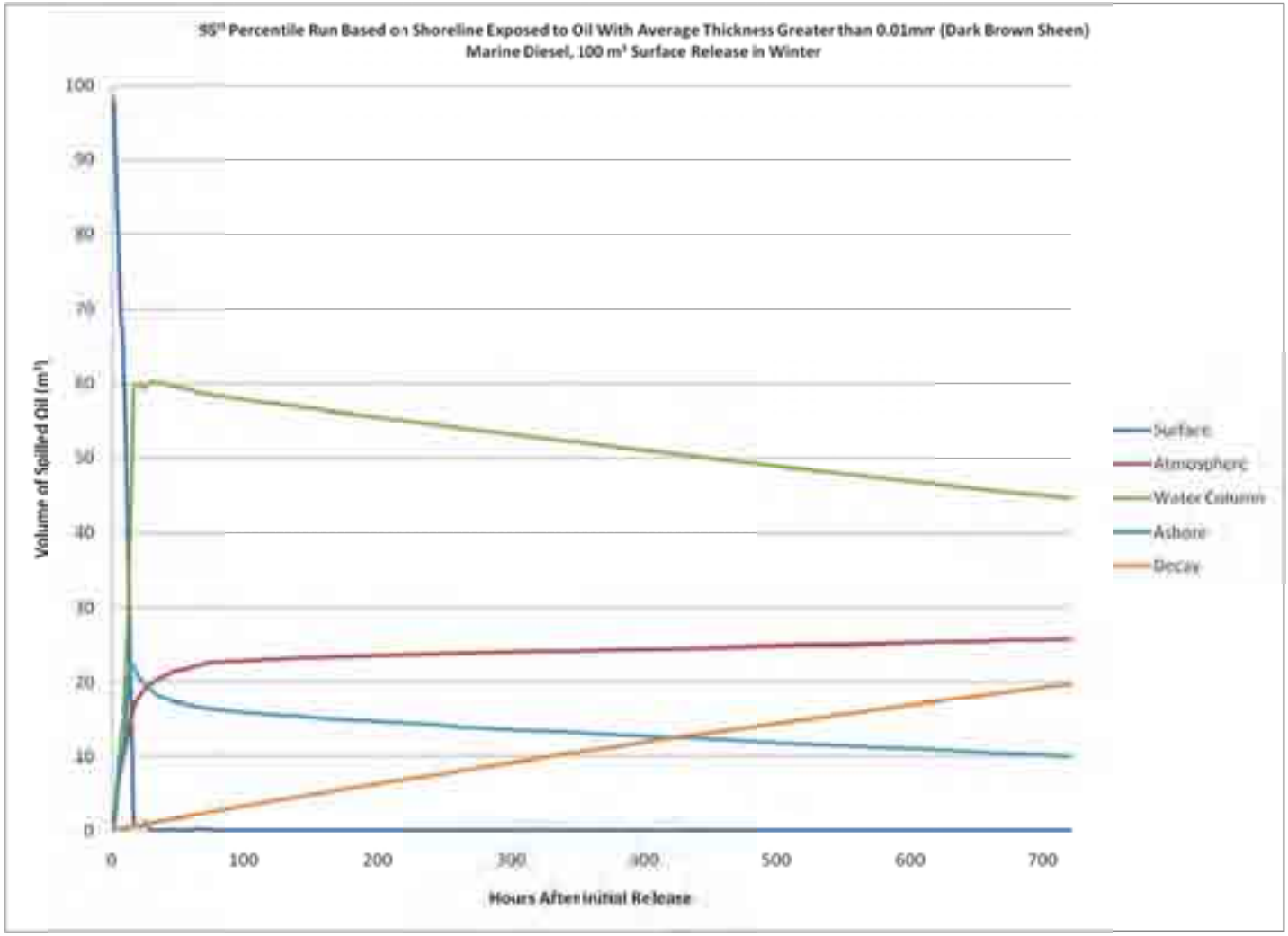

Figure C10. Mass balance graph for 95th percentile run based on area of shoreline oiled with average thickness greater than 0.01mm (dark brown sheen) for a 100 m^3 release of marine diesel in the winter.

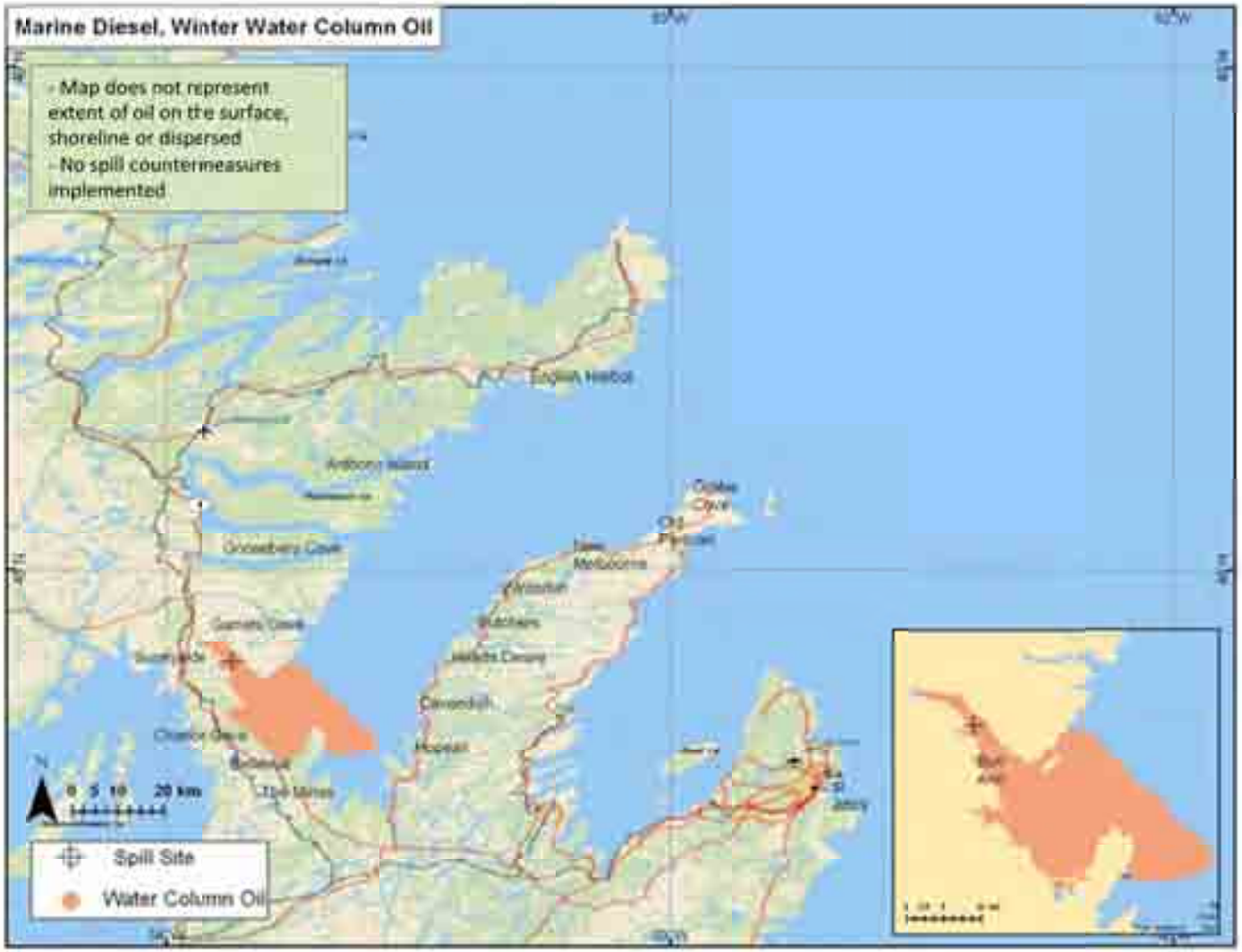

Figure C11. Area where the water column is exposed to a total hydrocarbon concentration exceeding 10ppb based on the 95th percentile run for a 100 m^3 release of marine diesel in the winter.

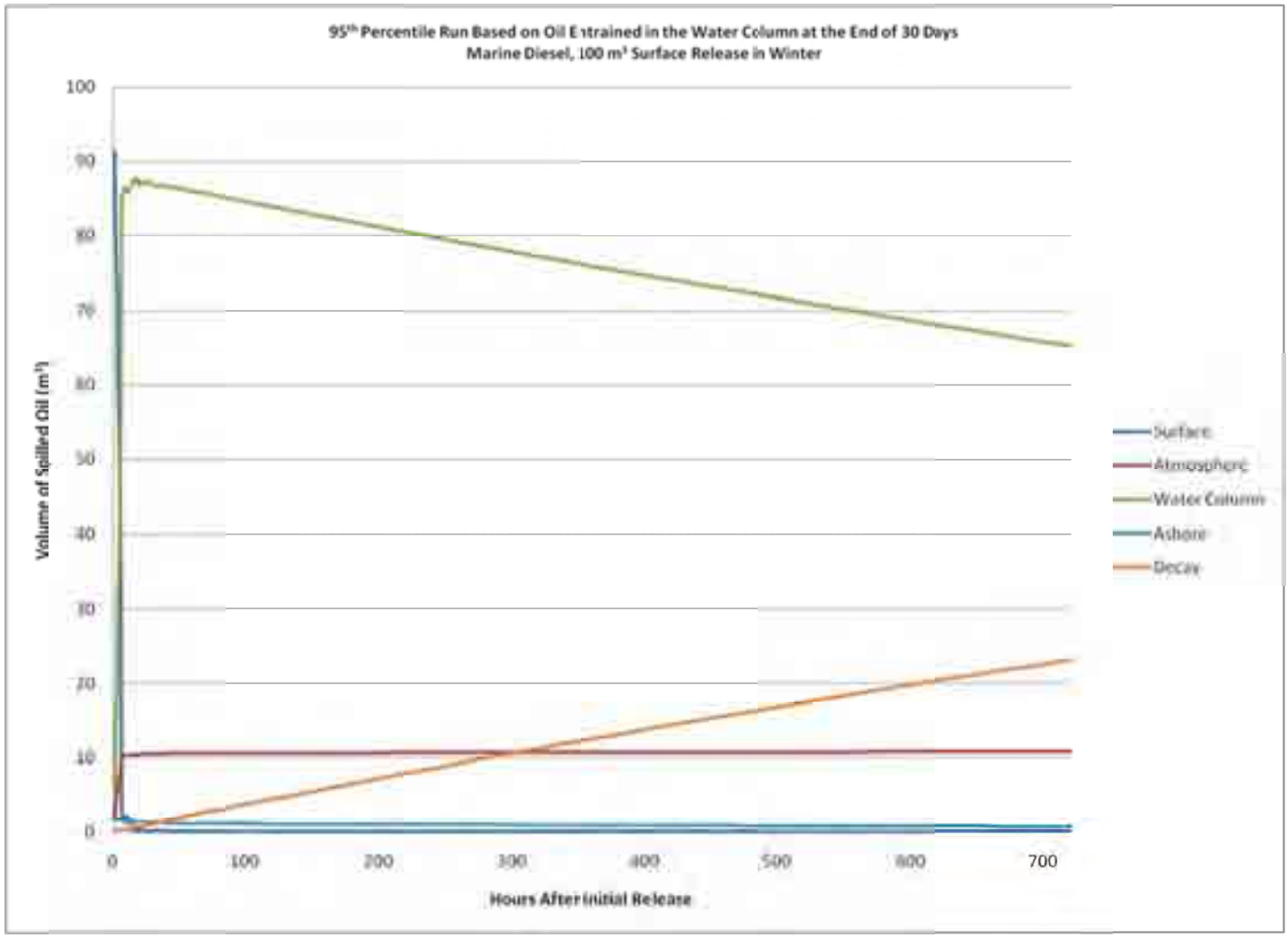

Figure C12. Mass balance graph for 95th percentile run based on subsurface oil entrained in the water column after 30 days for a 100 m^3 release of marine diesel in the winter.

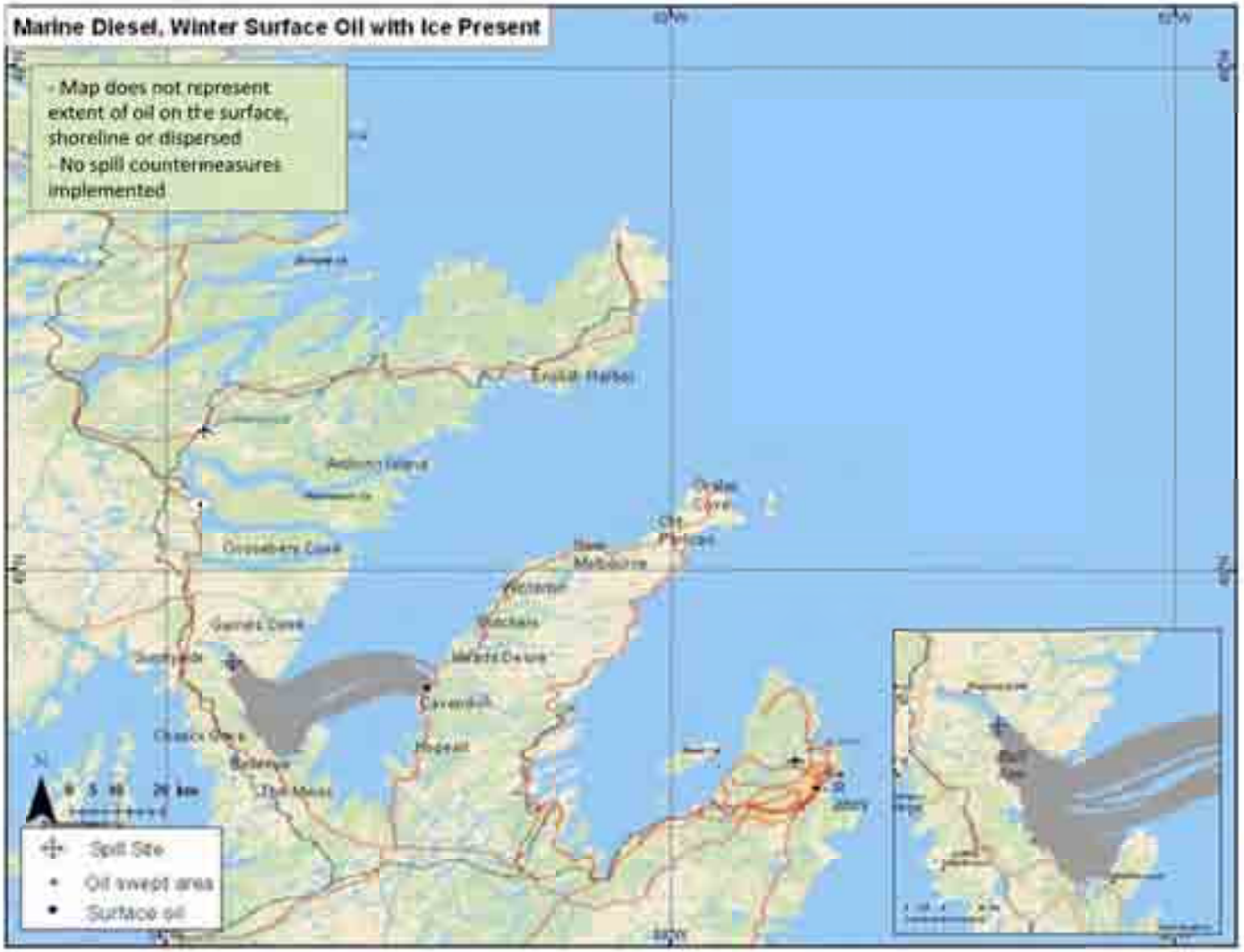

Figure C13. Water surface exposure to surface oil for 95th percentile run based on water surface area exposed to surface oil with average thickness greater than 0.01mm (dark brown sheen) for a 100 m^3 release of marine diesel in the winter with 65% ice coverage. Gray depicts the area of the sea surface swept by surface oil over the 30-day period, not a continuous surface slick. Black areas depict oil on the water surface at the end of the 30 day simulation.

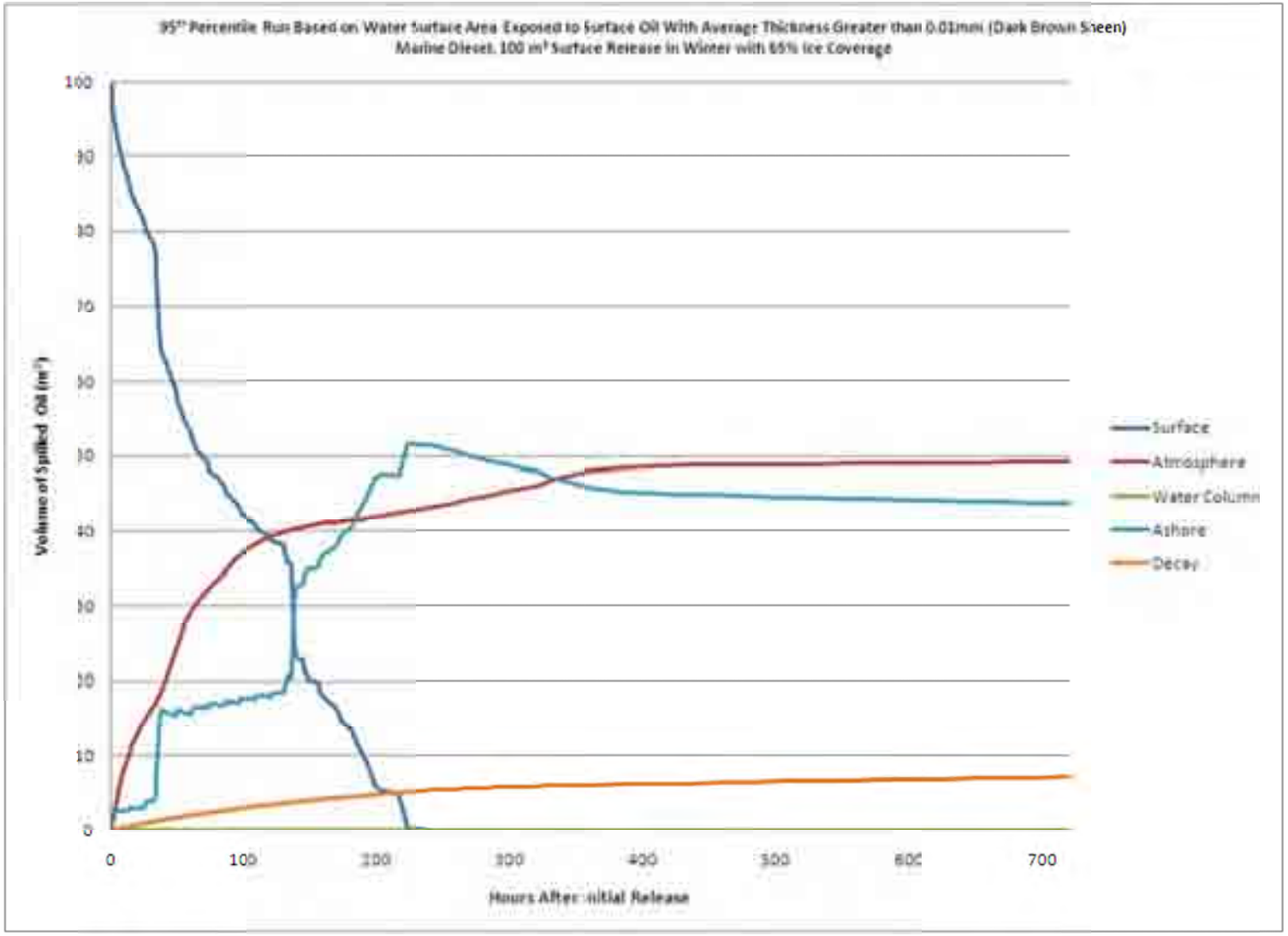

Figure C14. Mass balance graph for 95th percentile run based on water surface area exposed to surface oil with average thickness greater than 0.01mm (dark brown sheen) for a 100 m^3 release of marine diesel in the winter with 65% ice coverage.

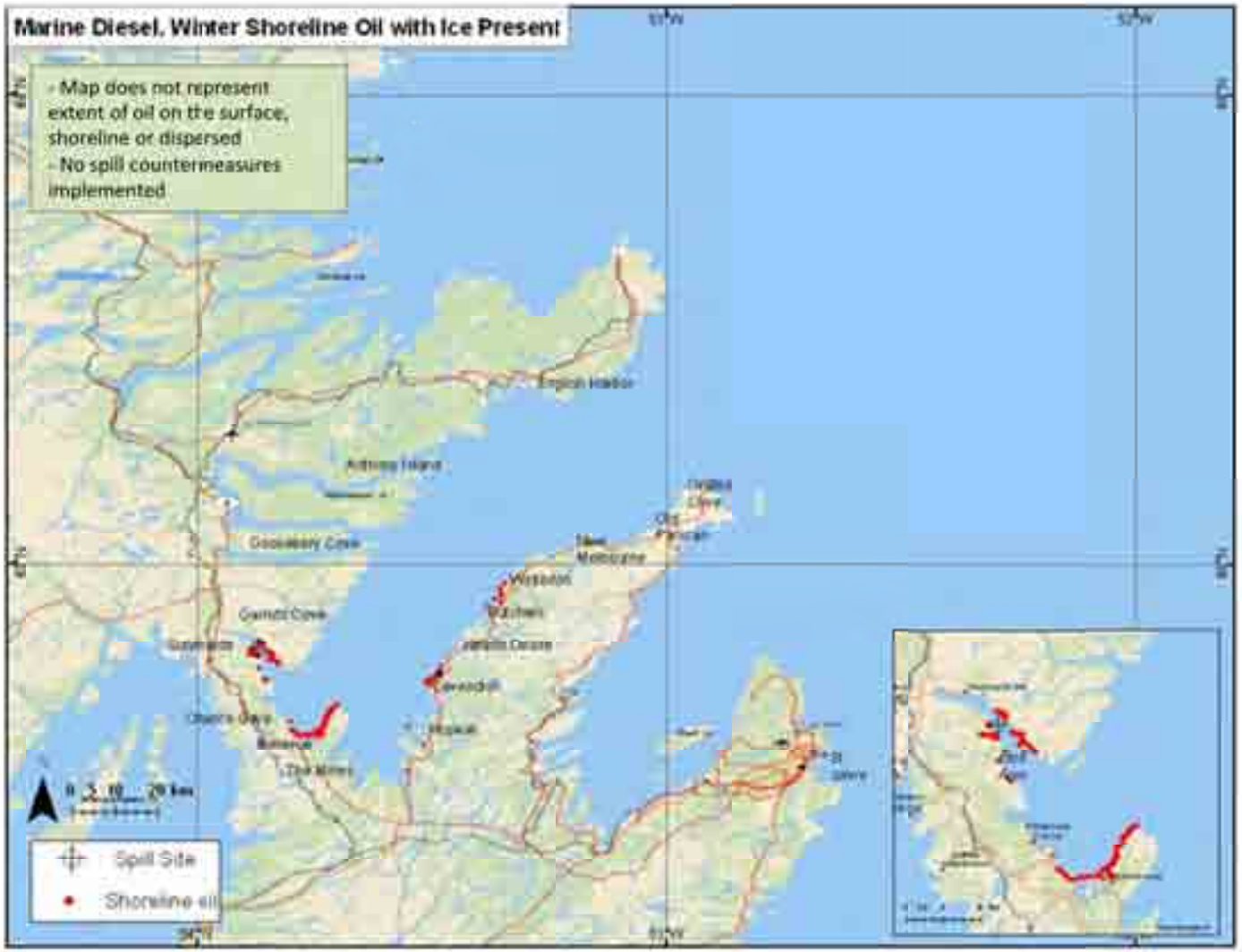

Figure C15. Shoreline exposure to hydrocarbons (mm) for 95th percentile run based on area of shoreline oiled with average thickness greater than 0.01mm (dark brown sheen) for a 100 m^3 release of marine diesel in the winter with 65% ice coverage. Red color highlights the areas of predicted shoreline oiling.

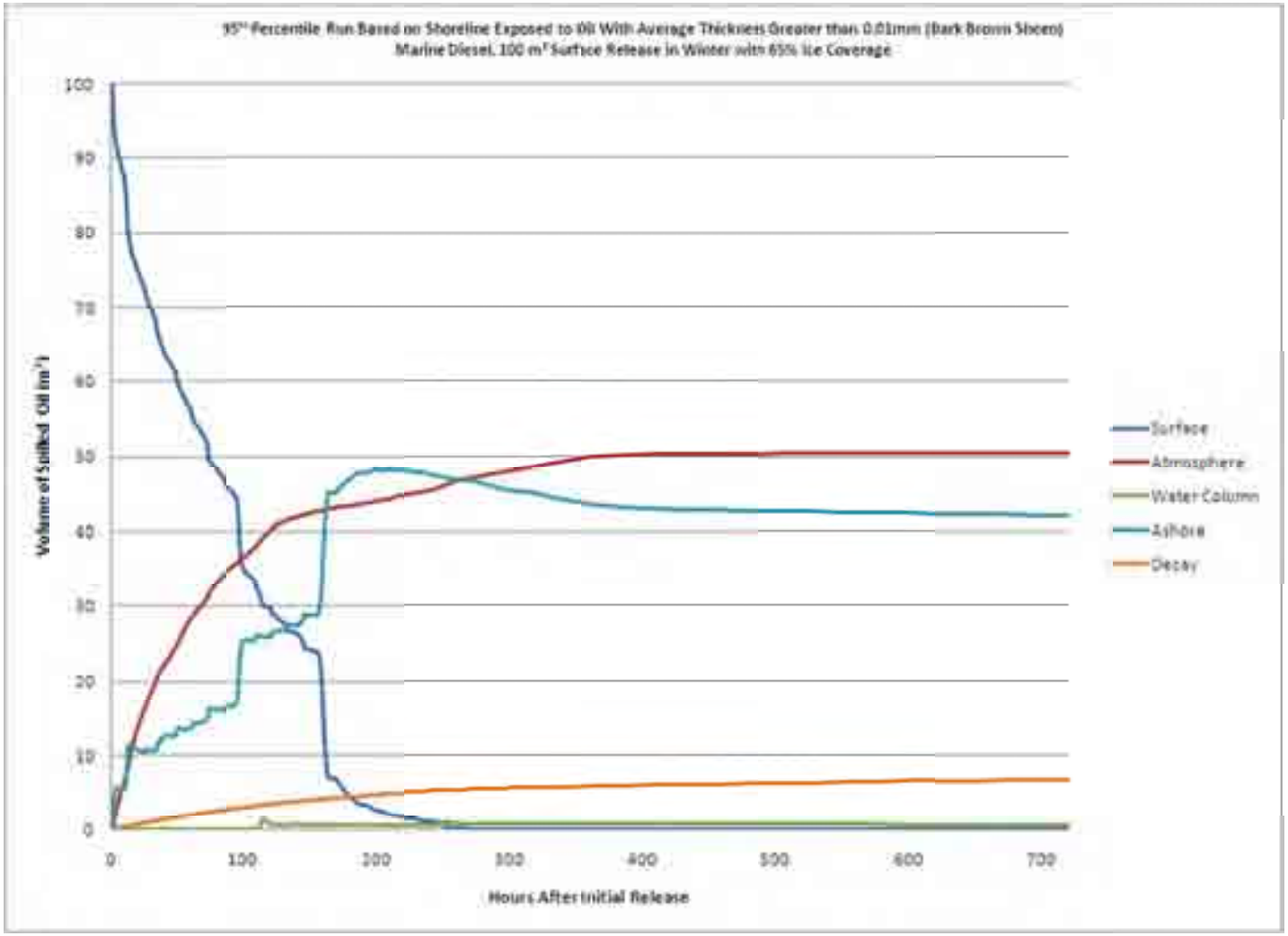

Figure C16. Mass balance graph for 95th percentile run based on area of shoreline oiled with average thickness greater than 0.01mm (dark brown sheen) for a 100 m^3 release of marine diesel in the winter with 65% ice coverage.

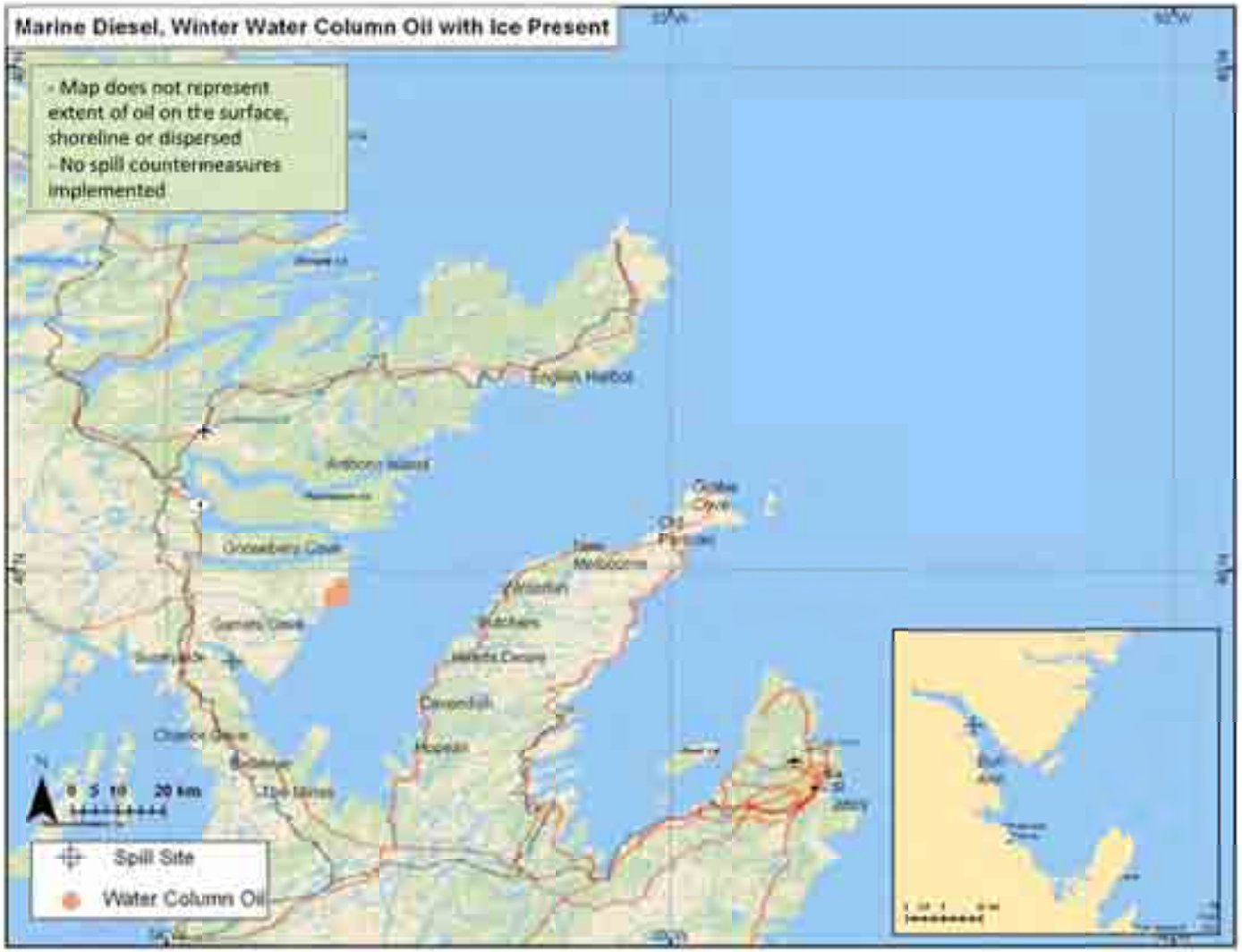

Figure C17. Area where the water column is exposed to a total hydrocarbon concentration exceeding 10ppb based on the 95th percentile run for a 100 m^3 release of marine diesel in the winter with 65% ice coverage.

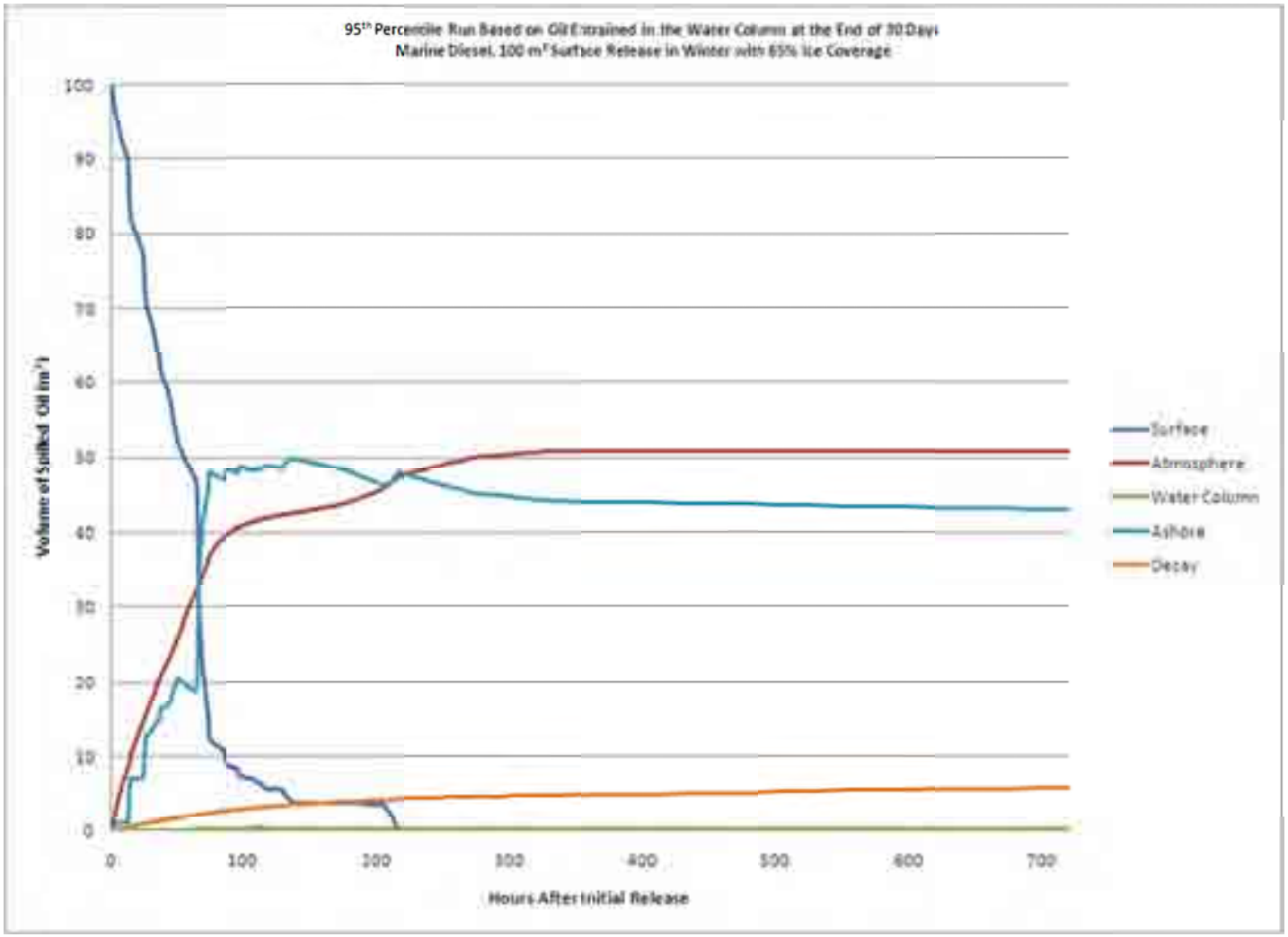

Figure C18. Mass balance graph for 95th percentile run based on subsurface oil entrained in the water column after 30 days for a 100 m^3 release of marine diesel in the winter with 65% ice coverage.

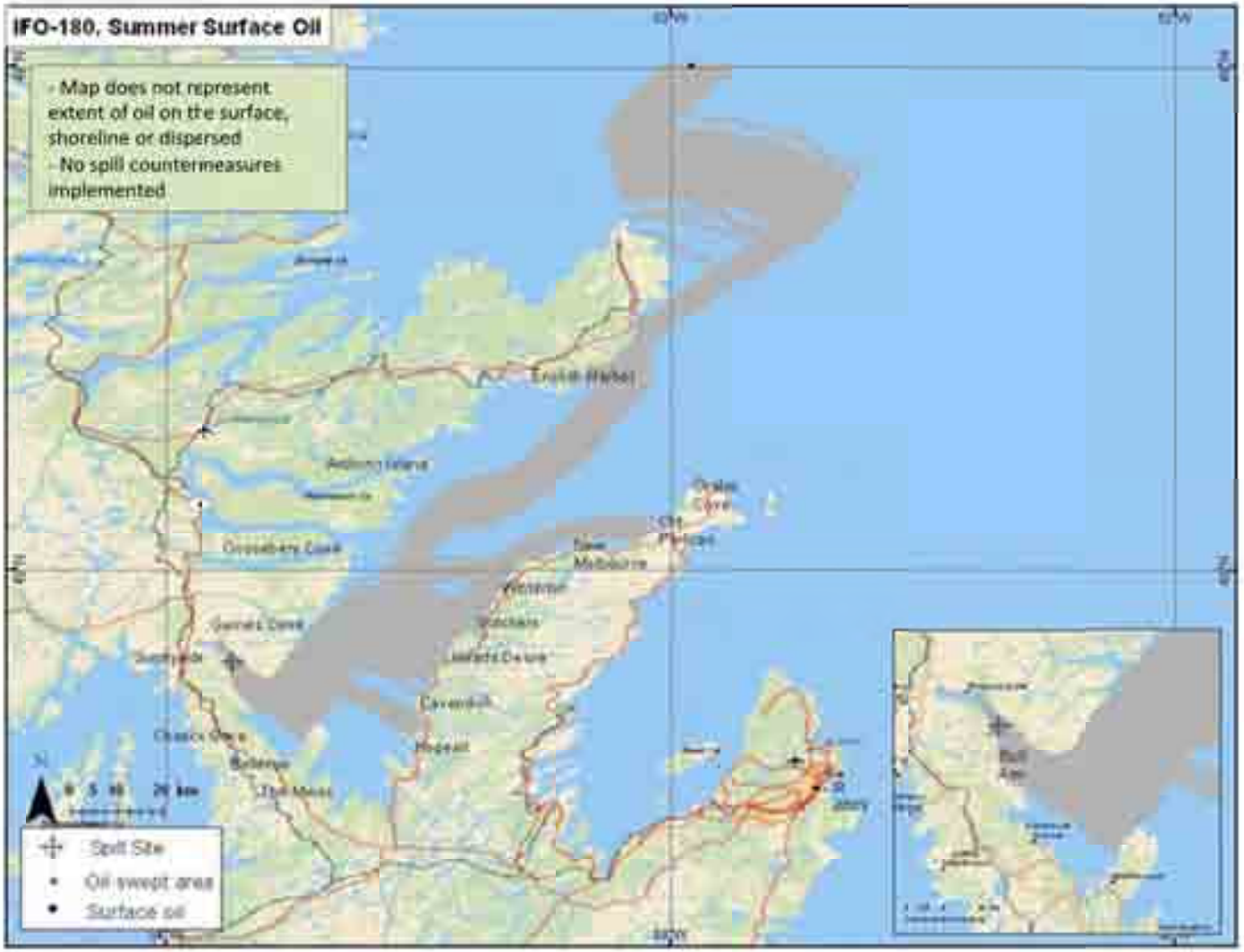

Figure C19. Water surface exposure to surface oil for 95th percentile run based on water surface area exposed to surface oil with average thickness greater than 0.01mm (dark brown sheen) for a 1000 m^3 release of IFO-180 in the summer. Gray depicts the area of the sea surface swept by surface oil over the 30-day period, not a continuous surface slick. Black areas depict oil on the water surface at the end of the 30 day simulation.

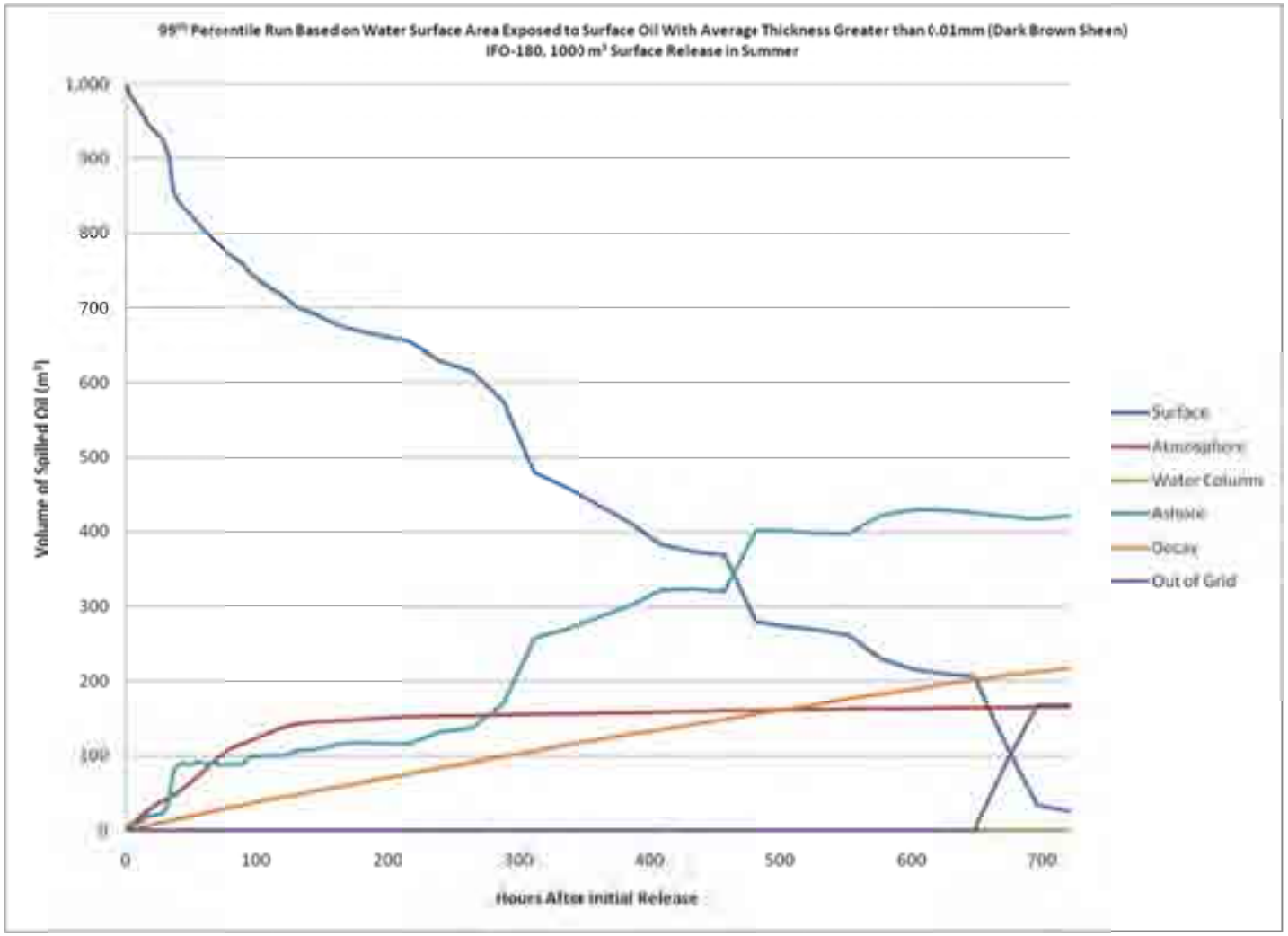

Figure C20. Mass balance graph for 95th percentile run based on water surface area exposed to surface oil with average thickness greater than 0.01mm (dark brown sheen) for a 1000 m^3 release of IFO-180 in the summer.

Figure C21. Shoreline exposure to hydrocarbons (mm) for 95th percentile run based on area of shoreline oiled with average thickness greater than 0.01mm (dark brown sheen) for a 1000 m^3 release of IFO-180 in the summer. Red color highlights the areas of predicted shoreline oiling.

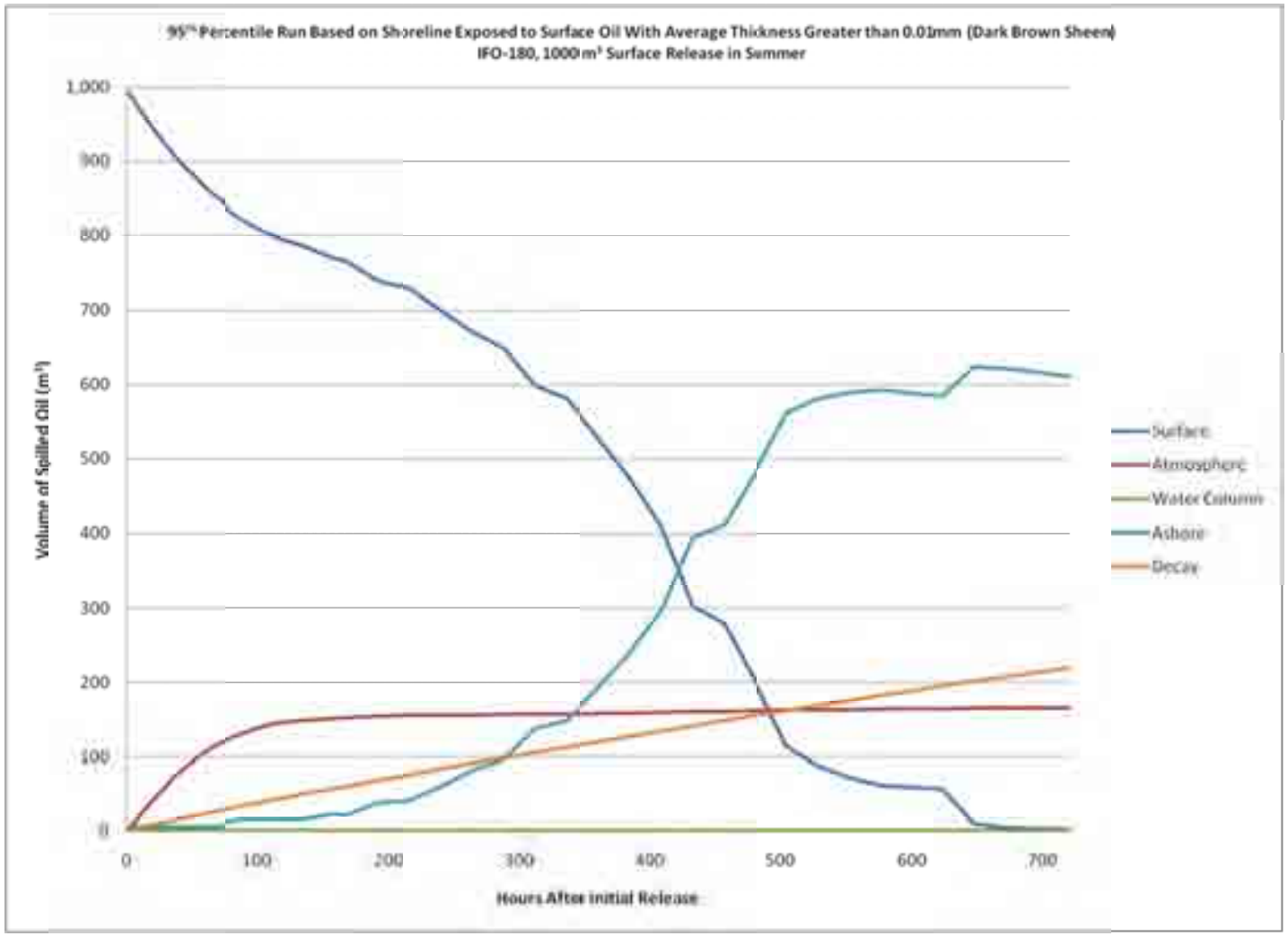

Figure C22. Mass balance graph for 95th percentile run based on area of shoreline oiled with average thickness greater than 0.01mm (dark brown sheen) for a 1000 m^3 release of IFO-180 in the summer.

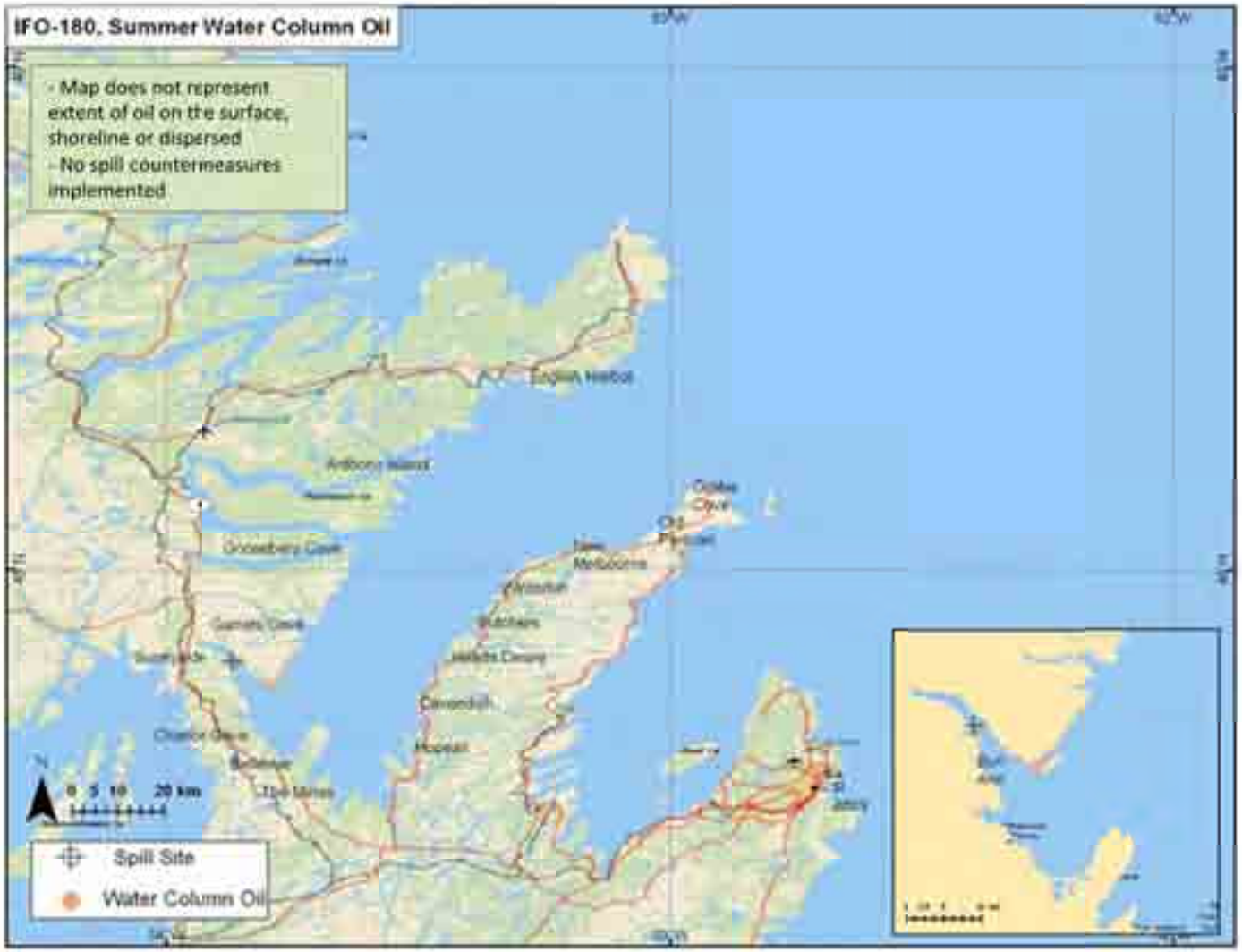

Figure C23. Area where the water column is exposed to a total hydrocarbon concentration exceeding 10ppb based on the 95th percentile run for a 1,000 m^3 release of IFO-180 in the summer.

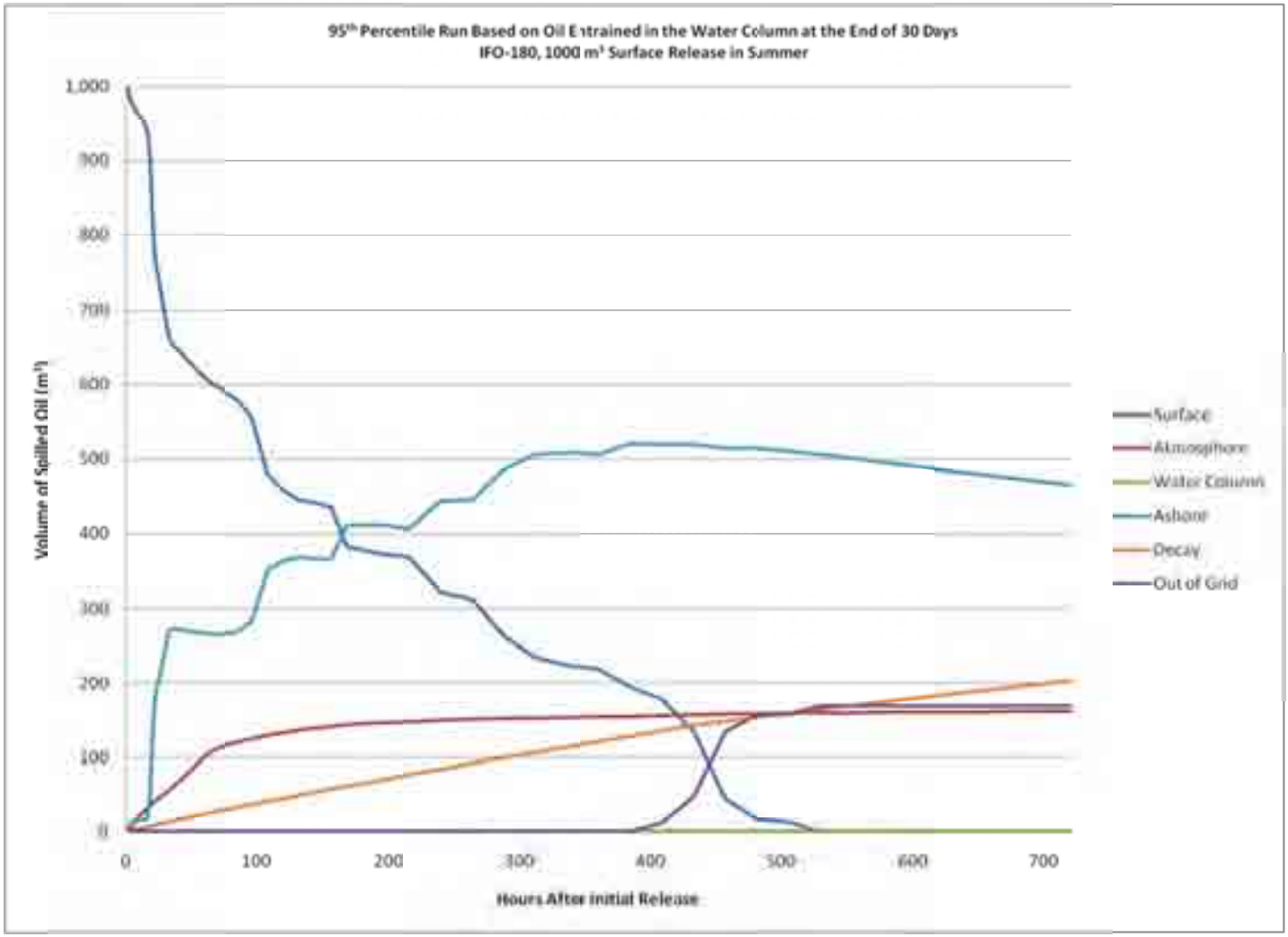

Figure C24. Mass balance graph for 95th percentile run based on subsurface oil entrained in the water column after 30 days for a 1000 m^3 release of IFO-180 in the summer.

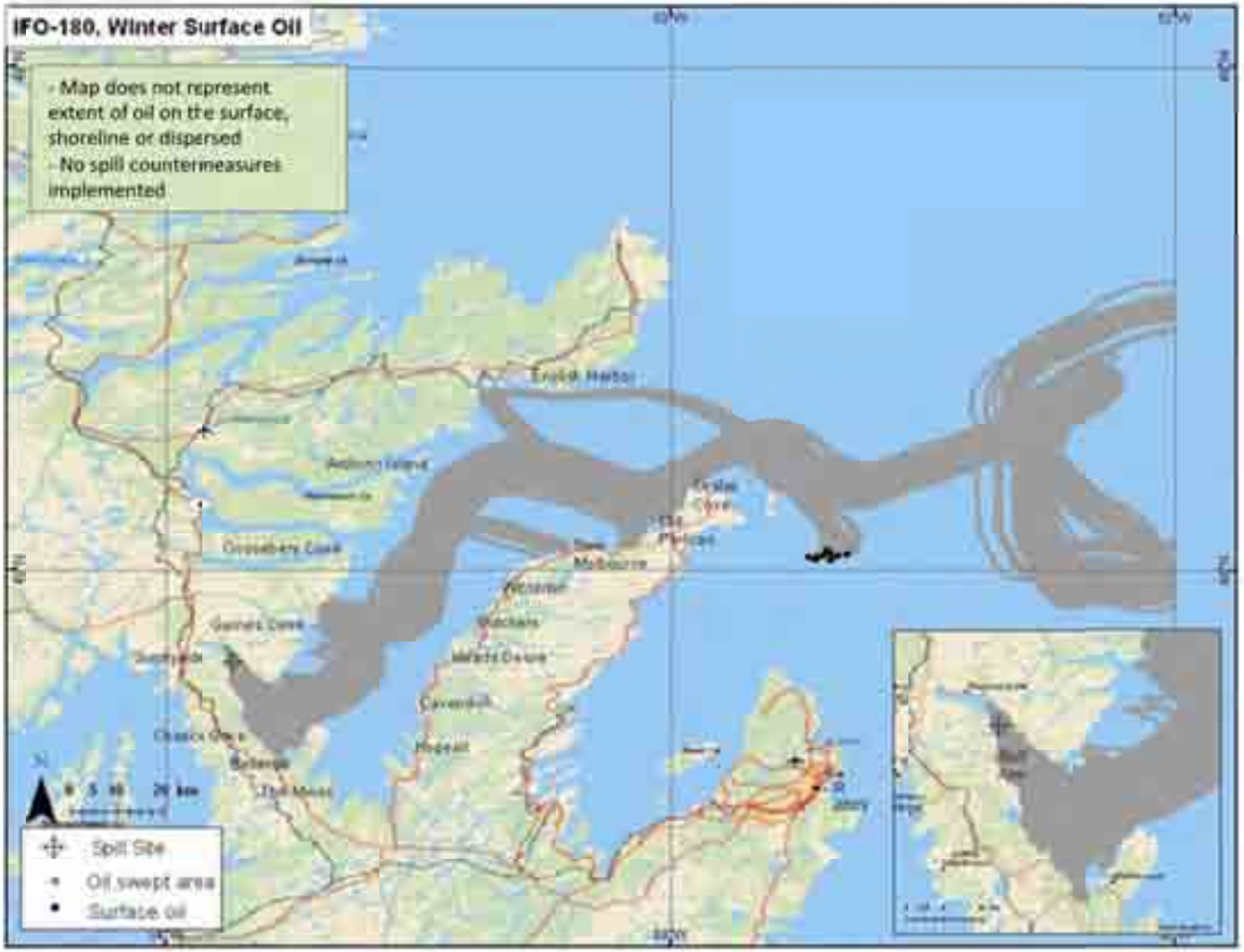

Figure C25. Water surface exposure to surface oil for 95th percentile run based on water surface area exposed to surface oil with average thickness greater than 0.01mm (dark brown sheen) for a 1000 m^3 release of IFO-180 in the winter. Gray depicts the area of the sea surface swept by surface oil over the 30-day period, not a continuous surface slick. Black areas depict oil on the water surface at the end of the 30 day simulation.

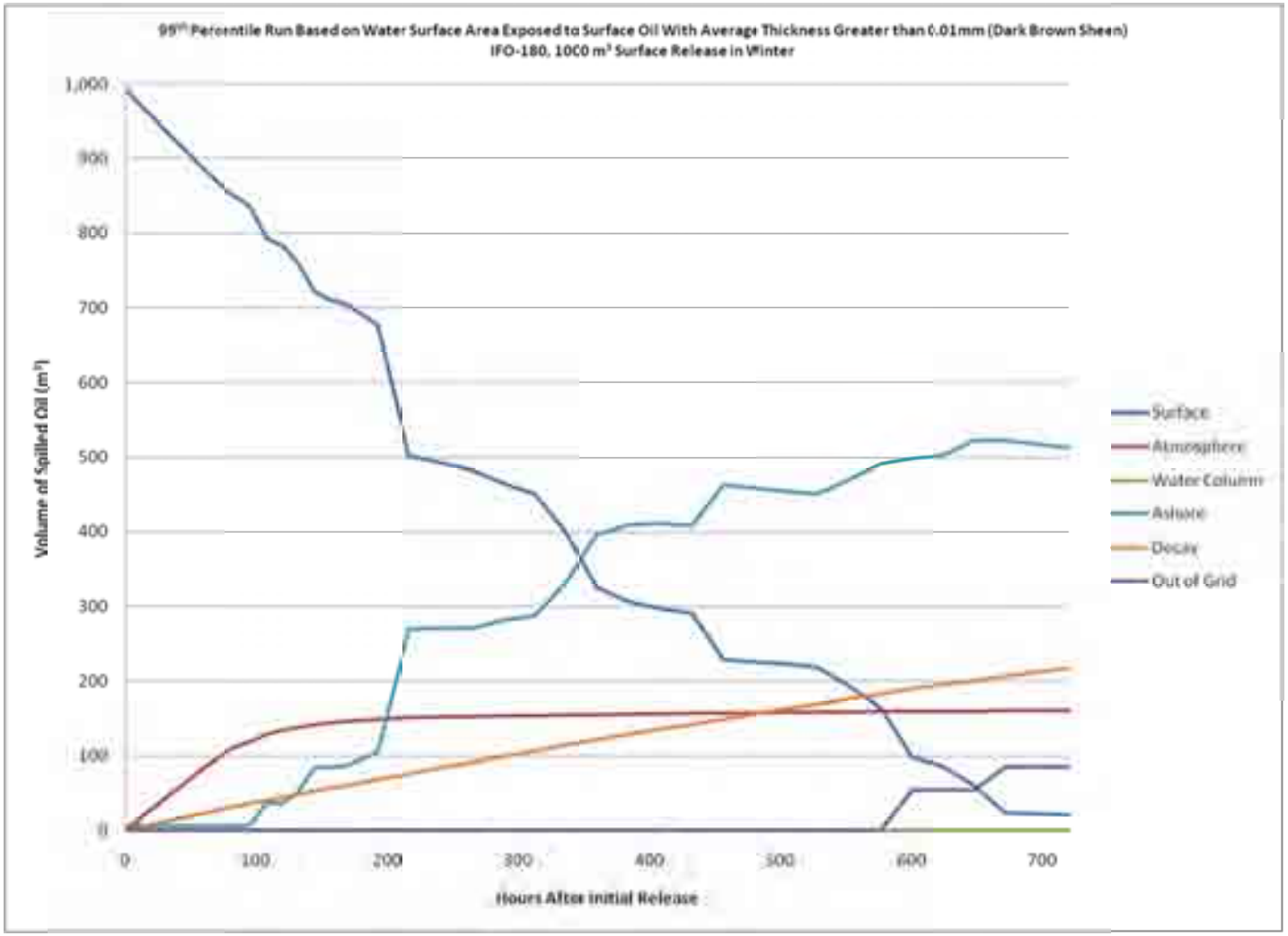

Figure C26. Mass balance graph for 95th percentile run based on water surface area exposed to surface oil with average thickness greater than 0.01mm (dark brown sheen) for a 1000 m^3 release of IFO-180 in the winter.

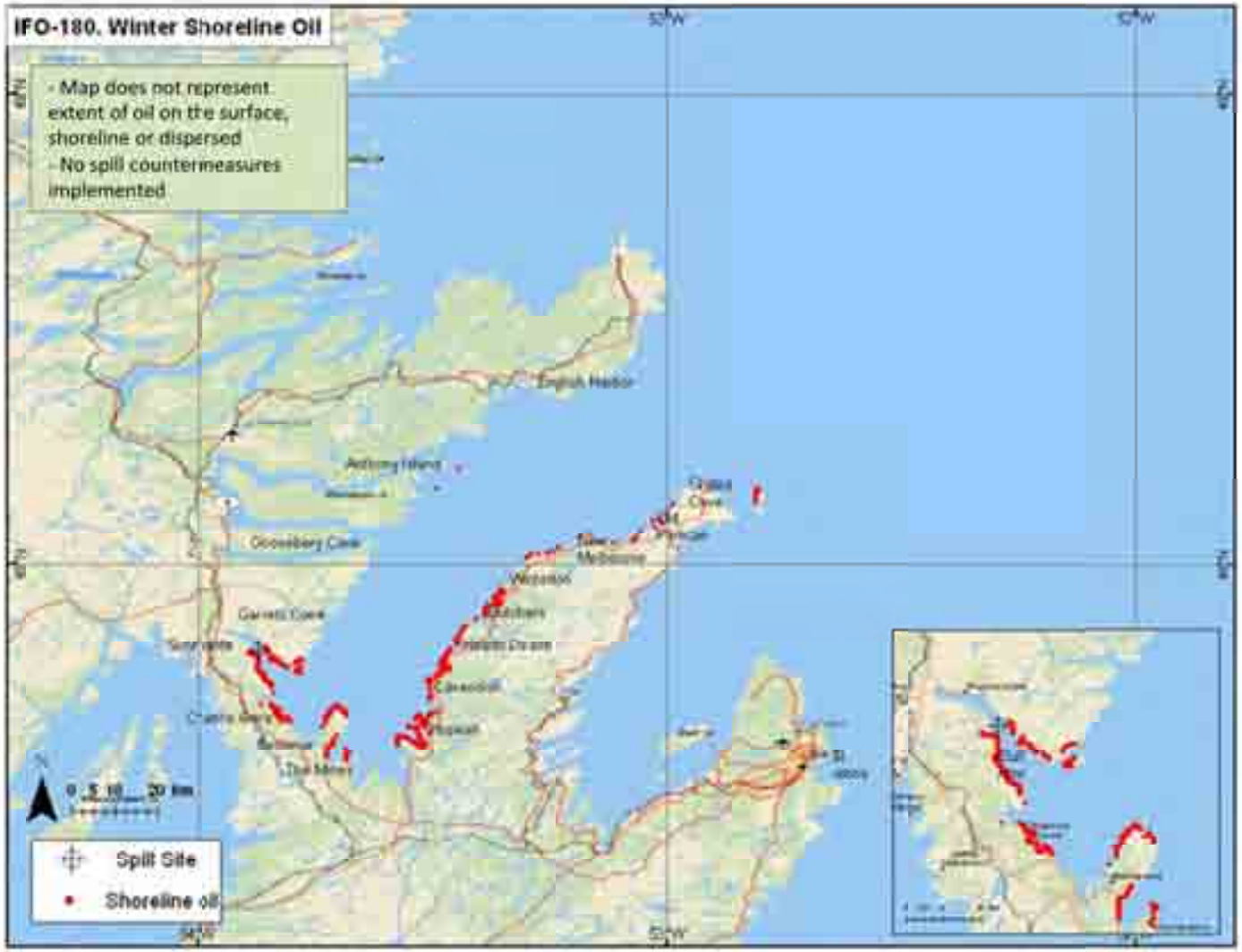

Figure C27. Shoreline exposure to hydrocarbons (mm) for 95th percentile run based on area of shoreline oiled with average thickness greater than 0.01mm (dark brown sheen) for a 1000 m^3 release of IFO-180 in the winter. Red color highlights the areas of predicted shoreline oiling.

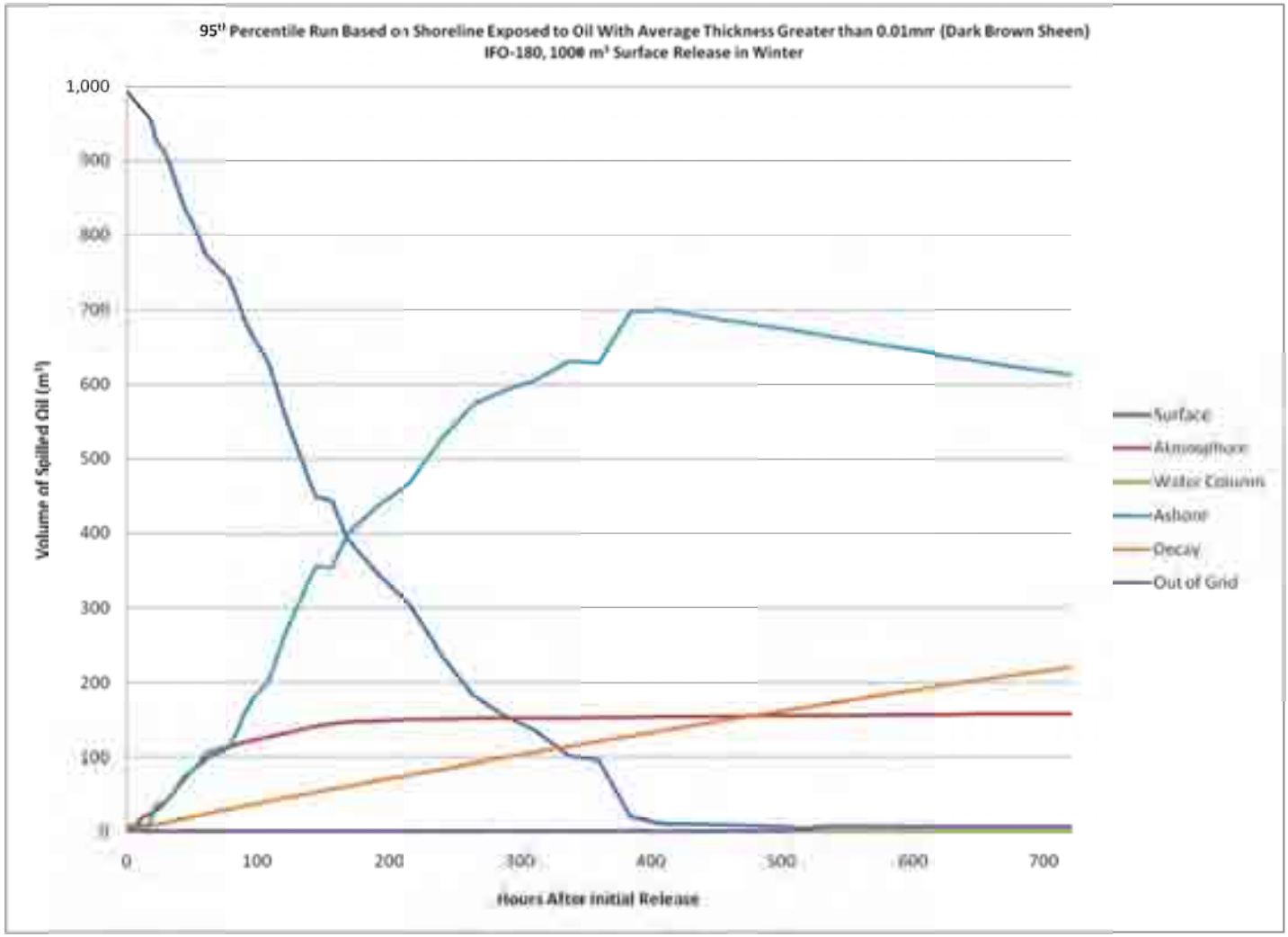

Figure C28. Mass balance graph for 95th percentile run based on area of shoreline oiled with average thickness greater than 0.01mm (dark brown sheen) for a 1000 m^3 release of IFO-180 in the winter.

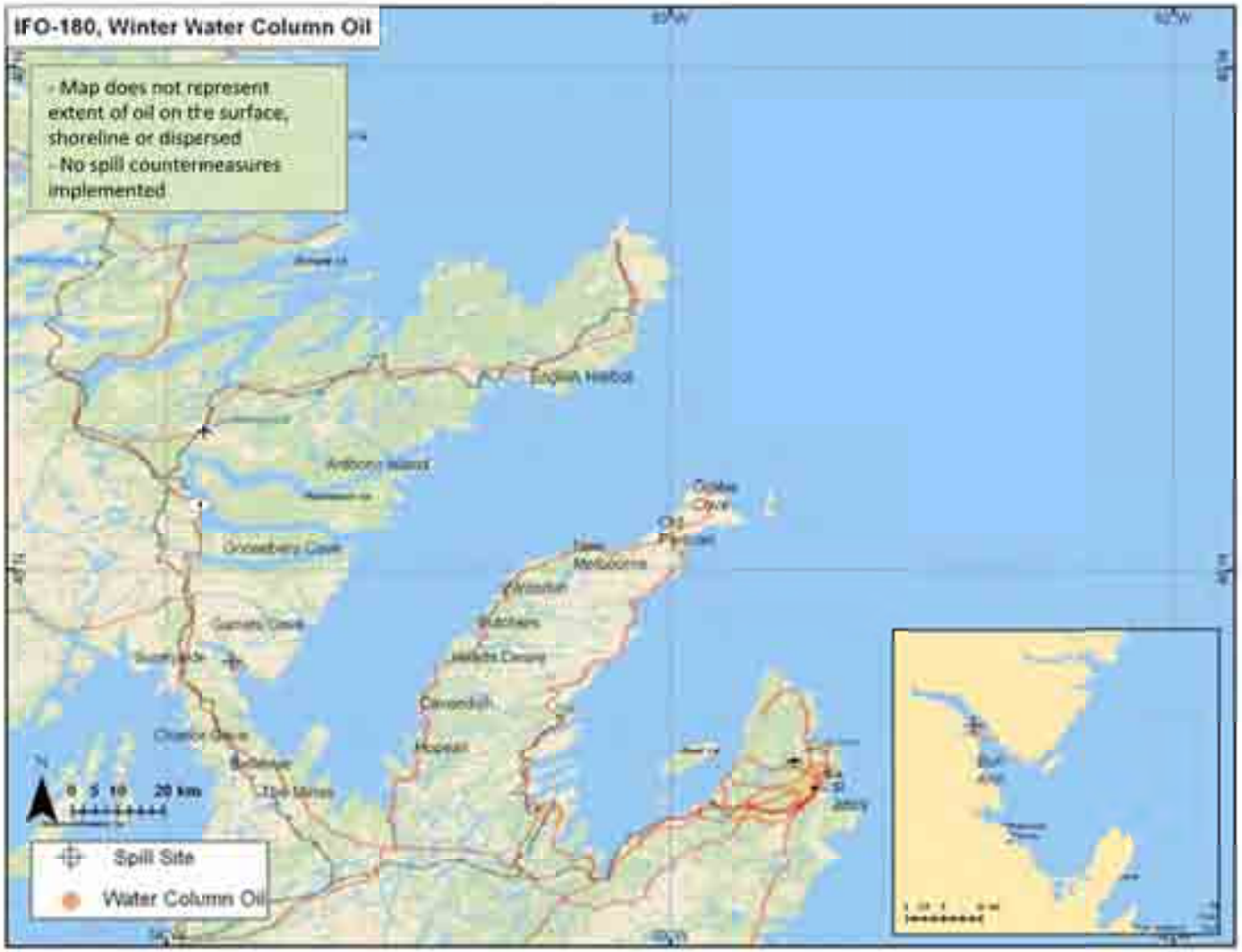

Figure C29. Area where the water column is exposed to a total hydrocarbon concentration exceeding 10ppb based on the 95th percentile run for a 1,000 m^3 release of IFO-180 in the winter.

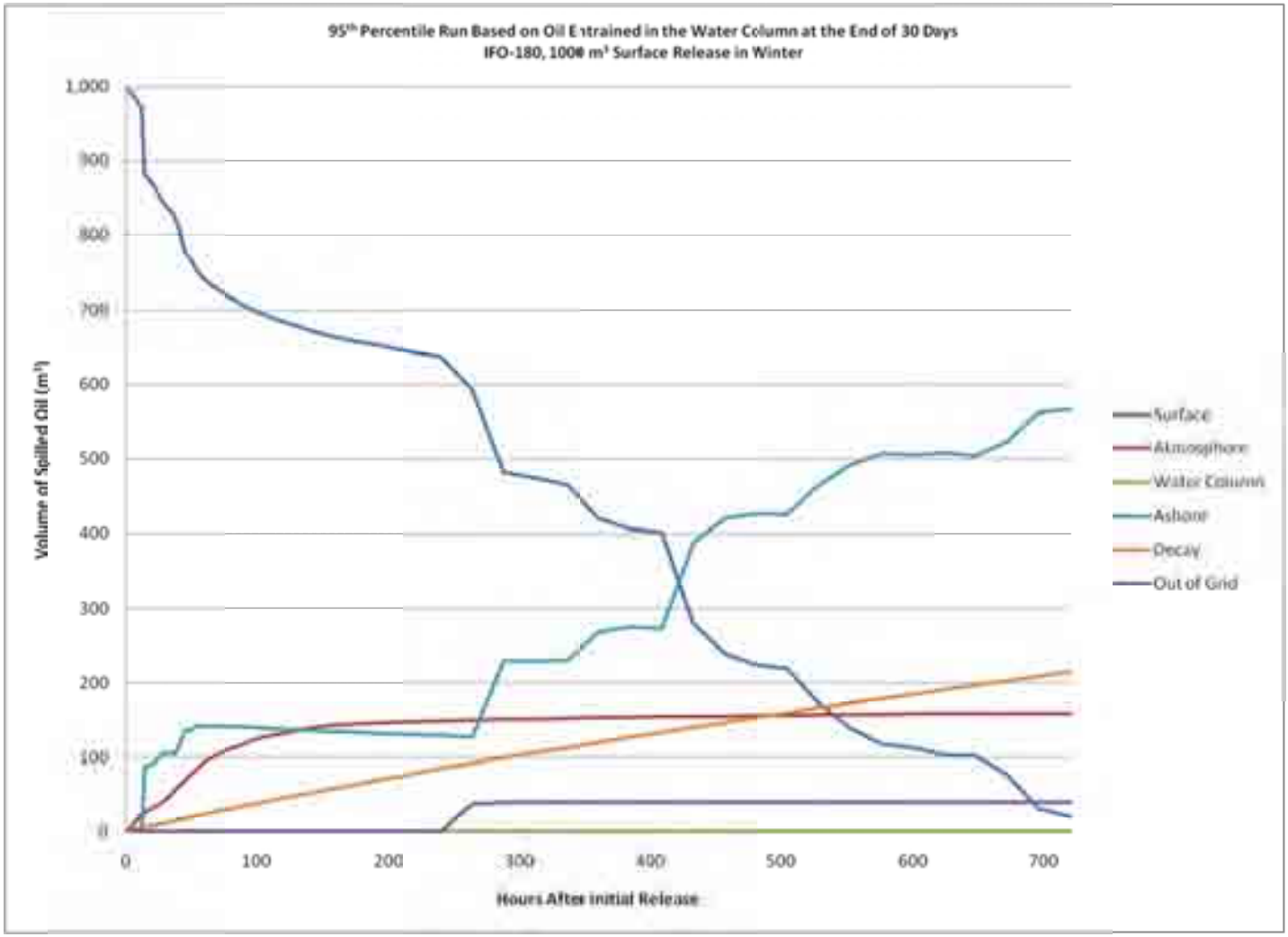

Figure C30. Mass balance graph for 95th percentile run based on subsurface oil entrained in the water column after 30 days for a 1000 m^3 release of IFO-180 in the winter.

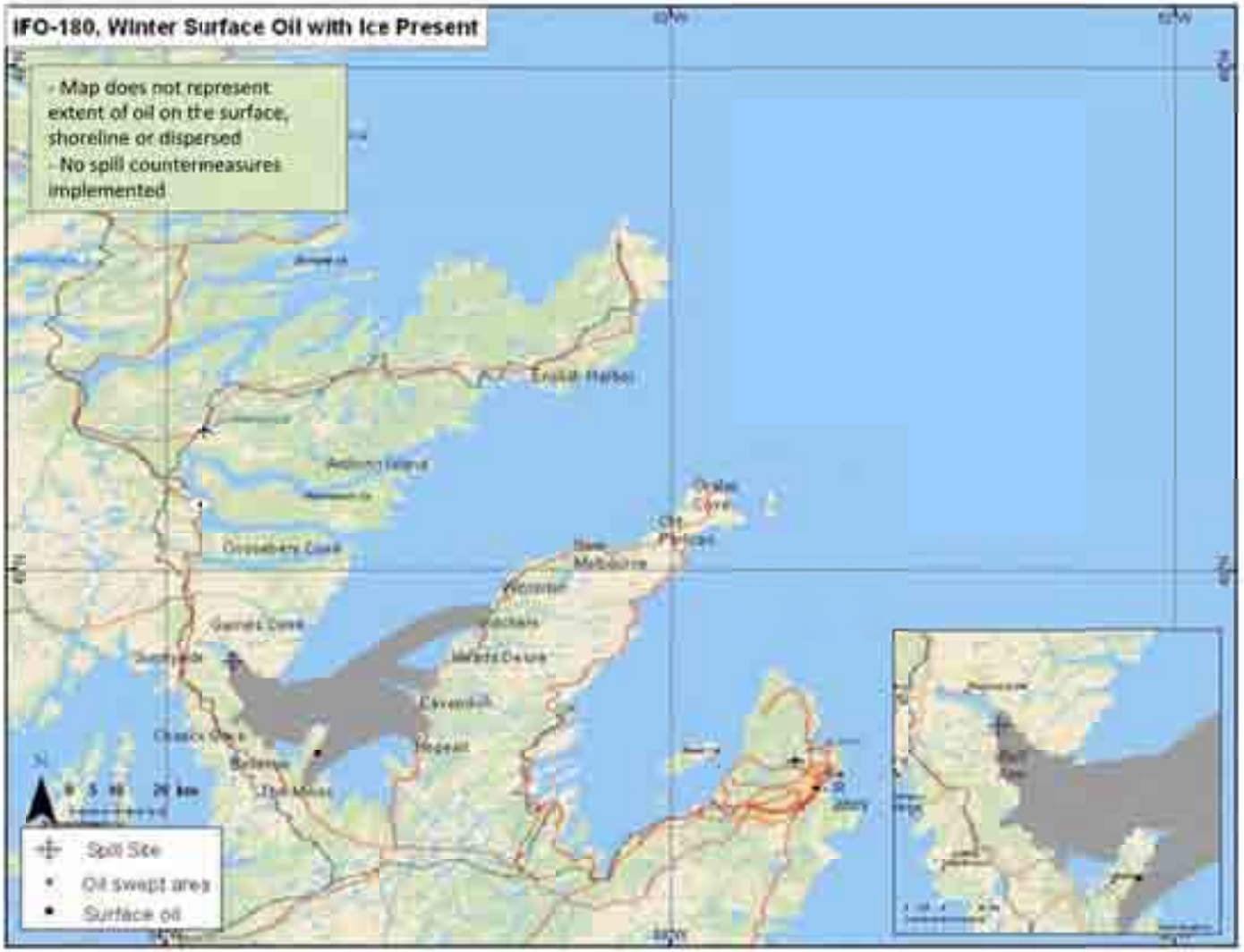

Figure C31. Water surface exposure to surface oil for 95th percentile run based on water surface area exposed to surface oil with average thickness greater than 0.01mm (dark brown sheen) for a 1000 m^3 release of IFO-180 in the winter with 65% ice coverage. Gray depicts the area of the sea surface swept by surface oil over the 30-day period, not a continuous surface slick. Black areas depict oil on the water surface at the end of the 30 day simulation.

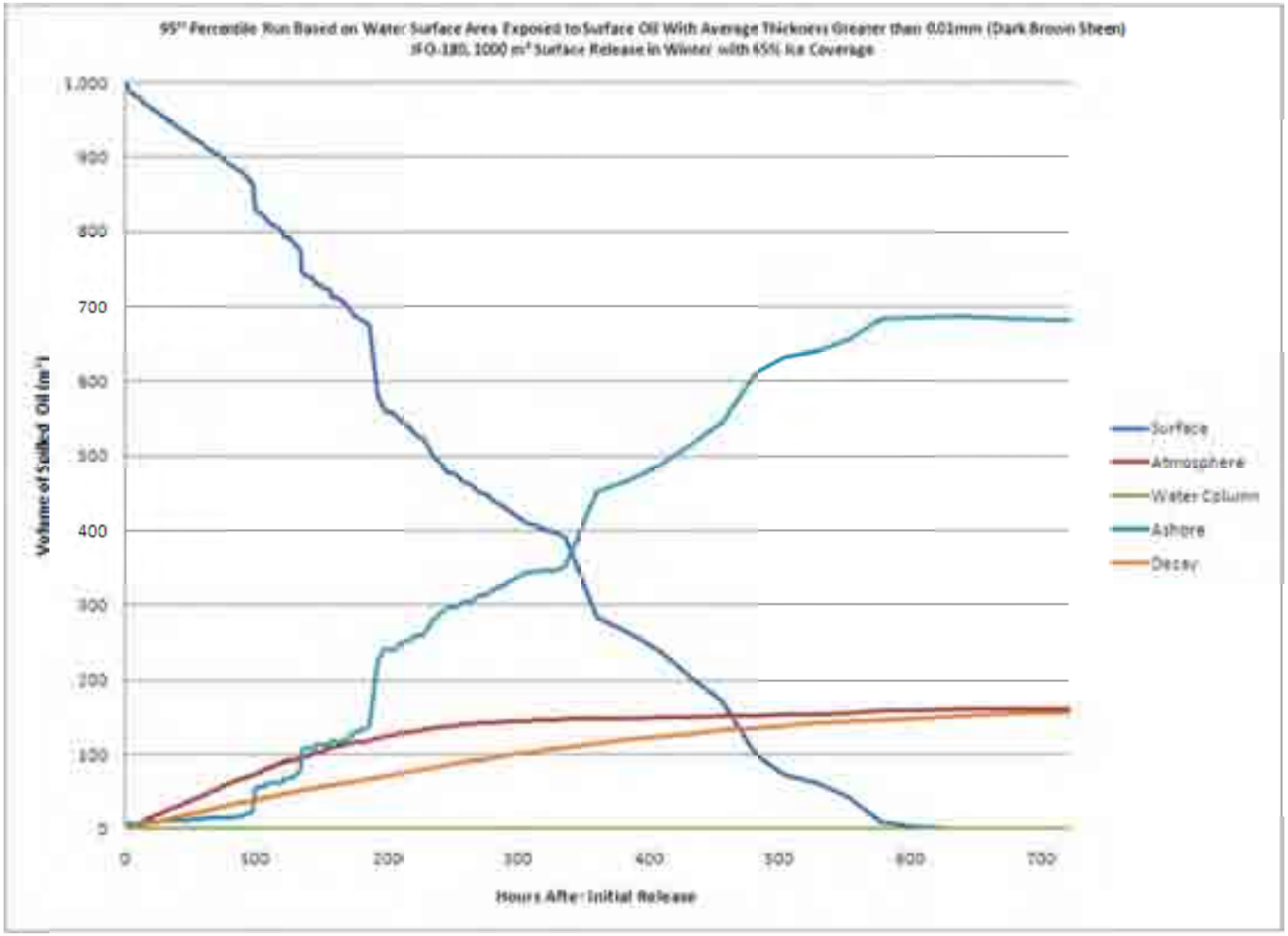

Figure C32. Mass balance graph for 95th percentile run based on water surface area exposed to surface oil with average thickness greater than 0.01mm (dark brown sheen) for a 1000 m^3 release of IFO-180 in the winter with 65% ice coverage.

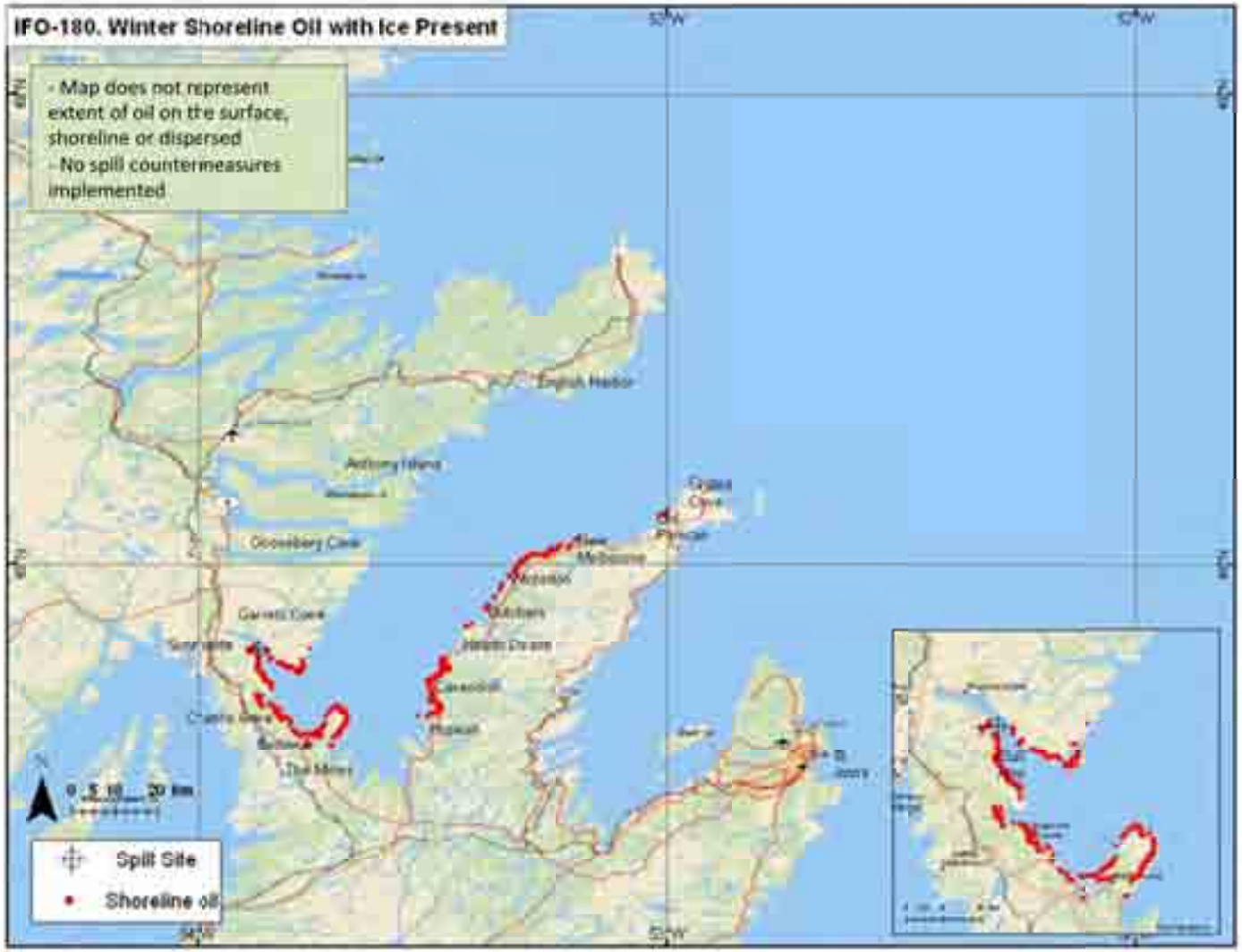

Figure C33. Shoreline exposure to hydrocarbons (mm) for 95th percentile run based on area of shoreline oiled with average thickness greater than 0.01mm (dark brown sheen) for a 1000 m^3 release of IFO-180 in the winter with 65% ice coverage. Red color highlights the areas of predicted shoreline oiling.

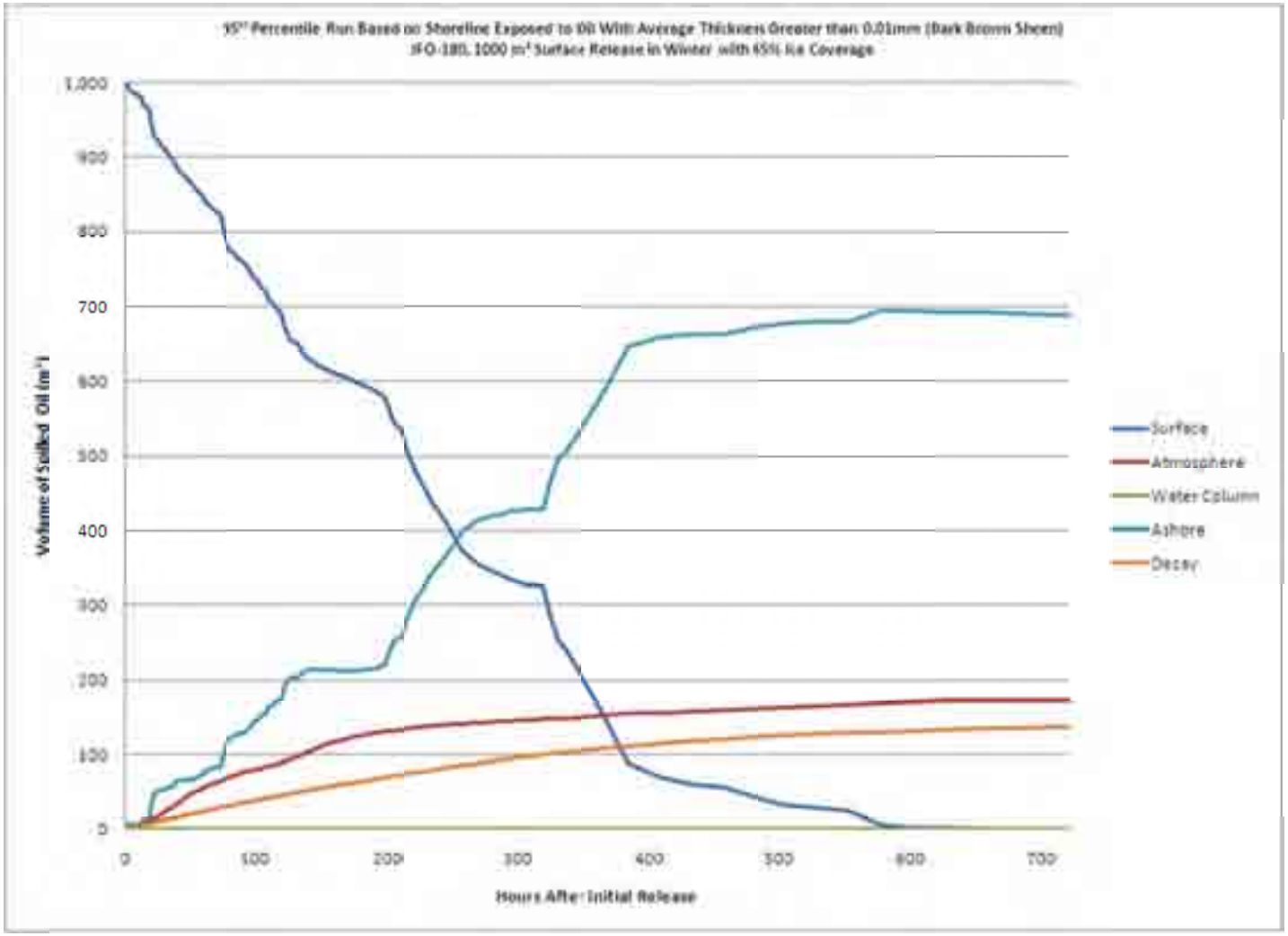

Figure C34. Mass balance graph for 95th percentile run based on area of shoreline oiled with average thickness greater than 0.01mm (dark brown sheen) for a 1000 m^3 release of IFO-180 in the winter with 65% ice coverage.

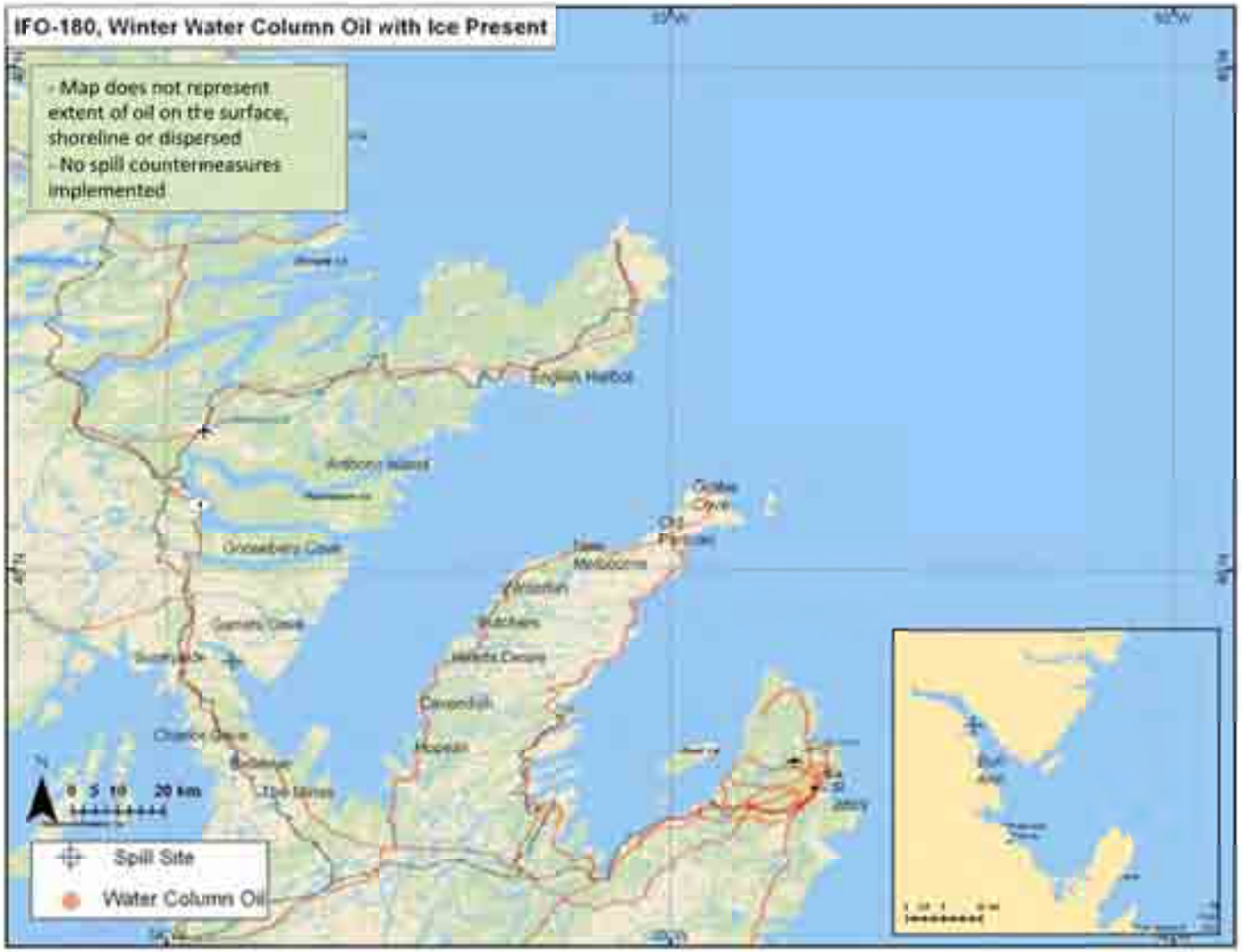

Figure C35. Area where the water column is exposed to a total hydrocarbon concentration exceeding 10ppb based on the 95th percentile run for a 1,000 m^3 release of IFO-180 in the winter with 65% ice coverage.

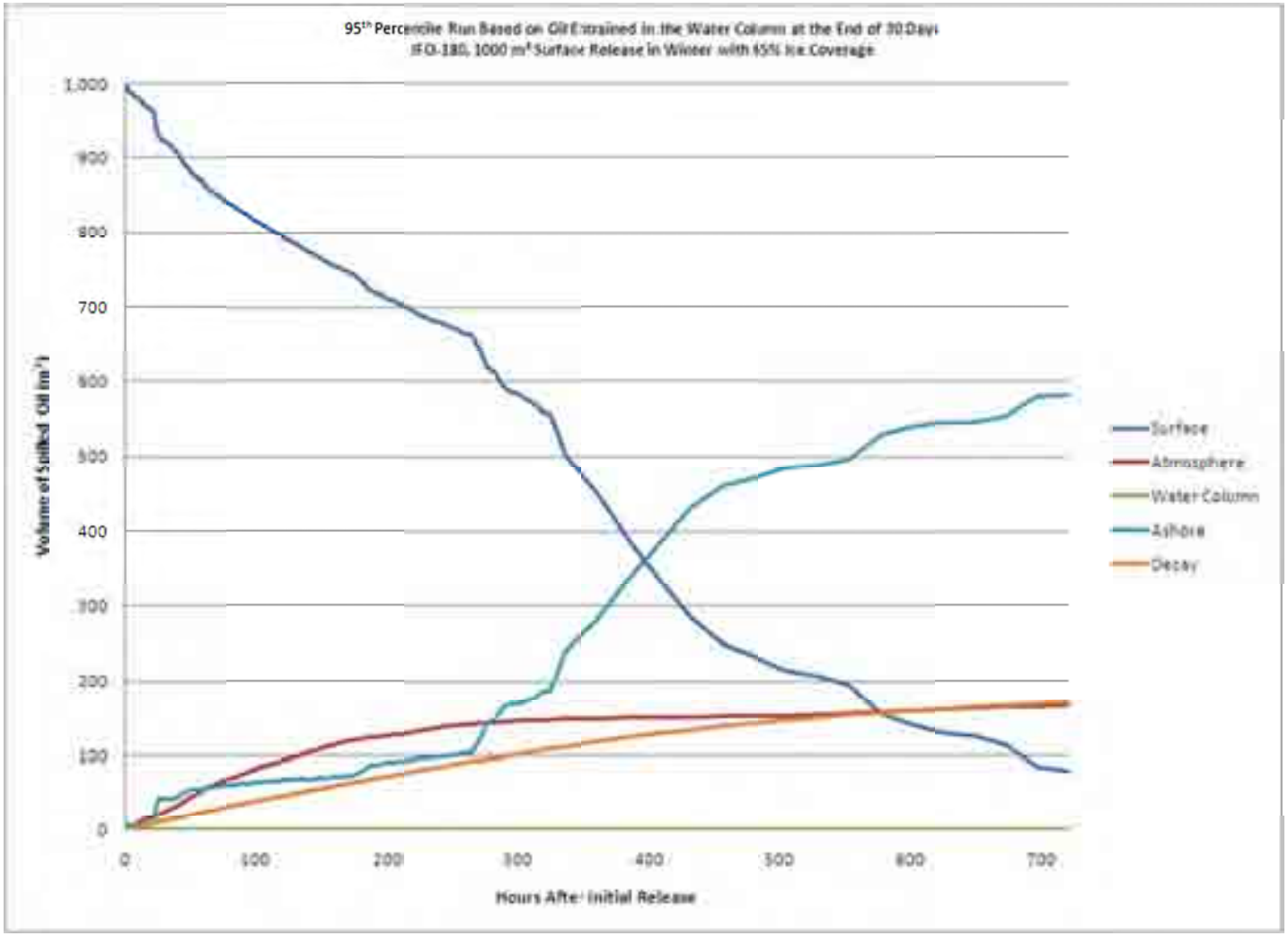

Figure C36. Mass balance graph for 95th percentile run based on subsurface oil entrained in the water column after 30 days for a 1000 m^3 release of IFO-180 in the winter with 65% ice coverage.